ANALYSIS AND DESIGN OF POWER CONDITIONING SYSTEMS FOR FUEL CELL POWERED SYSTEMS

A Dissertation

by

MAJA HARFMAN TODOROVIC

Submitted to the Office of Graduate Studies of
Texas A&M University
in partial fulfillment of the requirements for the degree of

DOCTOR OF PHILOSOPHY

May 2008

Major Subject: Electrical Engineering

ANALYSIS AND DESIGN OF POWER CONDITIONING SYSTEMS FOR FUEL CELL POWERED SYSTEMS

A Dissertation

by

MAJA HARFMAN TODOROVIC

Submitted to the Office of Graduate Studies of
Texas A&M University
in partial fulfillment of the requirements for the degree of

DOCTOR OF PHILOSOPHY

Approved by:

Chair of Committee,	Prasad Enjeti
Committee Members,	Hamid Toliyat
	Aniruddha Datta
	Anthony J. Appleby
Head of Department,	Costas Georghiades

May 2008

Major Subject: Electrical Engineering

ABSTRACT

Analysis and Design of Power Conditioning Systems for Fuel Cell Powered Systems.

(May 2008)

Maja Harfman Todorovic, B.S., University of Belgrade;

M.S., Texas A&M University

Chair of Advisory Committee: Dr. Prasad Enjeti

A combination of high prices of fossil fuels and the increased awareness of their negative environmental impact has influenced the development of new cleaner energy sources. Among various viable technologies, fuel cells have emerged as one of the most promising sources for both portable and stationary applications.

Fuel cell stacks produce DC voltage with a 2:1 variation in output voltage from no load to full load conditions. Hence, to increase the utilization efficiency and system stability, a power conditioner consisting of DC-DC and DC-AC converters is required for load interface. The design of power conditioners is driven by the application. This dissertation presents several different solutions for applications ranging from low-power portable sources for small electronics and laptop computers to megawatt-power applications for fuel cell power plants. The design and analysis for each power conditioner is presented in detail and the performance is verified using simulations and prototypes.

Special consideration is given to the role of supercapacitors who act as the additional energy storage elements. It is shown that the supercapacitor connected at the terminals of a fuel cell can contribute to increased steady state stability when powering constant power loads, improved transient stability against load transients, and increased fuel efficiency (i.e. reduced hydrogen consumption).

ACKNOWLEDGEMENTS

I would like to express my gratitude to my advisor, Dr. Prasad Enjeti, for his technical and theoretical support, guidance and encouragement throughout my graduate studies. I would like to thank all my committee members, Dr. Toliyat, Dr. Datta and Dr. Appleby, for their help, time and concern. Also, I would like to thank all my fellow students working in the power electronics and power quality laboratory at Texas A&M University, especially Leonardo Palma, and Mirunalini Chellappan for their help and guidance.

Most of all, I am grateful to my parents Radmila and Vitomir Harfman, my husband Milos, and our daughter Ema for their love, support and encouragement.

TABLE OF CONTENTS

CHAPTER Page

CHAPTER Page

LIST OF FIGURES

Page

Page

Page

Page

LIST OF TABLES

CHAPTER I

INTRODUCTION

1.1 Introduction

Most of the present electric power demand in the world is met by fossil and nuclear power plants. In recent years, we have witnessed a steadily growing interest in ecologically clean and renewable energy technologies, such as the fuel cells, wind and solar power plants. The United States Department of Energy (DOE) has identified the fuel cell as a distributed energy technology that will soon be participating in the energy market in wide variety of applications including portable power, central, auxiliary, and transportation systems, stationary power for buildings and other distributed generation applications.

A fuel cell is an electrochemical device that produces a DC voltage from the hydrogen-rich fuel gas and air that flow over two cell electrodes. It is similar to conventional battery in that both produce a direct current by using an electrochemical process, and to combustion engine in that both will work continuously as long as the fuel (reactants) are supplied. The main difference between the fuel cell and a battery is that the fuel cell is not the energy storage element that needs energy from an external source for recharging purposes.

Portable electronic technologies such as PDAs, notebook computers, and cell phones have fueled a need for new, high-energy, small volume power supplies for both military

---

This dissertation follows the style of *IEEE Transactions on Industry Applications*.

and commercial markets. Several of these devices are currently limited to battery technologies, which, despite recent advances, are insufficient to provide long-term power. In a fuel cell, power is continuous as long as the fuel and oxygen are supplied, similar to the gasoline/engine system which is used to power a car. The engine is purchased once (with the car) and gasoline is replenished as needed for continuous operation. The same is true in small fuel cell systems, which are expected to someday help power portable electronic products such as notebook computers. Fuel capsules can be exchanged out quickly without the need to wait for recharging. Users could carry spare fuel cartridges, not extra batteries to extend operation and enhance convenience. Fuel cells, especially low-temperature types such as DMFC and PEMFC, are potentially good candidates to replace batteries as power sources for the next generation of portable applications thanks to the high energy content of their fuels.

Another very attractive application of fuel cells is uninterruptible power supply (UPS) systems, which can help fuel cell technology to become a commercial solution. A fuel cell's end of life can be extended by intermittent operation of UPS systems and the per kilowatt price associated with UPS operation, although currently one of the highest on the market, can be driven down in the long run by fuel cell technology [1]. It is important for the UPS system to be able to immediately take over the full load at the inception of the power outage or out-of-tolerance situation to avoid any data or production loss, uncontrolled system shutdown or malfunctioning of the devices. However, fuel processors have a delay as long as several tens of seconds, and the fuel cell cannot take over the full load if its membrane is not properly humidified [2]. For this

reason, a supercapacitor module is employed to compensate for these response delays by supplying the required instantaneous energy, which is stored during the normal operation.

In order to properly design a fuel cell's power conditioning systems, an in-depth analysis of fuel cell behavior is needed. Furthermore, the role of a supercapacitor in the design of fuel cell powered systems needs to be investigated fully. The additional energy storage provided by the supercapacitor connected at the terminals of a fuel cell influences steady state as well as transient stability and changes the fuel efficiency.

1.2 Fuel cell technology

Fuel cells are electrochemical devices that convert hydrogen rich fuels into electric energy directly with a high overall efficiency. Since the process of producing electric energy avoids the intermediate steps of producing heat and mechanical work, common in most conventional methods, fuel cells are not limited by thermal limitations such as the Carnot efficiency. Likewise, since the process does not involve any kind of combustion, fuel cells produce power with a minimal amount of pollutant gases.

Different types of fuel cells can be characterized by the electrolyte used. They are listed in Table I with their main features. All of these fuel cells function in the same basic way. A schematic representation of the fuel cell functionality is shown in Fig. 1.

At the anode, a fuel (usually hydrogen) is oxidized into electrons and protons, and at the cathode, oxygen is reduced to oxide species. Depending on the electrolyte, either protons or oxide ions are transported through the ion-conducting, but electronically

insulating, electrolyte to combine with oxide ions or protons, respectively, to generate water and electric power.

TABLE I
CURRENTLY DEVELOPED TYPES OF FUEL CELLS AND THEIR CHARACTERISTICS AND APPLICATIONS

Fuel Cell Type	Proton exchange membrane FC **PEMFC**	Alkaline FC **AFC**	Phosphoric acid FC **PAFC**	Molten carbonate FC **MCFC**	Solid oxide FC **SOFC**
Electrolyte	Solid polymer (such as Nafion)	KOH	Phosphoric acid	Lithium and potassium carbonate	Solid oxide electrolyte (yttria, zirconia)
Charge carrier	H^+	OH^-	H^+	CO_3^{2-}	O^{2-}
Fuel	Pure H_2 (tolerates CO_2)	Pure H_2	Pure H_2 (tolerates CO_2, approx. 1% CO)	H_2, CO, CH_4, other hydrocarbons (tolerates CO_2)	H_2, CO, CH_4, other hydrocarbons (tolerates CO_2)
Catalyst	Platinum	Platinum	Platinum	Nickel	Perovskites
Operation temperature	50–100°C	60–120°C	~220°C	~650°C	~1000°C
External reformer for CH_4	Yes	Yes	Yes	No	No
Product water management	Evaporative	Evaporative	Evaporative	Gaseous Product	Gaseous Product
Product heat management	Process Gas + Independent Cooling Medium	Process Gas + Electrolyte Circulation	Process Gas + Independent Cooling Medium	Internal Reforming + Process Gas	Internal Reforming + Process Gas
Electric efficiency	35–45%	35–55%	38%-45%	50%-60%	40%-55%
Power range /Application	Automotive, CHP (5–250kW), portable	<5 kW, military, space	CHP (200 kW)	200 kW–MW range, CHP and standalone	2 kW–MW range, CHP and standalone

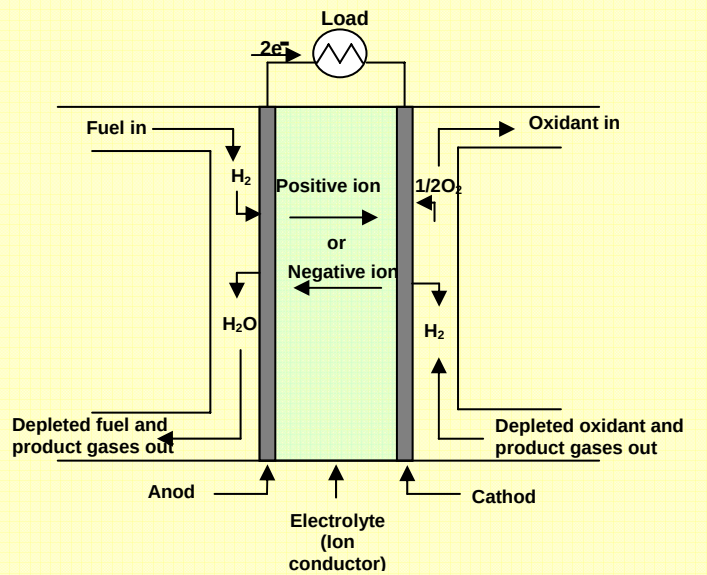

Fig. 1. Fuel cell diagram

Fuel cells produce DC power, water and heat from the combination of hydrogen produced from the fuel and oxygen from the air. In procedures where H_2O and CH_4 react in the cell to produce hydrogen, CO_2 is also a co-product. Reactions in fuel cells depend substantially on the temperature and pressure inside the cell. A system must be built around the fuel cell to supply air and clean fuel, convert the energy to a more usable form such as grid quality AC power, and remove the depleted reactants and heat that are produced by the reactions in the cells [3]. Figure 2 shows the basic structure of a fuel cell power plant.

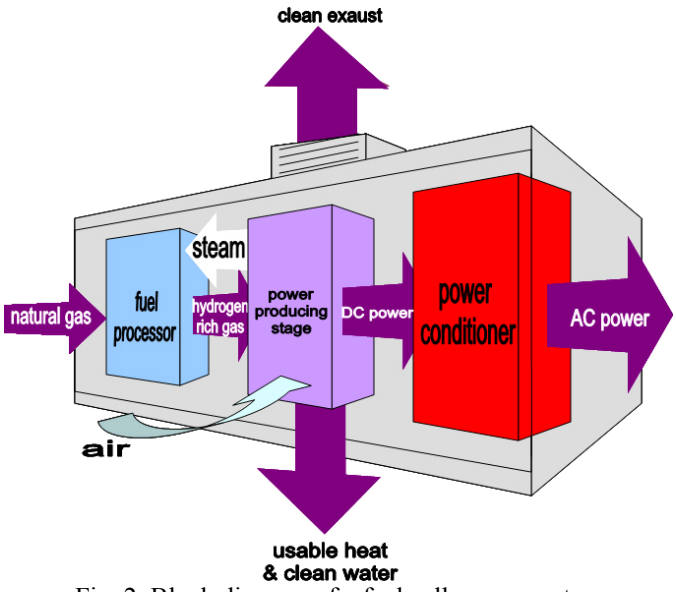

Fig. 2. Block diagram of a fuel cell power system

First stage of a fuel cell power system plant is a fuel processing unit where a conventional fuel (natural gas, methanol, coil, naphtha, or other gaseous hydrocarbon) is purified into a gas containing hydrogen. The following stage converts chemical energy to DC electricity using the stacks of individual fuel cells. The number of stacks used in the power producing section unit depends on the specific power application. Finally, a power conditioner converts DC power generated by the fuel cell stacks into the regulated AC or DC power suitable for customer usage.

1.3 Fuel cell promise

As mentioned before, fuel cells can be classified based on the type of electrolyte. Although the electrolyte is the primary mean of characterizing the cell, the operating temperature also plays an important role. There are low-temperature operating fuel cells (PEMFC, AFC, PAFC) and high-temperature operating fuel cells (MCFC, SOFC); in

latter type the temperature is high enough so that the reforming processing of fuel, such as natural gas, occurs within the cell.

Among them the proton exchange membrane fuel cell (PEMFC) has gained a wide acceptance due to several advantages, such as compact design, long operating life, quick start-up times, and high efficiency. A PEMFC generates electricity directly from hydrogen fuel through two electrochemical reactions which take place at the proton exchange membrane/catalyst interface at low temperatures (<80° C). Chemical reactions that take place inside a PEMFC fuel cell are presented in the following:

$$\text{Anode: } 2H_2 \rightarrow 4H^+ + 4e^-$$

$$\text{Cathode: } O_2 + 4H^+ + 4e^- \rightarrow 2H_2O \qquad (1)$$

$$\text{Net reaction: } 2H_2 + O_2 = 2H_2O\,.$$

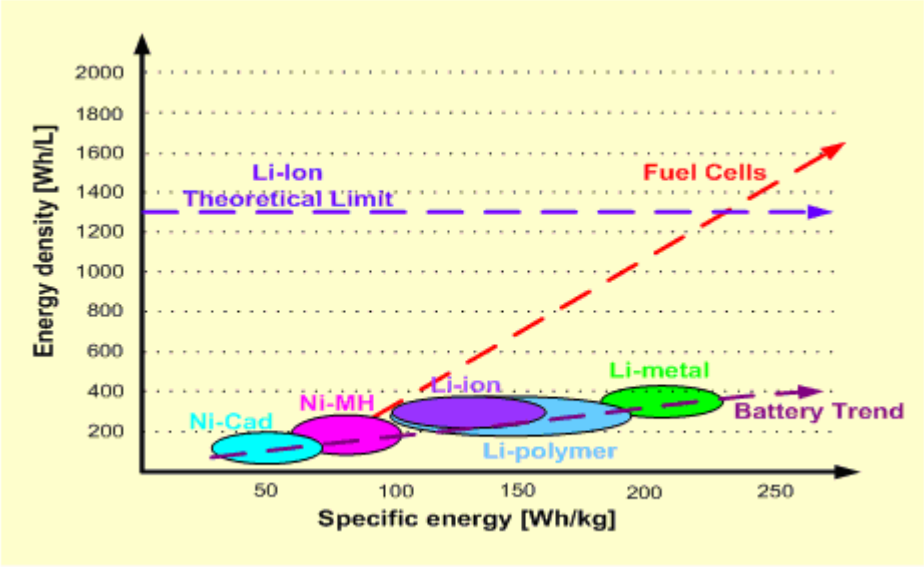

Fig. 3. Fuel cell and battery energy density vs. specific energy

The PEMFC is attractive for transportation applications, and portable power, and are a major competitor for stationary power applications less than 100 kW, particularly in combined heat and power (CHP) generation.

Since the introduction of portable electronics in the mid 1950's batteries have been their de facto source of energy. However the amount of energy that can be stored in batteries is limited and their improvement does not keep up with the energy requirements of modern devices. In contrast the energy density of fuel cells is up to 4 times higher than energy density of currently available batteries. This can be observed from Fig. 3. Furthermore, fuel cells offer an energy density even higher that the theoretical limit of their closes competitor (Li-Ion).

Another strong point of fuel cells emerges when the cost of producing 1 kW of energy is compared against batteries. As can be observed from Table II the total cost of generating 1 kW of energy using a fuel cell is up to 5.8 times lower than using existing reusable battery technologies.

Also the life span of fuel cells is up to four times longer than popular battery technologies such as Li-Ion and Ni-MH. For these reasons fuel cells are a very promising candidate for replacing batteries in portable devices in the coming years. However there are still issues that have to be resolved in order to make fuel cells popular in the marketplace.

TABLE II
COST OF GENERATING 1 KW OF ENERGY

Power source	Investment of equipment to generate 1 kW	Lifespan of equipment before major overhaul or replacement	Cost of fuel per kWh	Total cost per kWh, including maintenance and equipment replacement
Ni-MH	**$9400** Based on 7.5 V, 1000 mAh at $70/pack	**500h** based on 1 C discharge	**$0.15** for electricity	**$18.50**
Li-Ion	**$12000** Based on 7.2 V, 1200 mAh at $100/pack	**500h** based on 1 C discharge	**$0.15** for electricity	**$24.00**
Rechargeable Alkaline	**$1000** Based on 7.2 V, 1400 mAh at $6/pack	**10h** based on 1 C discharge	**$0.15** for electricity	**$95.00**
Ni-Cd	**$7000** Based on 7.2 V, 1000 mAh at $50/pack	**1500h** based on 1 C discharge	**$0.15** for electricity	**$7.50**
Fuel Cell	**$3000-7500**	**2000h**	**$0.35**	**$1.85-4.10**

1.4 Designing a hybrid source

One of the key disadvantages of the fuel cell is the long start-up time and slow dynamic response. Due to the nature of power demand in portable electronics supercapacitors seem to be very attractive for applications that require immediate power or a peak (burst) delivery of power [4].

TABLE III
SHORT AND LONG-TERM RESERVE ENERGY SOURCES FOR BACKUP POWER

Characteristic	Fuel cell with fuel	Supercapacitor	Lead-acid battery
Energy storage	Very good, depends on fuel available, fuel cells use stored energy (hydrogen)	Poor, limited to seconds of use; not a candidate for energy storage greater than 1 minute	Good, requires linear scaling; thus, large banks for large energy storage
Power delivery and acceptance/ power density	Can not accept regenerative current; provides rated power at about 50% efficiency	Very good and highly efficient; can discharge and accept high current	Reasonable power delivery; recharging is slower and must be managed
Electrical behavior	Generates energy electrochemically	Generates energy by dropping voltage and ramping current and is highly predictable	Generates energy at constant voltage and variable current
Life and maintenance	Expected life is good and steadily improving; "hot-swappable" cartridges can eliminate downtime	Very good, has many years of useful life, health monitoring simple and non-destructive	Limited life requires destructive health monitoring and maintenance over the life of the application
Operating temperature range	0^{o} to 50^{o}C; limited by cold weather below 0^{o}C	-40^{o}C to $+65^{o}$C	-20^{o}C to $+55^{o}$C
Cost-effectiveness for stationary and portable power	High value proposition in applications requiring system reliability	Cost competitive with batteries, especially where portability or reliability is required	Low initial cost, but has high maintenance cost and low reliability for critical applications
Footprint	Highly scalable from small (cell phones) to mid-sized generation plants (250kW); runtime is a function of incremental fuel storage	Highly scalable, lightweight power; very high power density; small combined with fuel cell or other energy source	Heavy weight and size; requires one-to-one scaling for more runtime; can provide power and energy
Integration potential	Can be optimized for most economical design at rated power with power buffer included	Lasts the life of application so can be intergraded into the solution; suitable partner with energy generator	Requires maintenance and replacement not fully integrated into the solution
Efficiency	50% fuel-efficient at rated power; at reduced load, efficiency varies up to 100%	Highly efficient at high loads charging or discharging-about 95%	Highly efficient at low loads-about 90%; low efficiency at high-rate charging-about 50%

Their main attribute is high power capability and long life. Supercapacitors are suited for short-term power backup requirements in the range from seconds to a few minutes,

while the primary source device provides continuous power for a longer time. Taking this into consideration the supercapacitor is an ideal device to connect in parallel with the fuel cell to form a hybrid source as shown in Fig. 4, capable of satisfying both steady-state and peak power demand [5]. They are environmentally benign and can provide a reliable source of backup power demanded by a wide variety of applications as shown in Table III.

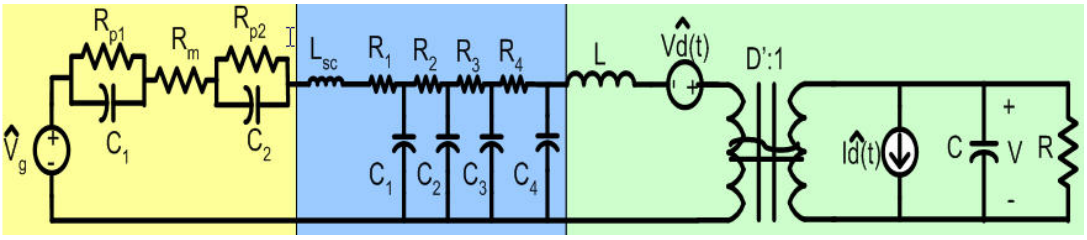

Fig. 4. Small signal representation of portable system powered by hybrid source

In-depth analysis of the benefits of combining supercapacitor and fuel cell technologies in portable electronics applications need to be investigated. The additional energy storage provided by the supercapacitor connected at the terminals of a fuel cell can contribute to: (a) increased steady state stability when powering constant power loads, (b) improved transient stability against load transients, and (c) increased fuel efficiency (i.e. reduced hydrogen consumption).

In order to design the optimum combination and realize the advantages listed above, detailed performance information in the form of a comprehensive electric circuit model is needed for each component. This information is usually unavailable from product data sheets for fuel cells as well as supercapacitors and has to be experimentally determined.

1.5 Distribution architecture for laptop computers

As mentioned in the literature [6], the "power gap" is simply the difference between the ever-increasing power demands of mobile electronics, such as notebook PCs, PDAs, and portable DVD players, and the amount of power available in today's battery technologies. The "power gap" is driven by three main trends:

1) Mobile electronics are more fully-featured than ever before, demanding more power;
2) Users are increasingly dependant on these mobile devices and are spending ever-longer periods of time without access to ac energy sources; and
3) Improvements in today's battery technology have leveled out and are unlikely to meet the ever-increasing power needs in the future.

This could be surmounted by using the low-temperature fuel cells instead the batteries. One example of a PEM fuel cell powering the laptop computer in the Power Electronics and Fuel Cell Power Systems Laboratory at Texas A&M University is shown in Fig. 5.

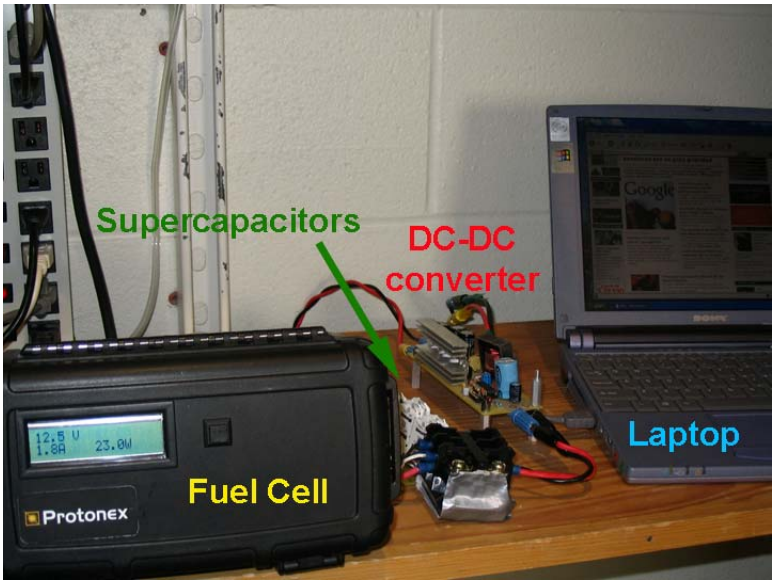

Fig. 5. Fuel cell with supercapacitors powering the laptop computer

Conventional power distribution systems in laptop computers (Fig. 6) have variable voltage levels which depend on whether the wall adapter is connected or not. Normally the bus voltage of the distribution system varies between 19.5 V when the wall adapter is connected and 14.8 V when the laptop is running from the four-cell Li-Ion battery [7]. This power distribution architecture poses a problem from the voltage regulator module (VRM) point of view. The operating voltage of these devices is normally in the range of 0.6 V to 3.3 V to increase the speed of the computer, thus a large voltage reduction is needed and therefore the power conversion efficiency is reduced. The most common method for stepping the high DC bus distribution system voltage to lower levels is by employing a non-isolated buck converter, which in this type of configuration have low efficiency and limited high switching frequency operation.

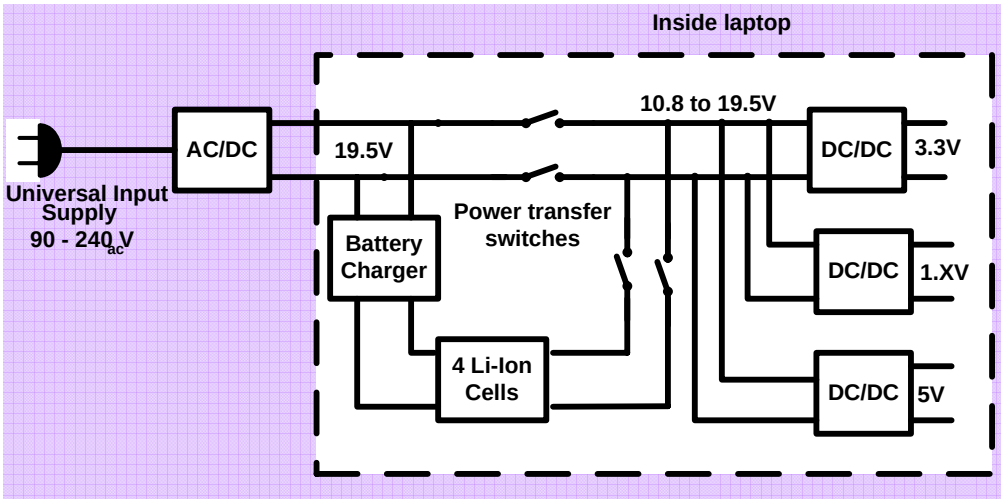

Fig. 6. Conventional laptop power management architecture

For this reason, four new power distribution architectures for fuel cell powered laptop computers are investigated in this dissertation and for each architecture, advantages/disadvantages are highlighted. Power consumption of two different laptop computers is measured for different types of loads to determine transient and steady state needs of the system. Furthermore, a hybrid multi-input bi-directional DC-DC converter for applications in fuel cell powered laptop computers has been proposed. The purpose of this multi-input converter is to suitably control the energy flow from multiple energy sources to enable all day computing. The AC-DC adapter and the fuel cell and its components are integrated with the converter in an external unit while the conventional Li-Ion battery is placed within the laptop casing.

The advantages of this architecture are:

- The Li-Ion battery charging function is transferred to the AC-DC adapter and hybrid DC-DC converter external to the laptop, thereby reducing the heat

dissipation and saving space inside the laptop. This reduction in heat dissipation and space can now accommodate more complex features and/or additional memory functions.

- Changes to AC-DC adapter are minor and do not contribute to higher cost.
- Minimized fan power and noise requirements within the laptop.
- Better overall efficiency and power savings.

1.6 Fuel cell powered UPS

As previously stated, UPS provide electric power for critical applications when the quality of the energy source, i.e. utility power, is not adequate or when it fails entirely. Conventional UPS employ batteries and/or engine generators as their main power sources. However, batteries contain toxic heavy metals such as cadmium, mercury, and lead and may cause serious environmental problems if they are discarded without special care; furthermore, these batteries suffer from life expectancy, footprint and weight issues. Similarly, engine generators have issues with startup, maintenance, noise and emission. Recently other methods of energy storage such as fuel cells, flywheels, supercapacitors and combinations of the above have come into use.

Among various kinds of fuel cells, PEM fuel cells are compact and lightweight, provide a high output power density at room temperature, as well as ease of start-up and shut down operations [8]. Additionally, fuel cells can continuously provide power as long as the reactants are supplied, which is especially useful when the duration of the power outage is uncertain.

Forming a hybrid source with supercapacitor is also very beneficial in this kind of application to compensate for fuel cells response delays and to handle overload conditions.

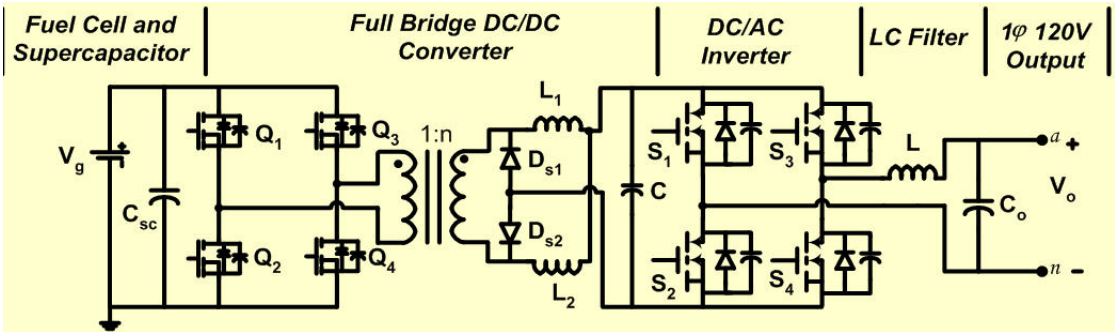

Fig. 7. Circuit topology of the proposed fuel cell powered UPS system

Motivated by the situation described above, this dissertation investigates the design considerations for a 1.5 kVA single–phase fuel cell powered passive stand-by UPS system shown in Fig. 7, with one hour of backup power employing modular (fuel cell and power converter) blocks. Interactions between the internal impedance of the fuel cell and steady state and transient stability are also considered.

1.7 High megawatt converter topologies for fuel cell based power plants

High temperature fuel cells have sufficient potential in terms of overall system efficiency and operation costs to compete with conventional power plants in the mega watt (MW) power range. Typical efficiency of conventional power plants ranges from 38% to 40%, whereas the efficiency of these fuel cells is in the range of 55-60%; consequently, fuel cell based plants have efficiency around 20% higher that conventional

systems. On the other hand the cost of generating power in a fuel cell based plant is slightly higher than in conventional systems (0.12 $/kWh) [9].

The fuel cell stack is interfaced with the AC grid, usually at the medium voltage distribution level, via a converter transformer unit [10]. Since each individual cell produces only 0.6 V, there is a maximum number of the cells that one can stack before thermal/water management issues arise. Additionally, electrostatic potential to ground within the fuel cell stack needs to be limited for safe operation. Considering the above limitations, the maximum voltage that a fuel cell stack can safely produce is around 350 V [11].

The power converter is usually constructed using a two stage approach having a DC-DC converter connected in series with a DC-AC inverter. A conventional approach is to have each fuel cell stack connected to a dedicated power electronic converter (DC-DC and DC-AC) interfaced to electric utility. There are other possible power electronics topology configurations that will be presented in this Dissertation.

The switching mode nature of the power converters generates common mode voltage with respect to ground. The presence of high frequency common mode voltage contributes to circulating ground currents which can interfere with ground fault protection system and also contribute to neutral shift and electro magnetic interference (EMI). In order to properly design the converter it is necessary to analyze common mode voltage in the converter topologies and implement one of several possible mitigation methods.

1.8 Previous work

The concept of hybrid sources is not new. There are several studies that show the applicability of such sources in high power applications such as electric vehicles and residential power generation [4, 5, 12]. Although these studies cover the complexity of fuel cell/supercapacitor integration the electric equivalent circuit models of those elements used in analysis are too simplified. There are also papers that suggest the use of hybrid sources in portable applications but no deeper analysis related to system integration and behavior is given [13-14].

Over the years many equivalent circuit models have been proposed [15-17], which vary in complexity and accuracy. Using one of these equivalent circuit models the effect of the load current in the performance of the fuel cell has been studied by Choi and Enjeti, but their work focused only on the effect of low frequency ripple.

A number of supercapacitor equivalent circuit models [18-20] have been presented. Among them the equivalent circuit model proposed in [20] is one of the few that uses the voltage dependent capacitor. However, this model is obtained using the constant current test and is not suited for transient behavior analysis. Nyquist plots for various charge states are shifted in both Re and Im directions, which implies that at least one resistance and capacitance in the model need to be charge dependent. Also the effects of capacitances increase with the increase in voltage across the supercapacitor terminals has not been analyzed.

The effect on the dynamics of the DC-DC converter due to the internal impedance of the fuel cell has not been studied so far. However analytical tools exist that can facilitate

this analysis [21]. The use of a fuel cell as a power source for DC-DC converters can be treated in a similar fashion to when a filter is connected between the power source and a DC-DC converter. An approach to analyze this problem is presented by Erickson and Maksimović in [21], and it is shown that for the case of using a filter the stability and dynamics of the system may be compromised.

One way to efficiently facilitate the use of fuel cells in portable electronics is to connect them via bi-directional DC-DC converter. The purpose of this multi-input converter is to suitably control the energy flow from multiple energy sources to enable all day operation. An example of such bi-directional converter is given in [22]. This topology reduces the number of components and simplifies the power management and the use of a microcontroller and high-speed analog PWM enhances the laptop power management system. Coremans suggested the use of fuel cells to power laptop computers and investigated the fuel cell sizing issues [23], but has not provided an in-depth analysis of the interaction between the fuel cell and the computer's power distribution system. The work presented here builds on the above concepts and introduces four distinct power distribution architectures for laptop computers powered by fuel cells.

Several approaches have been suggested for the design of the fuel cell powered UPS system [2, 24-25]. While references [2, 24, 25] mainly discuss the conceptual design, reference [26] shows the design and the actual implementation of system where the power supplied from the utility is transferred to the load via UPS. When the power outage occurs, energy stored in the battery is used to support the load. As the power

outage continues and voltage becomes lower than the pre-determined value, the signal-output unit outputs an operation signal to start the fuel cell system. The fuel cell system begins to warm up and incorporated inverter starts to generate the 100V AC power. Power transfer is performed by the synchronization-switch system. However, since this system requires a power conditioning stage for both batteries and fuel cell, the system is expensive. Further, it is disadvantageous in terms of efficiency because the power is always processed by the UPS.

The UPS system topology suggested in [24] uses a bi-directional DC-DC converter with a battery module as an active filter to compensate for the power mismatch between the fuel cell and load. However, this approach also employs the problematic batteries in the system and thus the system is not environmentally clean.

UPS system topology presented in [8] uses complicated system of two fuel cells and supercapacitor bank which are connected by three separated DC-DC converters to common isolated DC-DC converter and finally DC-AC inverter. Therefore this system suffers from limited efficiency and very complex control algorithm.

The fuel cell stack is interfaced with the AC grid, usually at the medium voltage distribution level, via a converter transformer unit [10]. Multilevel converters have been used previously to integrate several fuel cell modules for high power applications [11]. Low voltage fuel cell multi input systems were investigated in [27]. Different approaches for integrating numerous fuel cells modules for residential use and their evaluation and comparison in terms of cost, control complexity, ease of modularity and fault tolerance was given in [28]. The investigation of common mode noise in adjustable

speed drives has been carried out in the past. These systems are normally composed of a three phase rectifier cascaded with a three phase inverter. Most of the previous work focuses on reducing the common mode noise by placing passive filters at the output of the inverter [29-31] or by modifying the switching patterns in order to cancel out most of the common mode voltage [32-35]. However, little attention has been given to the common mode problem in systems used for co-generation, such as utility connected fuel cell systems. These systems are normally composed of a DC-DC converter cascaded with a DC-AC inverter; thus, there are two potential common mode sources in such systems. Therefore analysis of the common mode issue is required.

1.9 Research objective

The objective of this dissertation is to analyze and design power conditioning systems for fuel cell applications. The starting point in the analysis is to obtain an adequate equivalent circuit for the fuel cell and the supercapacitor. For this, the frequency spectroscopy method is used to acquire and systemize the element values in the equivalent circuit. This equivalent circuit is then used to analyze the effects of combining the fuel cell with supercapacitor in parallel in order to form the hybrid source. This is done both analytically and experimentally and the main focus is on determining static and dynamic stability conditions as well as hydrogen fuel consumption.

The interaction between the DC-DC converter and the fuel cell stack is studied. The benefits obtained in steady state stability of the power conditioner when powered by the hybrid source are analyzed to investigate if such configuration possesses any advantages

from the energy management point of view. For transient stability analysis, the effect of fuel cell internal impedance (extra element) along with the impedance of the supercapacitor (nonlinear) on the transfer function of the DC-DC converter is analyzed. Also, the effect on the operation of the DC-DC converter produced by the periodical release of by-products by the fuel cell was studied. The outcome of this should be design criteria for optimizing the operation of the power converter.

The design of the hybrid source and its interaction with the portable electronics is analyzed in detail with the four proposed power distribution architectures for fuel cell powered laptop computers. For each architecture advantages/disadvantages will be highlighted. Power consumption of two different laptop computers will be measured for different types of loads to determine transient and steady state needs of the system. As a result of this comparison, an optimal DC-DC converter for applications in fuel cell powered laptop computers will be proposed. The purpose of this converter is to suitably control the energy flow from multiple energy sources to enable all day computing. A design example highlighting the parameters of the fuel cell stack, Li-Ion battery, and supercapacitor modules appropriately sized for a typical load on a laptop computer will be shown. Simulation and experimental results will be used to verify the performance of the system under various input and output power conditions.

Subsequently, a fuel cell powered single-phase UPS system will be evaluated in detail. The proposed topology will provide stable power to the load when the utility is interrupted. A mathematical approach to analyze the interactions between the internal impedance of the fuel cell and the DC-DC converter closed loop control to verify steady

state and transient stability will be presented. A method to size the supercapacitor module will be incorporated to overcome the load transients such as instantaneous power fluctuations, slow dynamics of the fuel preprocessor and overload conditions.

Converting DC power produced by fuel cell to AC power suitable for utility interface can be accomplished by a variety of converter topologies and their interconnections. It is beneficial to study the various possibilities and compare them with respect to performance, component count, cost, usage of magnetics, etc. The switching mode nature of the power converters generates common mode voltage with respect to ground. The presence of high frequency common mode voltage contributes to circulating ground current which can interfere with ground fault protection system and also contribute to neutral shift and electro magnetic interference (EMI). The existence of the analysis of common mode voltages in the converter topologies is necessary for developing possible mitigation methods.

1.10 Dissertation outline

Chapter I of this dissertation presents the reasons behind the increased interest in fuel cells as an alternative power source for residential, transportation and portable applications. The basic operation principle of the fuel cell is described as well as its most relevant characteristics. Also this chapter compares fuel cells with batteries in terms of energy densities and cost. It is shown that in both aspects the fuel cell appears as a good alternative for powering portable devices and UPS systems. The characteristics of forming the hybrid source from fuel cell and supercapacitor are discussed and the

benefits are presented. More efficient distributed architecture for laptop computers is presented. In addition a fuel cell powered single-phase UPS system is discussed. Finally the research objective of this work is presented.

Chapter II focuses on the modeling of the fuel cell and supercapacitor in order to obtain an electrical equivalent circuit, and a method to extract the parameters of the equivalent circuit is presented. This chapter provides an in depth analysis of the benefits of combining supercapacitor and fuel cell technologies in portable electronics applications. This additional energy storage provided by the supercapacitor connected at the terminals of a fuel cell can contribute to: (a) increased steady state stability when powering constant power loads, (b) improved transient stability against load transients, and (c) increased fuel efficiency (i.e. reduced hydrogen consumption). Chapter II also deals with the effect of the internal impedance of the fuel cell on the dynamic characteristics of the DC-DC converter. For this the output impedance and input impedance of the fuel cell and DC-DC converter along with the transfer function of the converter are derived and analyzed. In addition this Chapter discusses the effect of the purge of the fuel cell's by products on the stability of the system.

Chapter III investigates four power distribution architectures for fuel cell powered laptop computers. As a result of the comparison, an optimal DC-DC converter for applications in fuel cell powered laptop computers is proposed. The purpose of this converter is to suitably control the energy flow from multiple energy sources to enable all day computing. A design example highlighting the parameters of the fuel cell stack, Li-Ion battery, and supercapacitor modules appropriately sized for a typical load of a

laptop computer is shown. Simulation and experimental results are used to verify the performance of the system under various input and output power conditions.

Chapter IV presents the fuel cell powered single-phase UPS system. The proposed topology is providing stable power to the load when the utility is interrupted. A mathematical approach to analyze the interactions between the internal impedance of the fuel cell and the DC-DC converter closed loop control to verify steady state and transient stability is presented. A method to size the supercapacitor module to overcome the load transients such as instantaneous power fluctuations, slow dynamics of the fuel preprocessor and overload conditions is incorporated.

Chapter V deals with the high power co-generation systems based on fuel cells and various power conditioning topologies used to interface such systems with utility. Different topologies are compared with respect to the number of components, cost, usage of magnetics, etc. In addition, the problem of common-mode noise in fuel cell systems connected to the utility is investigated. The presence of common-mode voltages and currents produces conducted electromagnetic interference that may have harmful effects on the operation of neighboring equipment as well as on the converter itself and the fuel cell. Analysis of the problem for different system configurations is done and possible solutions are presented.

Finally Chapter VI presents the general conclusions and remarks obtained from this work.

CHAPTER II

THE ROLE OF SUPERCAPACITORS IN DESIGNING FUEL CELL POWERED PORTABLE APPLICATIONS

2.1 Introduction

Due to the nature of power demand in portable electronics, supercapacitors seem to be very attractive for applications that require immediate power or a peak (burst) delivery of power [4]. Their main attribute is high power capability and long life. Supercapacitors are suited for short-term power backup requirements in the range from seconds to a few minutes, while the primary source device provides continuous power for a longer time. In this chapter primary source is a fuel cell, which is a promising energy source increasingly used in portable applications due to its environmental friendliness and high efficiency. One of the key disadvantages of the fuel cell is the long start-up time and slow dynamic response. Taking this into consideration the supercapacitor is an ideal device to connect in parallel with the fuel cell to form a hybrid source capable of satisfying both steady-state and peak power demand.

The concept of hybrid sources is not new. There are several studies that show the applicability of such sources in high power applications, such as electric vehicles and residential power generation [4, 5, 12]. Although these studies cover the complexity of fuel cell/supercapacitor integration, the electric equivalent circuit models of those elements used in analysis are too simplified. There are also papers that suggest the use of

hybrid sources in portable applications, but no deeper analysis related to system integration and behavior is given [13-14].

This chapter provides and in-depth analysis of the benefits of combining supercapacitor and fuel cell technologies in portable electronics applications. It is shown that the additional energy storage provided by the supercapacitor connected at the terminals of a fuel cell can contribute to: (a) increased steady state stability when powering constant power loads, (b) improved transient stability against load transients, and (c) increased fuel efficiency (i.e. reduced hydrogen consumption).

In order to design the optimum combination and realize the advantages listed above, detailed performance information in the form of a comprehensive electric circuit model is needed for each component. This information is usually unavailable from product data sheets for fuel cells as well as supercapacitors, and has to be experimentally determined.

2.1 Fuel cell equivalent circuit

The starting point to analyze the dynamic behavior of the fuel cell stack is to obtain an electrical equivalent circuit model. This model has to provide an accurate response for steady state as well as transients. Over the years many equivalent circuit models have been proposed [15-17], which vary in complexity and accuracy. Among them the equivalent circuit model proposed in [17] is one of the few that link the chemical reactions taking place in the fuel cell and measurable electric parameters. The chemical reactions that occur in the anode and cathode of the fuel cell are given by:

$$H_2 \rightarrow 2H^+ + 2e^- \tag{2}$$

$$O_2 + 4H^+ + 4e^- \rightarrow 2H_2O \quad (3)$$

From these equations the equivalent circuit shown in Fig. 8 can be derived and the parameters can be obtained from the redox reactions that occur in both electrodes.

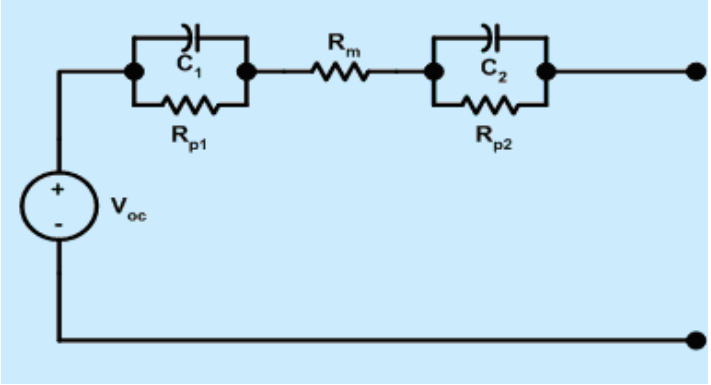

Fig. 8. Equivalent circuit for a PEM fuel cell

This equivalent circuit consists of the resistance of the membrane R_m, which is related to the electrolyte resistance. Also the model contains two parallel R-C blocks, R_{p1}-C_1 and R_{p2}-C_2, which are related to the time constant of each electrode. Specifically these time constants are related to the electron transport phenomena in the anode and cathode. These parameters can be calculated in terms of the fuel cell chemical parameters, but this information is rarely available to the power electronics designer. A straightforward method of obtaining these parameters is through frequency spectroscopy using a frequency response analyzer. The test setup for frequency spectroscopy using a frequency response analyzer is shown in Fig. 9. This method consists in drawing a DC current with a superimposed AC component from the fuel cell stack, and measuring the voltage ripple that appears in the output voltage of the stack.

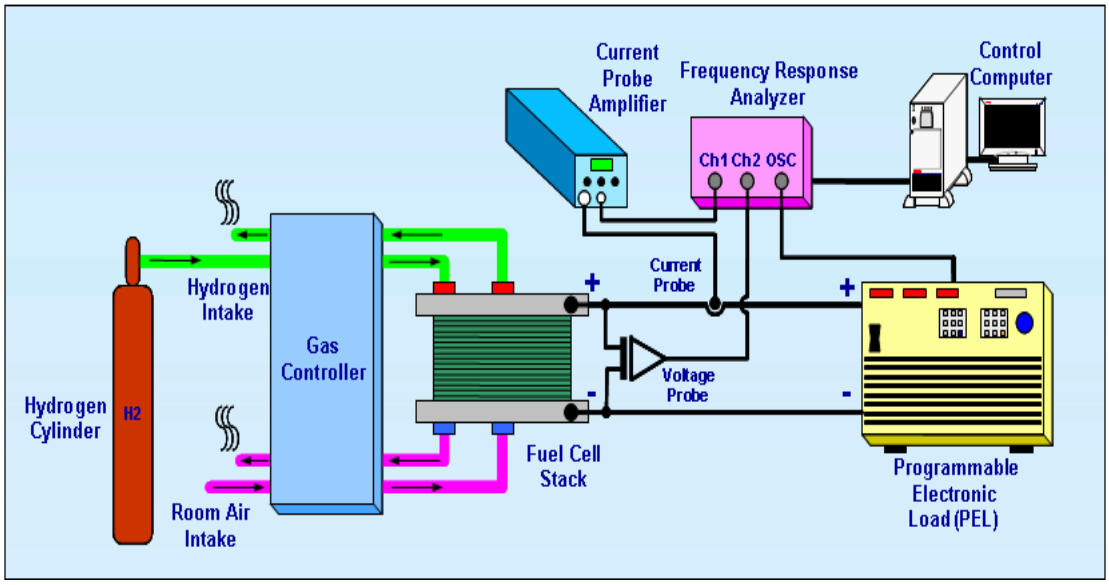

Fig. 9. Test setup for measuring the frequency respond of the PEM fuel cell

This is repeated for a wide frequency range in order to obtain the frequency response of the fuel cell. Fig. 10 shows a Nyquist plot of a 30 W fuel cell for different load conditions obtained experimentally by using this method. This figure shows the resistance and reactance of the fuel cell stack for three different load conditions and for frequencies ranging from 0.1 Hz to 10 kHz.

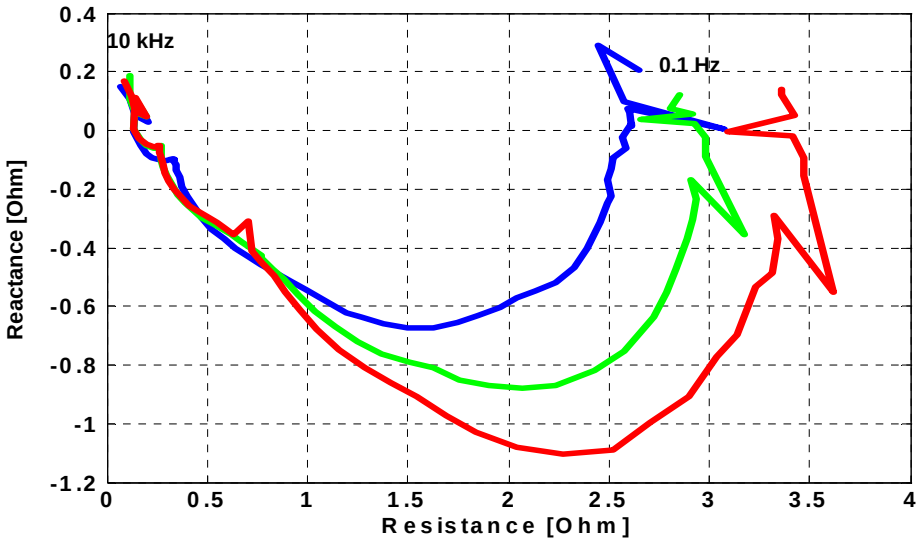

Fig. 10. Nyquist plot for a 30W fuel cell stack

From this plot it is simple to identify the main elements of the equivalent circuit model and to synthesize the parameters of the circuit model if the chemical data are not known. Each semicircle in the graph corresponds to one R-C time constant and its diameter is proportional to its resistive value while the vertex corresponds to its characteristic frequency. The value of the membrane resistance can be obtained from the graph at the point were the reactance becomes zero. The equivalent circuit parameters of the fuel cell whose response is shown in Fig. 10 are listed in Table IV.

It can be observed from Table IV and from the Nyquist plot from Fig. 10 that the fuel cell equivalent circuit parameters are a function of the output load.

TABLE IV
FUEL CELL EQUIVALENT CIRCUIT PARAMETERS

Load Condition	R_m[mΩ]	R_{p1}[mΩ]	C_1[mF]	R_{p2}[mΩ]	C_2[mF]
Light Load	100	684	0.622	1126	8.19
Half Load	100	620	0.987	1460	13.77
Full Load	100	615	1.277	1805	15.10

2.2 Nonlinear model of supercapacitor

A supercapacitor is characterized by the capacitive properties of the interface between an electronic (the electrode) and an ionic (the electrolyte) conductor, and its impedance depends on many parameters such as voltage, electrolyte concentration and temperature. Because of the porous nature of the electrodes, the capacitive interface is not localized in a plane but it spreads to the inside of the different pores [18]. As a result of this complexity a single resistor and capacitor are insufficient to model the supercapacitor. Hence, the theoretical model has to be composed of many nonlinear resistors and capacitors, leading to different time constants. A theoretical model of a supercapacitor is important for understanding the basic physical phenomena, but due to its complexity and the abundance of parameters to be identified is not very practical. For this reason, simple models are used to simplify the analysis. There are many equivalent circuit models [18-20], which vary in complexity and accuracy. Among them the equivalent circuit model proposed in [20] is one of the few that uses the voltage

dependent capacitor. However, this model is obtained using a constant current test and is not suited for transient behavior analysis.

In this chapter supercapacitor equivalent model was obtained in the same way as the fuel cell equivalent using a frequency response analyzer between 0.1 Hz to 100 kHz in order to obtain the accurate frequency response of the supercapacitor. Fig. 11 shows the impedance Nyquist plot for a 10 F/2.5 V supercapacitor (Maxwell PC-10) for different charge conditions.

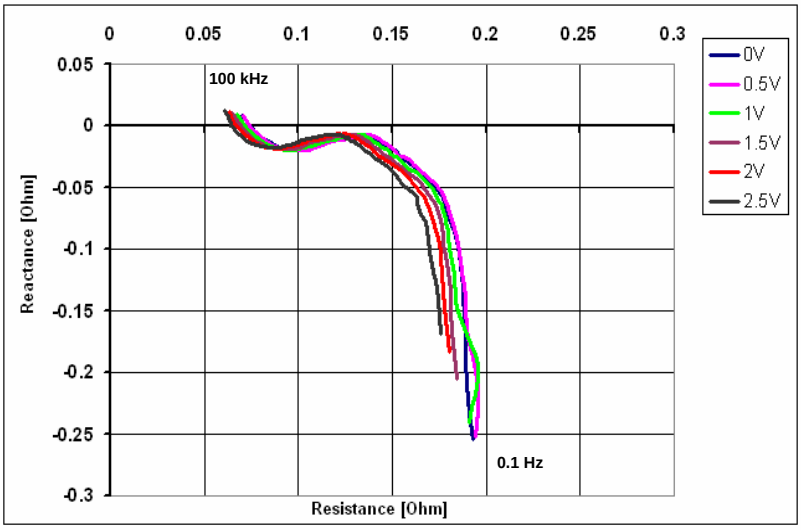

Fig. 11. Nyquist plot for a Maxwell PC10 supercapacitor

From Fig. 11 we can observe a vertical asymptote which appears at low frequency illustrating a purely capacitive behavior combined with an equivalent serial resistor. This resistance approaches its maximum value (ESR DC) at low frequencies and corresponds to the electric resistance of the terminals, electrodes, and electrolyte. For higher frequencies an oblique asymptote is found describing distributed impedance [19]. The

serial resistance decreases with the increased frequency and asymptotically reaches its minimum at high frequency (ESR HF). Finally, for frequencies higher than the resonance frequency the supercapacitor's behavior becomes inductive and can be expressed by a serial resistor ESR_HF in series with a low serial inductor. This behavior is due to the very porous nature of the electrodes and to the manufacturing process when using wound technology. Fig. 11 shows that the ESR DC and ESR for 1 kHz are in agreement with values found in manufacturer's datasheet.

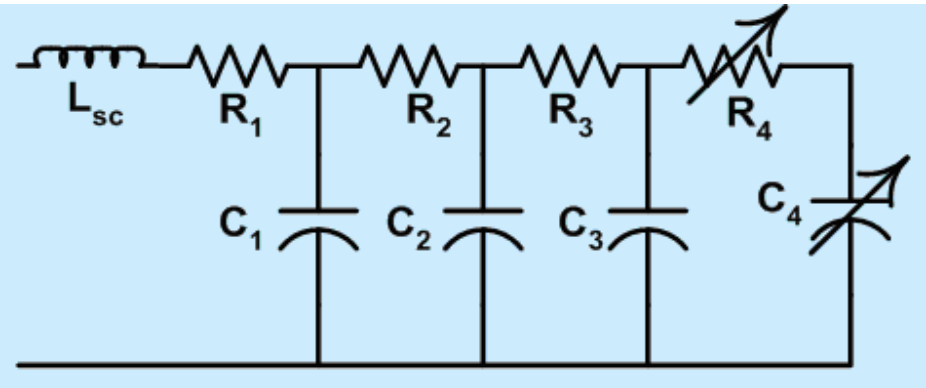

Fig. 12. Equivalent circuit for a PC10 supercapacitor

To fit the frequency response of the equivalent circuit to the experimental data a ladder R-C equivalent model was investigated and a multitude of different parameters combinations were examined. The proposed electric equivalent circuit is given in Fig. 12. The model is composed of a serial inductor and a network of four R-C branches. The unit-weighting fitting method was used to identify the combinations of parameters which most accurately fit the curves obtained from Nyquist plot.

TABLE V
SUPERCAPACITOR EQUIVALENT CIRCUIT PARAMETERS

U[V]	L_{sc}[nH]	R_1[mΩ]	C_1[μF]	R_2[mΩ]	C_2[mF]	R_3[mΩ]	C_3[F]	R_4[mΩ]	C_4[F]
0.0	17.9	75.9	358	45.9	42.2	20.9	1.64	83.5	4.50
0.5	18.3	75.7	334	47.0	37.4	20.9	1.67	84.0	4.55
1.0	19.8	72.6	347	46.3	41.7	20.2	1.78	82.0	4.94
1.5	21.2	70.1	359	45.2	45.3	19.5	2.02	78.5	5.82
2.0	22.4	67.9	379	44.1	52.0	19.6	2.27	78.0	6.53
2.5	24.3	65.1	414	43.0	65.6	20.0	2.56	80.5	6.90

Table V shows the supercapacitor equivalent circuit parameters as a function of the charge state. It can be seen that the R-C values depend on the charge state. Nyquist plots for various charge states are shifted in both Re and Im directions, which implies that at least one resistance and capacitance in the model need to be charge dependent (capacitance C_4 and resistance R_4 in Fig.12). The other parameters can have fixed values. Another trend shown in Table V is that capacitances increase with the increase in voltage across the supercapacitor terminals. This is beneficial for parallel connection with the fuel cell because it enhances the transient response of the hybrid source.

2.3 Power conditioner for portable fuel cell system

It is clear from earlier chapters of this thesis, that a fuel cell is a soft voltage source, due to the load dependent nature of its output voltage. A typical fuel cell stack output voltage experiences a 2 to 1 variation from no load to full load. Also, since each cell in a fuel cell stack has a low output voltage (0.6 V at full load), it is necessary to stack many in series to obtain a reasonable output voltage. Stacking many cells in series adds to the

complexity of the systems in terms of complicated plumbing to properly distribute the fuel and water/thermal management.

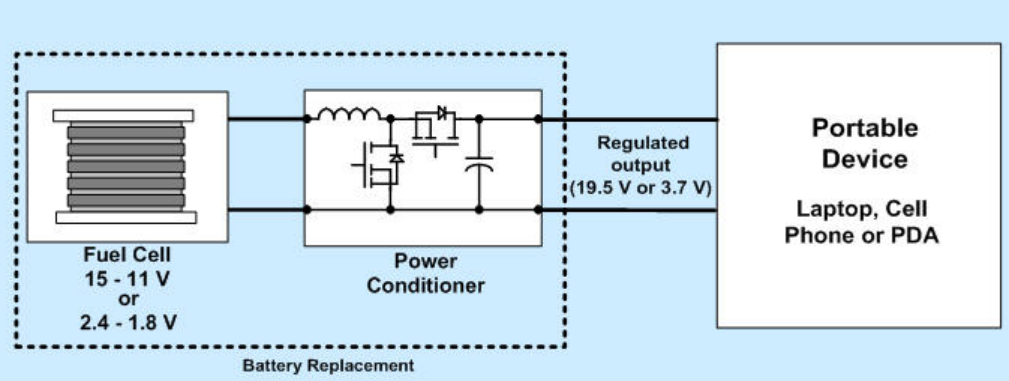

Fig. 13. Fuel cell powered portable system

Complexities arise when many cells are connected in series. Due to these limitations, a lower output voltage (3 V to 12 V) fuel cell (with fewer cells stacked in series) becomes the optimum configuration for fuel cells under 20 W. Attributable to the available lower output voltage, coupled with no-load to full-load variation of the fuel cell terminal voltage a DC-DC boost converter becomes necessary (Fig. 13). DC-DC converters can be operated either in continuous conduction mode or in discontinuous conduction mode. In the continuous conduction mode, the peak currents are lower, however, the inductor size is larger and the effect of diode reverse recovery contributes to additional switching losses. On the other hand the discontinuous conduction operation results in large peak currents, lower inductor size, zero current turn-on and the absence of reverse recovery phenomenon. In both cases the current supplied by the fuel cell contains high frequency ripple. The ripple current has an effect on the performance of the fuel cell that can be measured in terms of the temperature rise and hydrogen fuel consumption. An important

point when designing the DC-DC converter is to know the amount of ripple current that can be injected into the fuel cell without degrading its performance. From the converter point of view at light loads, it may be more efficient to operate in discontinuous conduction mode.

2.4 Fuel cell and DC-DC converter interaction

2.4.1 Steady state stability

In most practical portable applications, due to the low voltage of the fuel cell, the use of a boost type DC-DC converter is required as discussed previously. In general for a fuel cell powered DC-DC converter system to be stable in steady state the V-I characteristic of the fuel cell and the constant power locus of the DC-DC converter have to intersect at one point, which sets the operating condition of the system. If the two curves do not intersect the source is not able to meet the power demanded by the load. Fig. 14 shows the V-I characteristic (normal V-I) of the 30 W fuel cell whose parameters where obtained in section 2.1. This figure also shows the constant power locus of a 30 W boost converter for full and half load. As can be observed from Fig. 14 the constant power locus intersects the V-I of the fuel cell, and therefore the power requirements of the load are met.

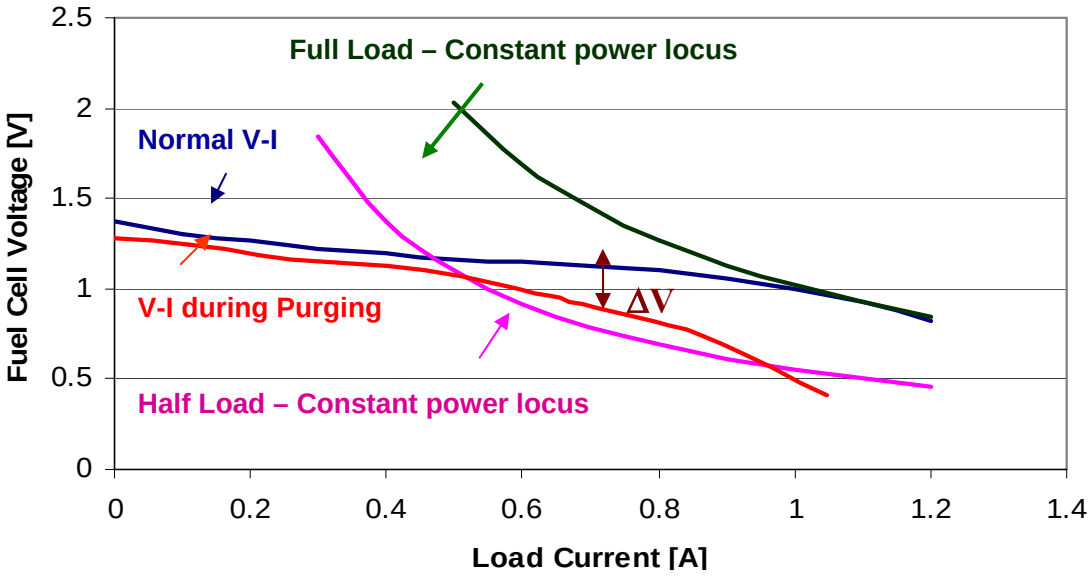

Fig. 14. Fuel cell V-I characteristic and load constant power locus

For low power applications, 150 W and below, dead ended PEM fuel cells are normally used. In this particular kind of fuel cell, hydrogen enters the stack at the anode, and there is a solenoid valve located at the cathode which opens at regular intervals to release the products of the chemical reaction. The opening of the valve is referred to as purging. During the purging interval the voltage produced by the fuel cell drops due to the reduction in internal pressure. The magnitude of this voltage drop is a characteristic of the fuel cell, and it is a function of the load current, fuel cell parameters, and the duration of the purging period. Figure 15 shows the voltage profile of the 30 W stack during a purge.

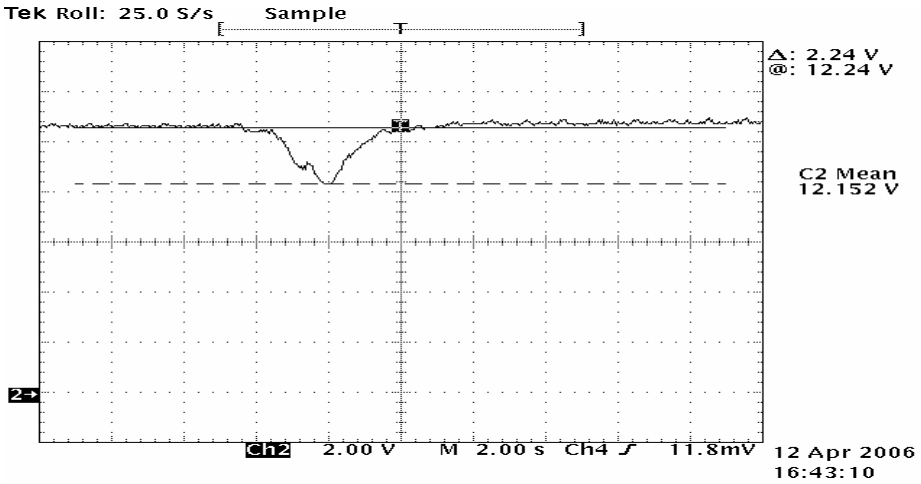

Fig. 15. Fuel cell voltage during the purging interval for a 30W stack supplying 1.73A

It can be seen from Fig. 15 that for this particular fuel cell the duration of the purging interval is 2.5 s and the voltage drops by 2.24 V for a load current of 1.73 A. Figure 14 shows the V-I characteristic measured for the 30 W fuel cell during the purge interval. As can be observed from Fig. 14 during the purge the fuel cell voltage drops by a quantity ΔV. In order to maintain the output power constant the DC-DC converter will require a higher current, which will produce an additional voltage drop at the fuel cell terminals. This in turn will produce an additional increase in the converter current. In other words a positive feedback takes place, which finally results in instability.

To avoid this problem, two approaches can be taken. One of them is to control the boost converter in order to limit its output load during the purging interval. But this approach has the disadvantage of degrading the total output power of the system. An alternative approach it to supply the power difference produced during the purge by using a supercapacitor. The size of the capacitor in our experimental setup was

calculated in terms of the energy that the capacitor has to supply during the duration of the purge, and can be calculated from:

$$C = \frac{2\Delta P_o t_p}{\Delta V^2}, \tag{4}$$

where ΔP_o is the difference between the power that the fuel cell can supply during the purge and the power required by the load, t_p is the duration of the purge and ΔV is the voltage drop in the capacitor. In the case of the 30 W fuel cell under study the duration of the purge is 2.5 seconds, and the voltage drops to 0.75 p.u at full load. In this case the supercapacitor needs to supply 25% of the output load during 2.5 seconds. If a maximum voltage drop of 2 V is allowed during the purge from (4) the required capacitance is 10 F.

2.4.2 Transient stability

The interaction of the DC-DC converter with the stand-alone fuel cell as well as with the hybrid source has been analyzed in order to investigate dynamic response as well as the stability of the overall system. The power converter controller is generally designed to provide appropriate amount of phase and magnitude margins in order to meet the stability criteria. But once the fuel cell is connected to the input terminals of the power converter, as shown in Fig. 16 the output impedance of the fuel cell alters system behavior.

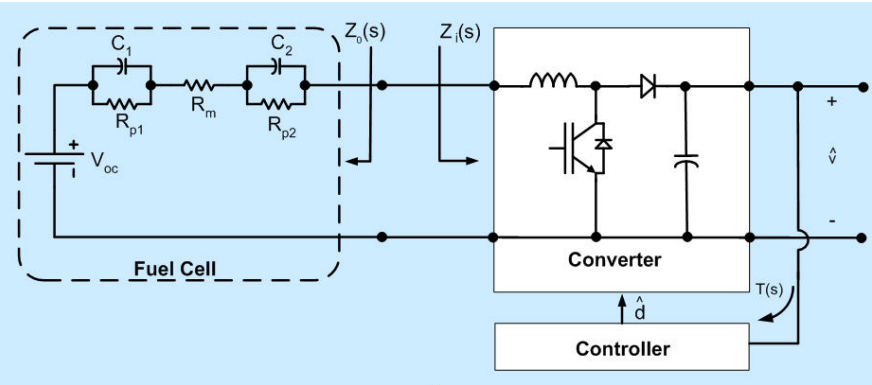

Fig. 16. Fuel cell DC-DC converter system

If the internal impedance of the fuel cell is considered, Middlebrook's extra element theorem [21] can be used to analyze the effect of the fuel cell onto the dynamics of the converter. Application of the theorem results in the system shown in Fig. 17, where the fuel cell output impedance is modeled as an extra element in the system.

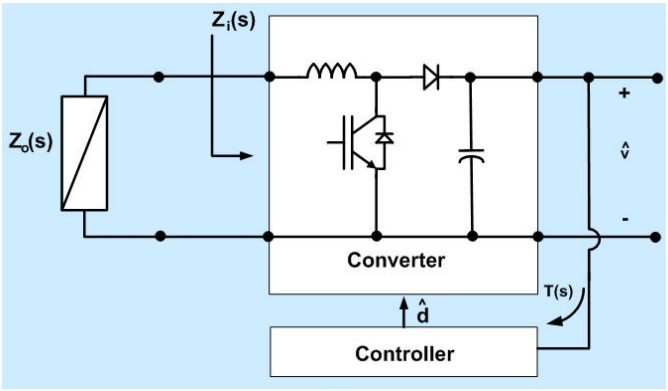

Fig. 17. Modeling of the fuel cell impedance effect

It can be found that the control to output transfer function of the converter when the fuel cell is considered is given by (4)

$$G_{vd}(s) = \left(G_{vd}(s)\big|_{Z_o=0} \right) \frac{1 + \frac{Z_o(s)}{Z_N(s)}}{1 + \frac{Z_o(s)}{Z_D(s)}} \tag{5}$$

Where $G_{vd}(s)\big|_{Z_o=0}$ is the converter transfer function when the supply is an ideal voltage source, $Z_N(s)$ is the input impedance of the converter under the condition that the feedback controller operates ideally, $Z_D(s)$ is the input impedance of the converter under the assumption that $\hat{d}(s) = 0$, and $Z_o(s)$ is the output impedance of the fuel cell. It is obvious that the transfer function of the converter is modified by the output impedance of the fuel cell. Moreover, it can be shown that by connecting the fuel cell to the DC-DC converter all the transfer functions are modified including the control-to-output and the line-to-output, and the converter output impedance. In order to minimize the effect in the dynamics of the converter it has been shown [21] that the following impedance inequalities have to be met.

$$\|Z_o\| << \|Z_N\| \tag{6}$$

$$\|Z_o\| << \|Z_D\| \tag{7}$$

Similarly the converter output impedance of the converter is not affected if

$$\|Z_o\| << \|Z_e\| \tag{8}$$

$$\|Z_o\| << \|Z_D\| \tag{9}$$

where Z_e is the converter input impedance when its output is shorted. A typical fuel cell power converter system is shown in Fig.13. Due to the low output voltage of the fuel cell the converter of choice for this kind of applications is a boost converter. The small signal

model for a boost converter is shown in Fig. 18a. If the fuel cell equivalent circuit model is added to the circuit the small signal equivalent shown in Fig. 18b is obtained. From Fig. 18a the converter transfer function when the supply is an ideal voltage source $G_{vd}(s)$, and input impedances of the system, $Z_N(s)$ and $Z_D(s)$ are given by:

$$G_{vd}(s) = G_{do}\frac{1-\frac{s}{\omega_z}}{1+\frac{s}{Q\omega_o}+\frac{s^2}{\omega_o^2}}$$
$$G_{do} = \frac{V_o}{1-D},\ Q = R(1-D)\sqrt{\frac{C}{L}} \qquad (10)$$
$$\omega_z = \frac{R(1-D)}{L},\ \omega_o = \frac{1-D}{\sqrt{LC}}$$

$$Z_N(s) = -(1-D)^2 R\left(1-\frac{sL}{(1-D)^2 R}\right) \qquad (11)$$

$$Z_D(s) = (1-D)^2 R\frac{1+s\frac{L}{(1-D)^2 R}+s^2\frac{LC}{(1-D)^2}}{1+sRC} \qquad (12)$$

where V_o is nominal output voltage, D is the converter duty cycle, L and C are the inductor and capacitor of the converter, and R is a load resistance.

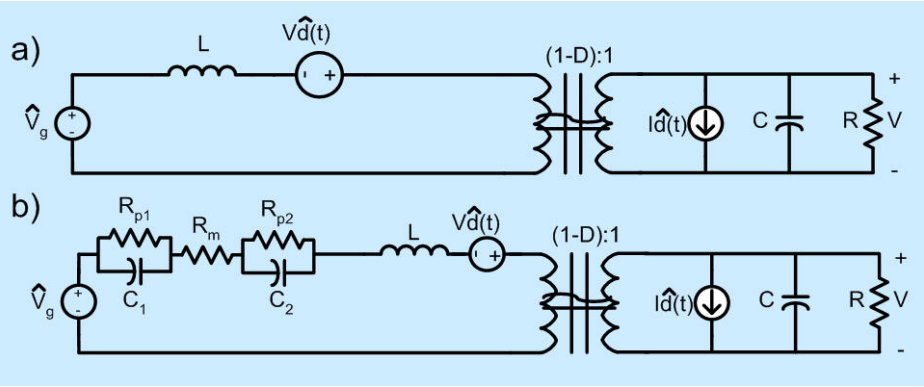

Fig. 18. a) Small-signal models for boost converter. b) When connected to a fuel cell

From the fuel cell equivalent circuit discussed in Section 2.1 its output impedance is given by (13).

$$Z_o = \frac{s^2(R_m R_{p1} R_{p2} C_1 C_2) + s(R_m(R_{p1}C_1 + R_{p2}C_2) + R_{p1}R_{p2}(C_1 + C_2)) + R_m + R_{p1} + R_{p2}}{s^2(R_{p1}R_{p2}C_1C_2) + s(R_{p1}C_1 + R_{p2}C_2) + 1} \quad (13)$$

By plotting the magnitudes of the converter input impedances and fuel cell output impedance (11-13) for the fuel cell parameters shown in Table IV and for a 30 W boost converter designed to operate in continuous conduction with a 250 μH inductance and 250 μF output capacitance, the graph in Fig. 19 is obtained.

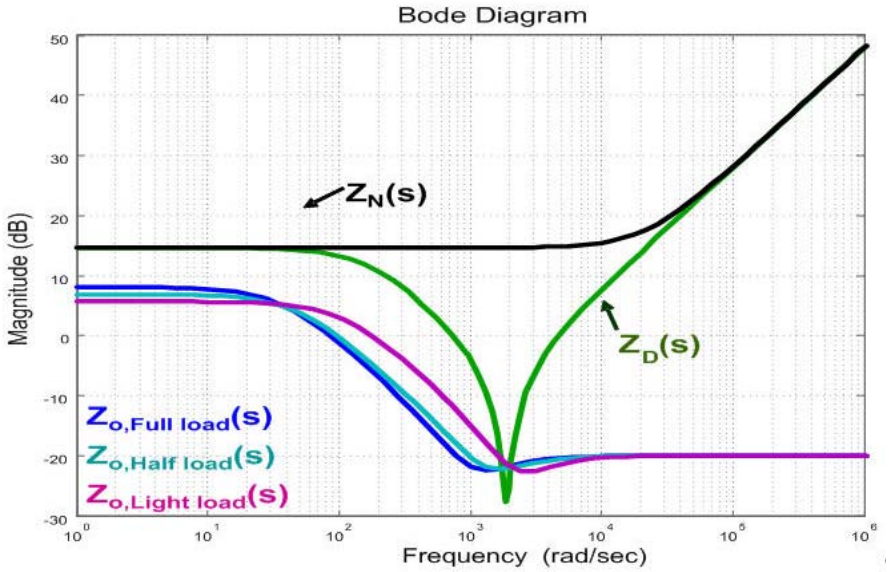

Fig. 19. Impedances for fuel cell boost converter system

It can be seen from Fig. 19 that the magnitudes of the converter input impedance and the fuel cell output impedance are of comparable magnitudes. From (6) in order to minimize the effect of the fuel cell on the dynamics of the system the impedance

inequalities (6)-(7) have to be met. Normally the “much greater than” condition (<<) can be considered to be true if there exist at least 6 dB of difference between the magnitude of the converter and fuel cell impedances. As can be seen from Fig. 19 the inequalities may not be satisfied for low frequencies and at the resonant frequency of the boost inductor and output capacitor. Therefore it is important to verify the stability of the system as part of the system design. At low frequencies the inequalities (6)-(7) are met as long as the DC-DC converter input power is less or equal to the rated power of the fuel cell. On the other hand to meet the design criteria at the resonant frequency of the input impedance of the boost converter either the converter or the fuel cell impedances have to be modified.

A method of modifying the output impedance of the fuel cell is by connecting a supercapacitor in parallel to form a hybrid source. A small signal equivalent model of the portable system powered by hybrid source is formed by combining the equivalent model of the fuel cell and equivalent model of the supercapacitor derived in Section 2.2, and is shown in Fig. 20. The effect of the parallel capacitor is displacement of the output impedance of the fuel cell to the left as shown in Fig. 21, which increases the distance between the output impedance of the fuel cell and the input impedance of the boost converter. This helps satisfying the impedance inequalities. The modified output impedance of the hybrid source system Z_{o_HS} can be calculated by solving ladder R-C form:

$$Z_{o\_HS} = \cfrac{1}{sC_4 + \cfrac{1}{R_4 + \cfrac{1}{sC_3 + \cfrac{1}{R_3 + \cfrac{1}{sC_2 + \cfrac{1}{R_2 + \cfrac{1}{sC_1 + \cfrac{1}{R_1 + sL_{sc} + Z_o}}}}}}}} \tag{14}$$

where C_1-C_4, R_1-R_4 and L_{sc} are parameters of the supercapacitor and Zo is the output impedance of the fuel cell (13).

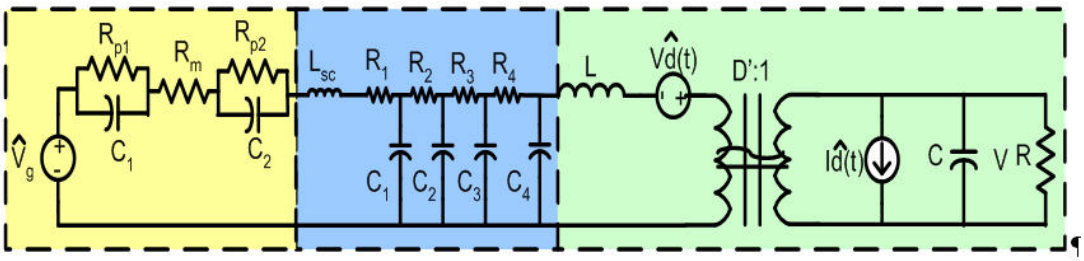

Fig. 20. Small signal representation of portable system powered by hybrid source

Figure 21 shows the fuel cell output impedance for the full load condition (13), and DC-DC input impedance frequency responses for six PC-10 supercapacitors connected in series in order to match fuel cell operating voltage range. The supercapacitor charge state is calculated assuming that the nominal fuel cell voltage (full load condition) is divided equally between the supercapacitors, and the parameters are given in Table V. As can be observed from this figure the capacitance needed to modify the output impedance of the fuel cell in order to satisfy (6)-(9) is relatively small. In general the amount of

capacitance calculated to compensate for the voltage drop during the purging period is sufficient to ensure that the impedance inequalities are met.

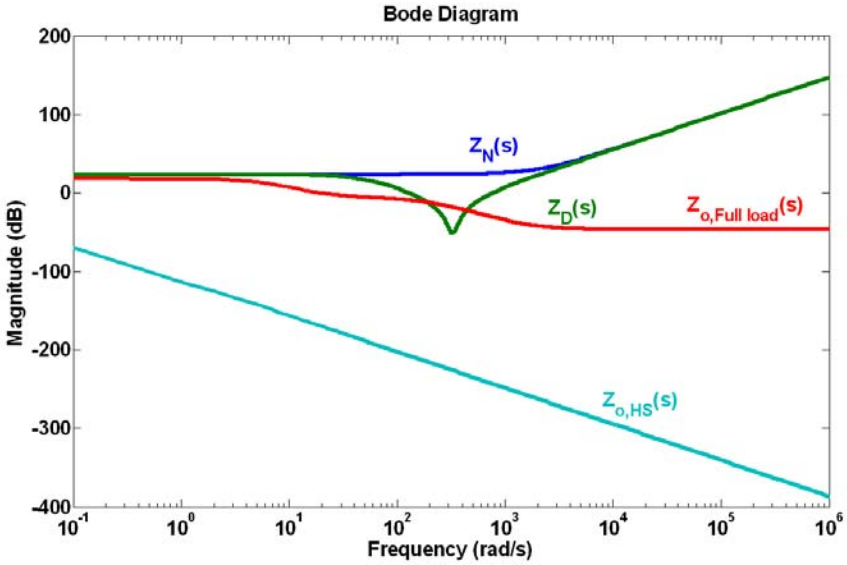

Fig. 21. Effect of forming the hybrid source

2.4.3 Experimental results

In order to verify the theoretical analysis experimental measurements were made. Figure 22a shows the response of the system for the load step from zero to full load when the fuel cell alone is used, while Fig. 22b shows the response of the system once the 10F supercapacitor bank is connected across the terminals of the fuel cell. The output voltage of the fuel cell varies from 16 V for no load to 10 V for full load and the boost converter is designed to maintain a 19.5 V output voltage and it is rated for 30 W, which is suitable for powering a laptop computer. The internal parameters of the fuel cell are shown in Table IV, while parameters for supercapacitor are shown in Table V. As can be

seen from Fig. 22a both input and output voltages oscillate widely until the load is removed, while Fig. 22b shows no oscillation in either input or output voltage.

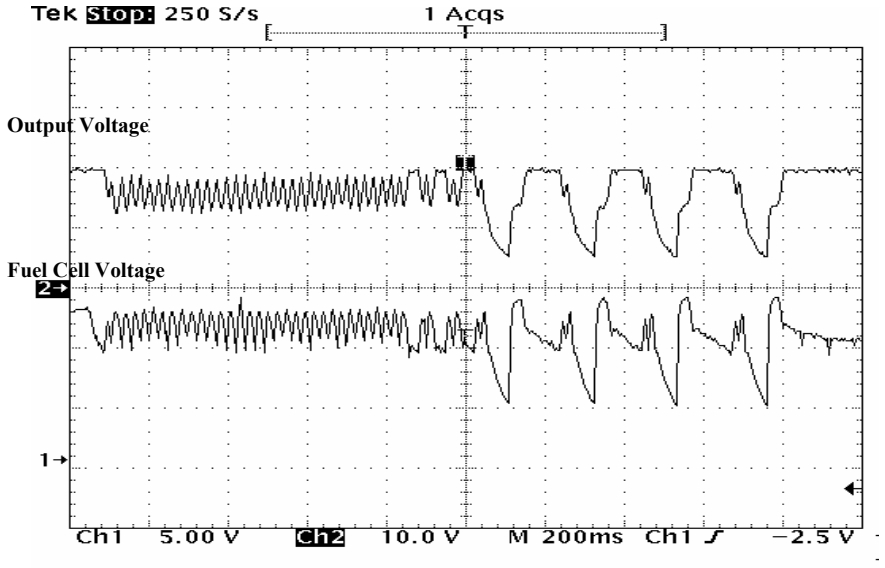

a

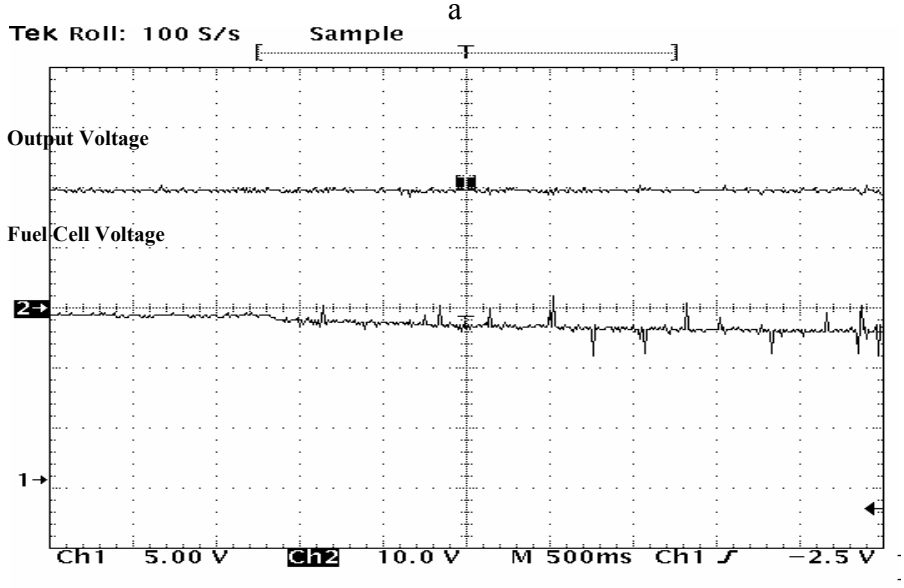

b

Fig. 22. Dynamic behavior of a) Stand-alone fuel cell system b) Hybrid source system

Also in Fig. 22b, the input voltage decreases slowly until the new steady state is reached. A conclusion can be drawn that the experimental comparison between the system with the stand-alone fuel cell and the system with the hybrid source showed that the latter had superior performance.

2.5 Influence of supercapacitor on hydrogen fuel consumption

In order to further investigate the benefits of using the hybrid source with the supercapacitor in parallel with the fuel cell hydrogen flow of two PEM fuel cells was measured. It is well known that current ripple injected from the DC-DC converter into the fuel cell has a degrading effect on its performance. In order to investigate the possible benefit of inclusion of the supercapacitor experimental measurements on the 20 W and 30 W fuel cell stacks were made with high frequency ripple currents. The measurements consisted of loading the stand-alone fuel cell and hybrid source with a square wave load current with 50% duty cycle. The peak value of the load currents was set to two times the nominal currents of the fuel cell stacks so that their mean values equaled their nominal values. The frequency of the load currents was varied from 10 Hz to 200 kHz, and the hydrogen consumption of the stacks was recorded.

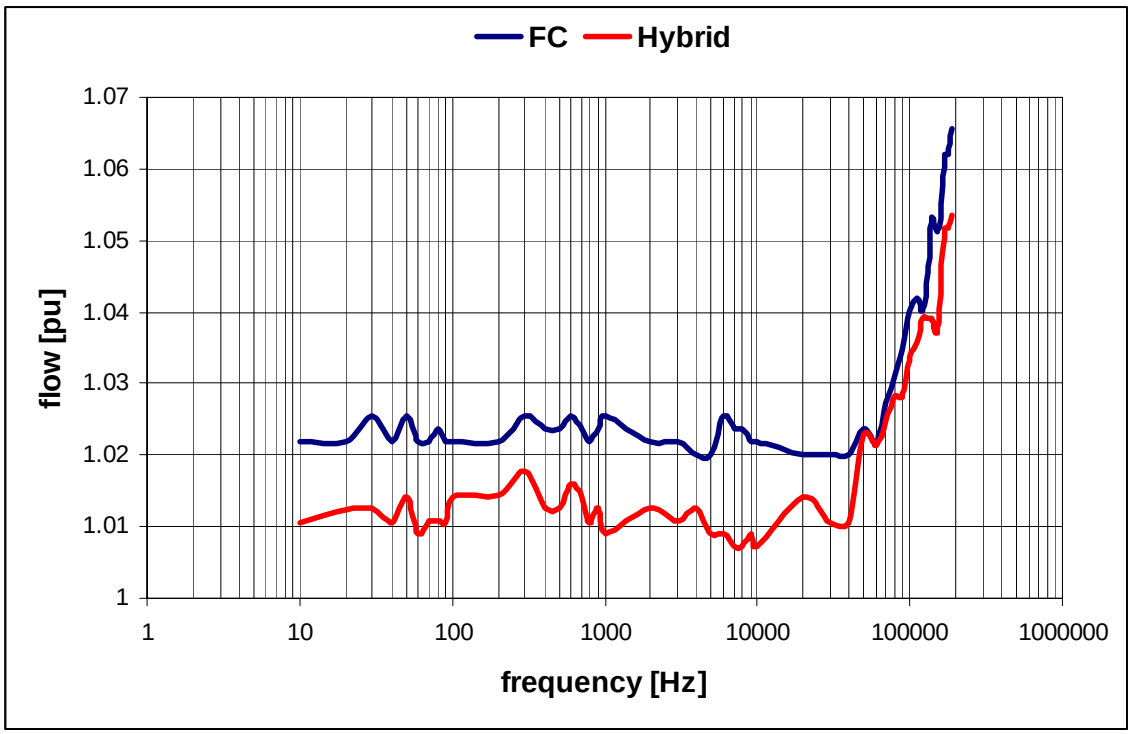

a

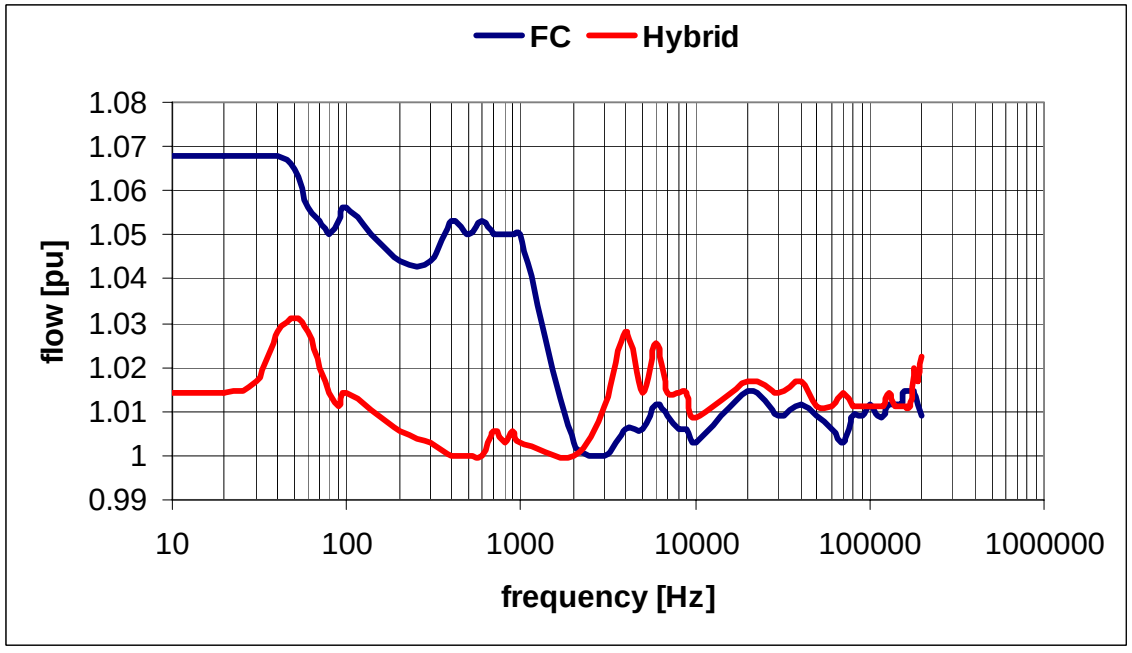

b

Fig. 23. Hydrogen flow for the a) 20W and b) 30W fuel cells as function of load current ripple frequency with hybrid configuration or working alone

Figure 23a and Fig. 23b, show the hydrogen consumption as a function of the load current frequencies measured from the 20 W and 30 W PEM fuel cells and the hybrid sources constructed with them. The hybrid sources for 20 W and 30 W fuel cells were made using the seven PC-10 and six PC-10 supercapacitors connected in series in order to match the open circuit voltage of 17 V and 16 V respectfully. It can be observed from Fig. 23 that the hydrogen consumption decreases for of the hybrid configuration. The magnitude of the decrease in the hydrogen consumption is a function of the frequency of the ripple current. The fuel cell voltage does not experience wide variation due to the high frequency ripple current in hybrid configuration, which directly transfers to the smaller demand on hydrogen flow. This proves that fuel cells in hybrid configuration can work longer with the same the amount of hydrogen then the fuel cells operating alone.

2.6 Conclusion

In this chapter, the role of a supercapacitor in the design of fuel cell powered systems is discussed. It is shown that the additional energy storage provided by the supercapacitor connected at the terminals of a fuel cell can contribute to: (a) increased steady state stability when powering constant power loads, (b) improved transient stability against load transients, and (c) increased fuel efficiency (i.e. reduced hydrogen consumption). Further, it is shown that the electric equivalent circuit of a fuel cell is essential to establishing a design procedure to size the required supercapacitor. The development of the equivalent circuit model for fuel cells and supercapacitors using frequency analysis is presented and results discussed. Additionally, the benefits obtained

in steady state stability of the power conditioner when powered by the hybrid source are analyzed and it is shown that such configuration possesses several advantages from the energy management point of view. For transient stability analysis, the effect of fuel cell internal impedance (extra element) along with the impedance of the supercapacitor (nonlinear) on the transfer function of the DC-DC converter is analyzed. Finally, experimental evaluation and comparison of fuel consumption in the conventional and hybrid systems is performed, showing that the hybrid source has improved fuel utilization.

From these results it is shown that the proposed approach permits the optimization of energy management and improvement of the dynamic performance of the power conditioner. Experimental results obtained on 20 W and 30 W PEM fuel cell/boost converter systems demonstrate the validity of the proposed approach.

CHAPTER III

A HYBRID DC-DC CONVERTER FOR FUEL CELL POWERED LAPTOP COMPUTERS

3.1 Introduction

Portable electronic technologies such as PDAs, notebook computers, and cell phones have fueled a need for new, high-energy, small volume power supplies for both military and commercial markets. Several of these devices are currently limited to battery technologies, which, despite recent advances, are insufficient to provide the long-term power. The resulting "power gap" [6] is simply the difference between the ever-increasing power demands of mobile electronics and the amount of power available in today's battery technologies. The "power gap" is driven by three main trends:

1. Mobile electronics are more fully-featured than ever before, demanding more power.
2. Users are increasingly dependant on these mobile devices and are spending longer periods of time without access to AC energy sources.
3. Improvements in today's battery technology have leveled out and are unlikely to meet the increasing power needs in the future.

The fuel cells are potentially good candidates to replace batteries as power sources for the next generation of laptop computers thanks to the high energy content of their fuels. Two types of low-temperature fuel cells are primary candidates for portable applications: Direct Methanol Fuel Cell (DMFC) and the Proton Exchange Membrane Fuel Cell

(PEMFC). In a fuel cell, power is continuous while fuel and oxygen are supplied, similar to the gasoline/engine system which is used to power a car. The engine is purchased once (with the car) and gasoline is replenished as needed for continuous operation. The same is true in small fuel cell systems, which are expected to someday help power portable electronic products such as notebook computers. Fuel capsules can be exchanged out quickly without the need to wait for recharging. Users could carry spare fuel cartridges, not extra batteries, to extend operation and enhance convenience. Fuel cells, especially low-temperature types such as DMFC and PEMFC, are potentially good candidates to replace batteries as power sources for the next generation of portable applications thanks to the high energy content of their fuels. An example, Toshiba Corporation's prototype of a small form factor DMFC for portable PCs [7] is shown in Fig. 24.

Fig. 24. Toshiba's DMFC for a laptop

The DMFC is a fuel cell which uses methanol as a fuel. Methanol is a particularly economical, commercially available, source of energy for small fuel cells. It comes in liquid form, can be easily transported and stored, and has a high energy density. However, there are some problems associated with this type of fuel cell. First of all, it

requires a lot of expensive platinum catalyst material (5 to 20 times more expensive than for the PEMFC) to ensure reaction, and secondly, its power density (i.e. the power achieved per unit membrane surface) is relatively low compared to PEM systems that use hydrogen. The DMFC is not as efficient as the PEM-cell (only 25% compared to 50%). In addition, methanol needs to be diluted with water into 3% solution to avoid so called crossover losses. This, however, presents a disadvantage in that it reduces the fuel cell energy density and requires additional and unnecessary water ballast to be carried around with the system. Some types of DMFCs get around this problem by using water generated by the chemical reaction in the cell to dilute the methanol.

The PEM fuel cell is fuelled by pure hydrogen. Hydrogen reacts with oxygen taken from the air or oxygen tank, producing electricity, heat and water. The PEM configuration combines good efficiency (in the order of 50%) and excellent weight characteristics of the fuel (hydrogen has a very high specific energy: 120 MJ/kg in comparison with e.g. gasoline: 50 MJ/kg). Most problematic task associated with PEMs is to store sufficient quantities of hydrogen into small volumes, due to their low energy per-volume (10.8 kJ/m^3). To minimize the volume, hydrogen can be stored in pressure vessels or metal-hydrate cartridges. A trade-off is that this reduces the weight advantages because of the relatively high weight of the storage medium (steel, or aluminum, or composites).

Several electronics manufacturers are now seeking to combine the advantages of methanol as a fuel with the high power density of PEM fuel cells by employing systems equipped with micro-reformers that create hydrogen from methanol [36]. The problem is

that developers are facing challenges yet to be solved with regard to the miniaturization of a complete system consisting of a reformer that produces hydrogen and the fuel cell itself, coupled with the challenge of ensuring reliable operation over long periods of time.

3.2 The power consumption of a laptop computer

The power consumption of a laptop computer typically ranges between 25 W and 50 W depending on its performance. Table VI shows the variation of power consumption for various tasks. Fig. 25 shows the time domain variation of power consumption when idle and while saving a Microsoft (MS) Word document. In general batteries for laptops have a voltage of 14.8 V and have a capacity ranging from 3000 mAh to 4000 mAh depending on device performance and functionality. All-day computing for an ultra-light notebook PC, typically requires about 120 Watt-hours (Wh) of energy for 8 hours of operation. A fuel cell system designed for this application needs to be flexible and able to work with the onboard battery and AC wall adapter unit.

TABLE VI
LAPTOP POWER CONSUMPTION

Task	Power Consumption [W]
0% CPU Bandwidth (backlight off)	8.23
0% CPU Bandwidth (backlight on)	13.13
100% CPU Bandwidth	30.01
Write to Hard Drive	18.2
Read from Hard Drive	18.4
Memory Read/Write	21.4
CD Playback	19.2

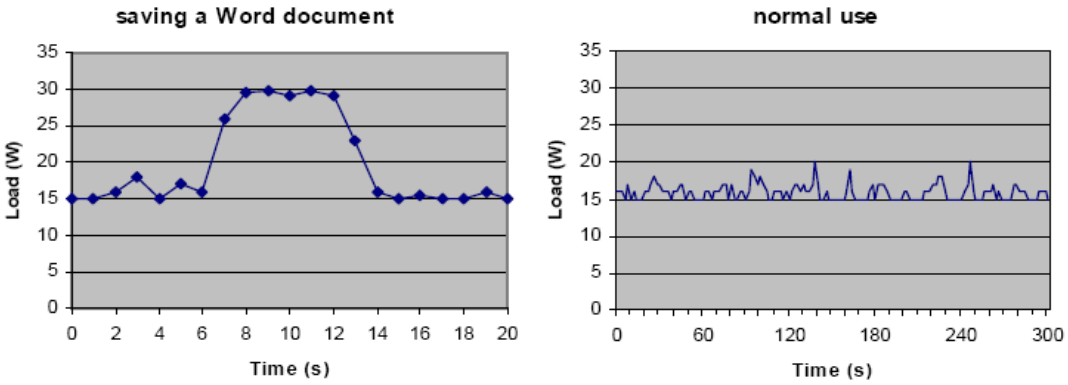

Fig. 25. Measured load on a Toshiba laptop computer [23]

3.3 Conventional power distribution architecture of a laptop computer

Conventional power distribution systems in laptop computers (Fig. 26) have a variable voltage level which depends on whether the wall adaptor is connected or not [22]. Normally the bus voltage of the distribution system varies between 19.5 V when the wall adaptor is connected and 14.8 V when the laptop is running from the four-cell Li-Ion battery. The voltage of a single battery itself is not constant, and varies from 2.7 V minimum to 4.2 V maximum. This creates the battery bank voltage range from 10.8 V to 16.8 V if four cells are used. This power distribution architecture poses a problem from the voltage regulator module (VRM) point of view. VRMs are connected to the distribution bus and step down the voltage to supply different devices such as the processor, memory, etc. The operating voltage of these devices is normally in the range of 0.6 to 3.3 V to increase the speed of the computer, thus a large voltage reduction is needed and therefore the power conversion efficiency is reduced. The most common method for stepping the high DC bus distribution system voltage to lower levels is by employing a non-isolated buck converter. In this type of configuration, the buck

converter's duty cycle is very small, which compromises the efficiency and high frequency operation.

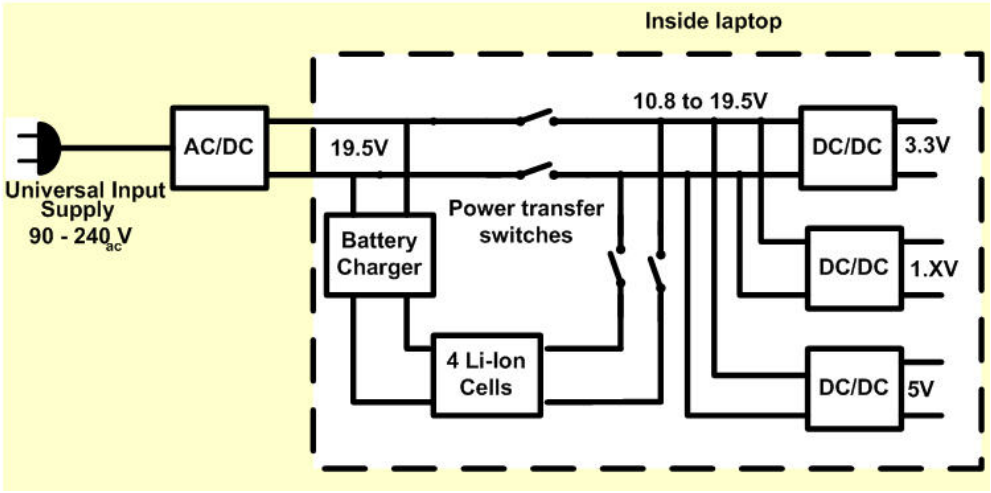

Fig. 26. Conventional laptop power management architecture

In the existing laptop power system architecture shown in Fig. 26 multiple power path switches are used to select the input source. When AC input is available, the horizontal switches are on, connecting the AC-DC converter with internal DC-DC power supplies. When the AC input is lost, vertical switches connect the battery bank with DC bus distribution system and the energy from the battery is used for operation of the laptop.

3.4 Power distribution architectures for laptop computers powered by a fuel cell

No matter what kind of fuel cell is used, in the proposed distribution systems for portable PCs inclusion of the fuel cell as an added energy source increases the run time of the laptop and can potentially decrease the size of the on-board Li-Ion battery. In conventional systems, multiple series-connected Li-Ion cells are used to provide efficient

energy storage. Using fewer batteries in series may reduce the voltage of the battery bank, but it increases the current requirements of the Li-Ion batteries. This higher current decreases the efficiency of energy conversion during charging and, more importantly, discharging (as a result of internal battery and contact resistance). In our system, the fuel cell as an additional power source decreases the power requirement on the battery bank, so the size of the battery can be reduced without above mentioned consequences.

Four possible power distribution system architectures are discussed in this chapter. The first three of the approaches discuss variations of a hybrid system consisting of an AC-DC adapter, fuel cell and Li-Ion battery. In these systems the fuel cell is rated to power the normal functions of the laptop and the AC-DC adapter is sized to power the laptop and simultaneously charge the battery. In the fourth proposal, the Li-Ion battery is eliminated and the AC-DC adapter and the fuel cell form one unit.

3.4.1 Proposed power distribution architecture # 1

This power distribution architecture shown in Fig. 27 is almost identical to the conventional system (Fig. 26) with an added difference of an AC-DC/fuel cell hybrid external adapter. When AC power is available, the DC bus distribution system is regulated at 19.5 V and power is supplied to the laptop. In addition, the AC-DC adapter has sufficient VA rating to also simultaneously charge the battery as well. However, when AC power is unavailable/disconnected, fuel cell operation is enabled and the DC bus distribution system is regulated at 19.5 V. The fuel cell is rated to supply the laptop power and is interfaced to the DC bus distribution system using the synchronous boost

converter (Fig. 28) to regulate the output voltage to 19.5 V. This is necessary because of the fluctuating output voltage of the fuel cell. This converter converts energy only in one direction, from the fuel cell to the DC bus distribution system. The fuel cell stack can be combined with a parallel connected supercapacitor module to improve its dynamic response in the event of sudden load current changes. From the aspect of control, battery charger operates as a voltage controlled current source. After the battery bank voltage matches the reference voltage, the controller maintains the voltage constant and decreases the current toward zero.

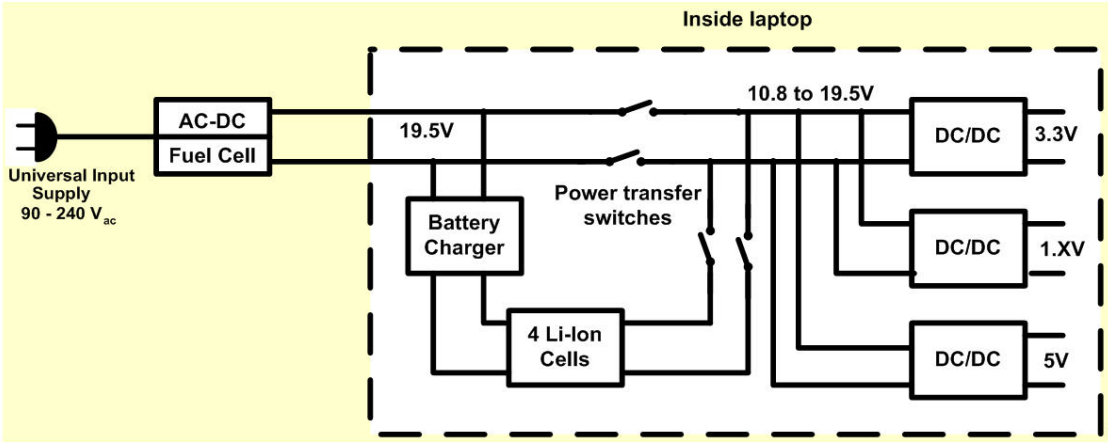

Fig. 27. Power distribution architecture #1with an external fuel cell

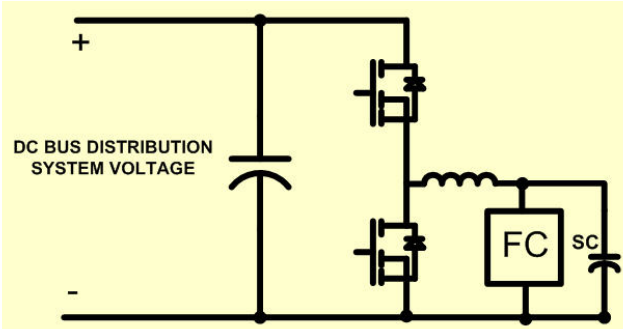

Fig. 28. Synchronous boost converter for fuel cell

The advantages of this power distribution architecture are as follows:

1) Utilizes the conventional variable DC bus distribution system (10.8 V to 19.5 V), hence reduces cost of development and time to market.
2) The fuel cell and AC adapter can be integrated into one external package.
3) The fuel cell, along with the synchronous boost converter is electrically interfaced to the AC adapter output.
4) In the absence of AC power, the fuel cell together with the on board Li-Ion battery can cater to all-day computing.
5) In the event the external AC adapter and the fuel cell are disconnected then the on board Li-Ion battery is capable of powering the laptop.

The disadvantages of this power distribution architecture are all inherited from the conventional power distribution system and they are listed below.

1) Additional weight, volume of the fuel cell/AC-adapter is an issue.
2) Wide voltage variation in the DC bus distribution system (10.8 V to 19.5 V) supplied to laptop's DC-DC converters. Power conversion cost, size and efficiency are all impacted by the range of input voltage.
3) The on-board battery charger contributes to power loss and adds to the complexity of thermal management and noise management.
4) Even if the power transfer switches are low in on-resistance, there is an inevitable voltage drop which further reduces efficiency.

3.4.2 Proposed power distribution architecture # 2

The architecture # 1 described in the previous section is identical to the conventional system built for Li-Ion batteries and external adapters. The main aim of the architecture # 2 shown in Fig. 29 is to transfer the battery charging function external to the laptop. This is accomplished by an external unit which consists of an AC adapter, fuel cell and a hybrid DC-DC converter (Fig. 30). This system requires the connection between the external unit and the laptop to have three wires (see Fig. 29). Fig. 30 shows the topology of the hybrid DC-DC converter block which resides in the external unit in proximity of the AC adapter and the fuel cell unit. The three wire connection (a, b, and g wires) between the external unit and the laptop. "g" denotes ground and "a" and "b" are positive (+) and negative (-) terminals. The power MOSFETs S_3 and S_4 constitute a DC-DC boost converter and regulate the fuel cell terminal voltage to an acceptable level for the laptop power distribution bus. The function of the MOSFET switches S_1 and S_2 in a bi-directional buck-boost converter is to accomplish both the battery charging (boost mode) and battery discharging function (buck mode). This configuration assumes that the voltage produced by the AC adapter (a-b terminals) is lower than the on board battery voltage. In the event the external unit (AC adapter and fuel cell) is disconnected from the laptop, the MOSFET switch S_5 internal to the laptop is controlled to turn on. This will now enable the laptop to function only on Li-Ion battery power. Therefore the architecture # 2 shown in Figs. 29 and 30 is highly versatile and employs hybrid power sources to power the laptop.

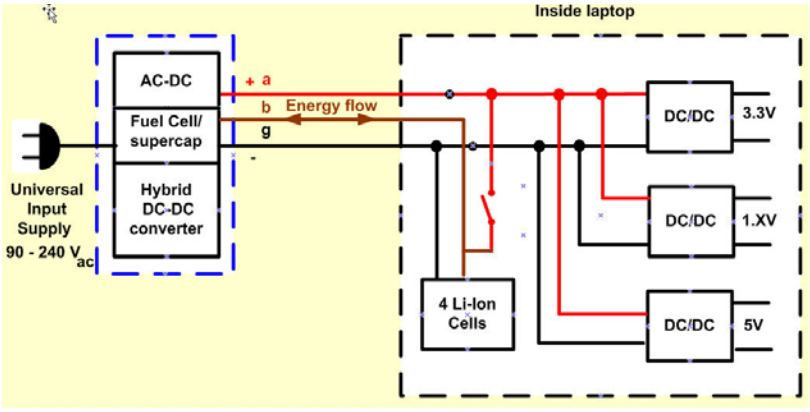

Fig. 29. Proposed power distribution architecture # 2

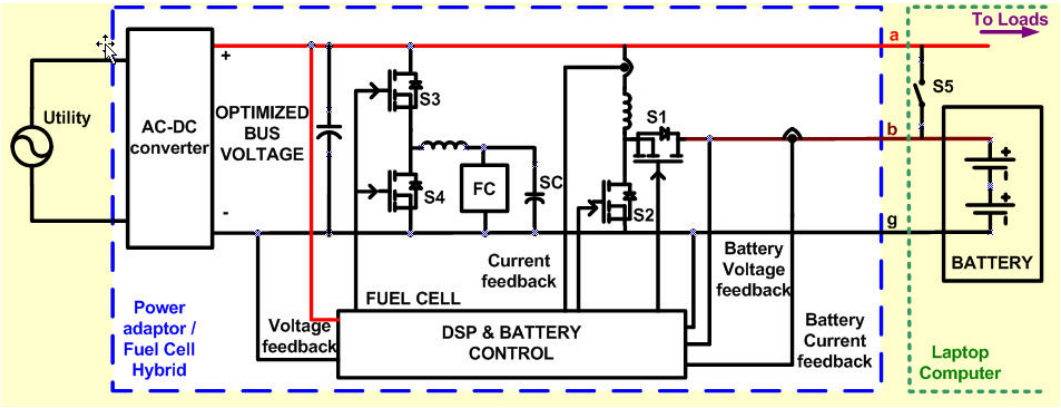

Fig. 30. Topology of the hybrid DC-DC converter block shown in Fig. 29

The advantages of this architecture are summarized as follows:

1) The Li-Ion battery charging function is transferred to the AC-DC adapter and hybrid DC-DC converter external to the laptop, thereby reducing the heat dissipation and saving space inside the laptop. This reduction in heat dissipation and space can now accommodate more complex features and/or additional memory functions.
2) Changes to AC-DC adapter are minor and do not contribute to higher cost.
3) Minimized fan power and noise requirements within the laptop.

4) Better overall efficiency and power savings.

3.4.3 Proposed power distribution architecture # 3

Another possible power distribution architecture is shown in Fig. 31. The proposed system employs lower DC voltages. This type of system is particularly suitable for AC-adapters and fuel cell systems that are mounted external to the laptop in close proximity (Fig. 24). In other words, there are no long wires connecting the external AC adapter to the laptop; safety standards limit the current carrying capacity of such long connecting wires to 5 A maximum. The architecture showed in Fig. 31 employs lower distribution voltages (9 V to 10 V) which improves the power conversion efficiencies of several onboard point of load DC-DC converters powering several loads. In order to employ a variable voltage Li-Ion battery, a bi-directional DC-DC converter is necessary to be installed inside the laptop (see Fig. 31).

When AC power is available, the DC distribution system bus is regulated at 10 V. When the fuel cell is operational the DC bus distribution system is regulated at 9 V. The bus voltage is reduced to enable the use of efficient, high frequency, low-voltage VRM converters placed at the points of load [22]. This results in smaller and more efficient computers and contributes to drastic reduction of generated heat.

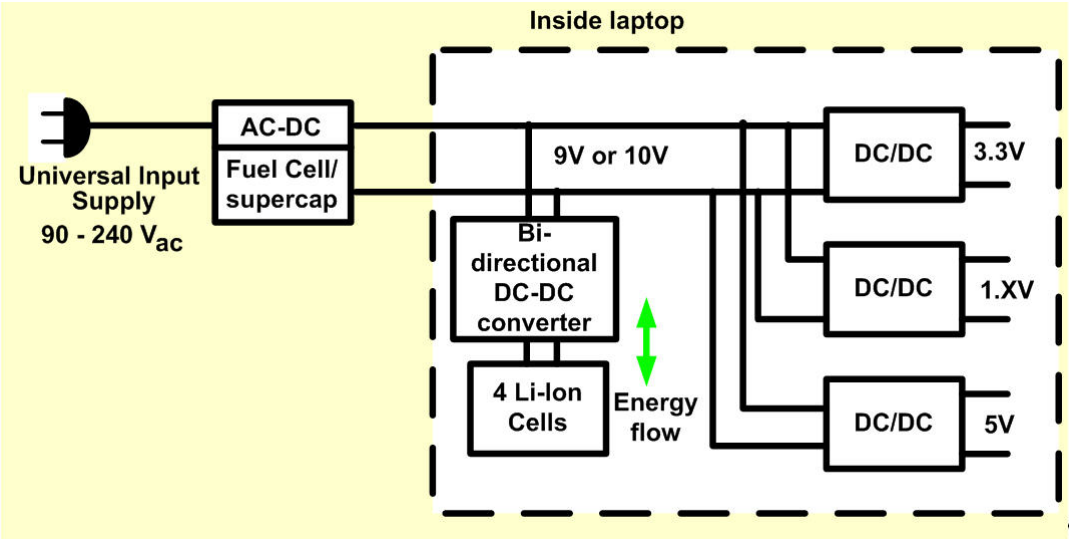

Fig. 31. Power distribution architecture #3

The onboard Li-Ion batteries are charged only when the AC-DC converter is connected to the DC bus distribution system. The bi-directional converter boosts the DC bus distribution system voltage to charge the battery bank. Without the AC-DC/fuel cell external adapter, the bi-directional converter steps down the battery bank voltage to provide the low DC bus voltage (9 V). The advantages of the power distribution architecture # 3 are as follows:

1) Single power train for battery charger (boost) and battery DC-DC converter (buck). This reduces the number of necessary power switches and switching regulators.
2) Provides the regulated low voltage input to laptop DC-DC converters. Power conversion cost and size are reduced while efficiency is increased as a consequence of the low input voltage.
3) Eliminates the need for power transfer switches.

4) Boosting the low voltage DC input to charge the battery minimizes the chopped input current typical of buck converters lowering the electromagnetic interference.

The associated disadvantages include:

1) Bi-directional DC-DC converter is placed inside the laptop where it dissipates the heat while charging or discharging the DC bus distribution system.
2) Bi-directional DC-DC converter also occupies a large area of motherboard PCB.
3) Large component count increases the cost of this topology.

3.4.4 Proposed power distribution architecture # 4

The power distribution architecture #4 is shown in Fig. 32. In this system the Li-Ion battery is eliminated and the AC-DC adapter and the fuel cell form one unit. When AC power is available DC bus distribution system is regulated at 7 V while when the fuel cell is operational the DC bus distribution system is regulated at 6 V.

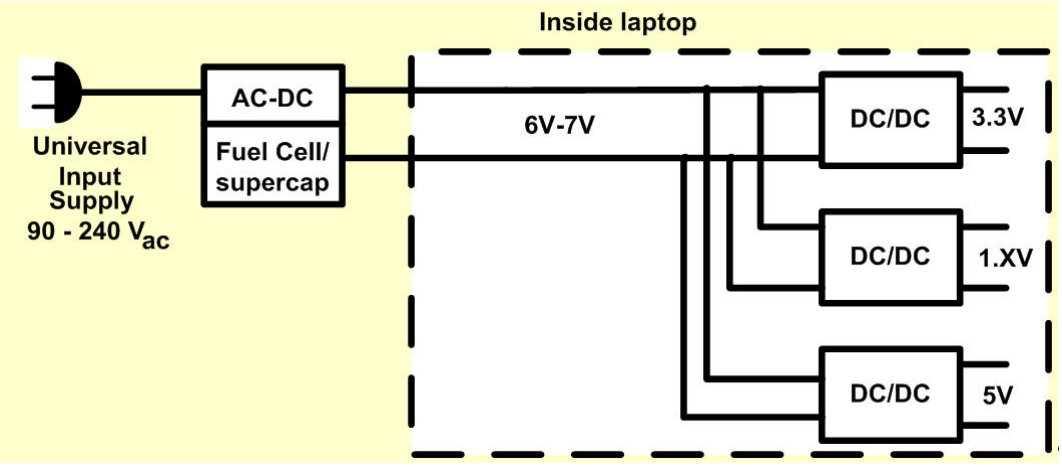

Fig. 32. Power distribution architecture # 4

The advantages of this architecture are as follows:

1) No Li-Ion battery; additional battery space can be used for other functions.
2) Lower AC-DC component ratings and drastic increase in operating efficiency due to low voltage (6-7 V) distribution bus.
3) Fuel cell is rated to supply the entire load.
4) Constantly controlled DC bus distribution system; therefore, easier design of the laptop DC-DC converters, which could be smaller and more efficient.
5) Simpler control without the battery managing function.
6) No need for additional hardware (charger/discharger).
7) Smaller size of the laptop providing more room for the fuel cell system.

The disadvantages of this power distribution architecture are as follows.

1) Due to the absence of Li-Ion battery, the fuel cell has to supply both constant and transient power needed, hence requiring a larger fuel cartridge.
2) In the absence of Li-Ion battery laptop cannot be operated without the fuel cell and/or the AC adapter unit.
3) Changes in the existing system, high cost of development.

3.5 Design example for proposed power distribution architecture # 2

The key point in implementing the proposed power distribution system # 2 is the design of a multi-input bi-directional DC-DC converter, shown in Fig. 30, to suitably interface the different energy sources (wall adapter, fuel cell, battery) to the loads. The integrated subsystem encompassing the AC-DC inverter, the fuel cell stack, the

supercapacitor and the proposed hybrid converter is placed outside the laptop casing as indicated in Figs. 29 and 30. The fuel cell is interfaced to the DC link using the synchronous boost converter to regulate the output voltage to 9 V. This is necessary because of the fluctuating output voltage of the fuel cell. This converter, together with S_3 and S_4 MOSFETs, converts the energy only in one direction from the fuel cell to the DC link; the S_4 MOSFET is gated while the S_3 acts as a diode preventing the energy from flowing in opposite direction. The fuel cell has a parallel-connected supercapacitor to improve the dynamic response during sudden load changes [37].

The battery bank is connected through the bi-directional buck/boost converter to the DC link. The bi-directional converter boosts the DC link voltage by gating the S_2 MOSFET to charge the battery bank. In case of the discharging, the bi-directional converter steps down the battery bank voltage by gating the S_1 MOSFET to provide the low 8 V DC bus voltage. The AC-DC converter regulates the voltage at its output to 10 V using conventional architecture.

The control function is realized using the Texas Instruments (TI) DSP 2407 and the battery manager system. The battery manager system consists of a set of sensors which collects precise battery data (temperature, voltage, charge and discharge currents). The DSP processes the battery manager's data and computes the charge time and the charging current. While charging, the bi-directional DC-DC converter operates as a voltage controlled current source. After the battery bank voltage matches the reference voltage, the controller maintains the voltage constant and decreases the current toward zero. Once the battery is fully charged the controller keeps the bi-directional converter

active by switching it between the buck and boost mode. This is necessary to maintain the average battery current zero while waiting for the possible loss of AC and fuel cell power.

Two loops are used to control the hybrid DC-DC converter. While operating in buck mode both loops are working simultaneously. The current control loop regulates the battery discharging current (positive current) and the voltage loop regulates the DC link voltage at 8 V. Operation in boost (battery charging) mode first employs just the current control loop to regulate the constant battery charging current (negative current) and when the battery voltage is high enough the negative current reference starts increasing slowly towards zero current and in that period the voltage loop regulates the constant battery voltage. A converter used to connect the fuel cell to the DC link is controlled with another voltage control loop to keep the DC link voltage at 9 V.

In the presence of the AC power DC link is powered through the AC-DC converter and both the fuel cell and the battery are inactive. If the DC link voltage drops below 9.8 V, the battery takes over the supply of the loads and the fuel cell gets activated but kept off the DC link until the start-up procedure is over. Once the fuel cell voltage reaches the nominal value, the fuel cell is connected to the DC link and the hybrid DC-DC converter switches to boost mode and starts charging the battery. After the battery is fully charged the fuel cell alone is supporting the DC link. This behavior is shown in simulation results in Fig. 33. The operating scenario is as follows: the AC power is disconnected at $t = 0.1$ *ms* and the battery takes over supporting the DC link. After the fuel cell start up procedure is completed at $t = 20$ *ms* it starts to power the DC link and charge the battery.

There is the change of load from half load to full load at $t = 50\ ms$; the DC link voltage is still regulated, although with the higher ripple. Finally, the AC power is back at $t = 80\ ms$ and the DC link is again supported through the AC-DC converter. The simulation results confirm the feasibility of the proposed hybrid DC-DC converter configuration.

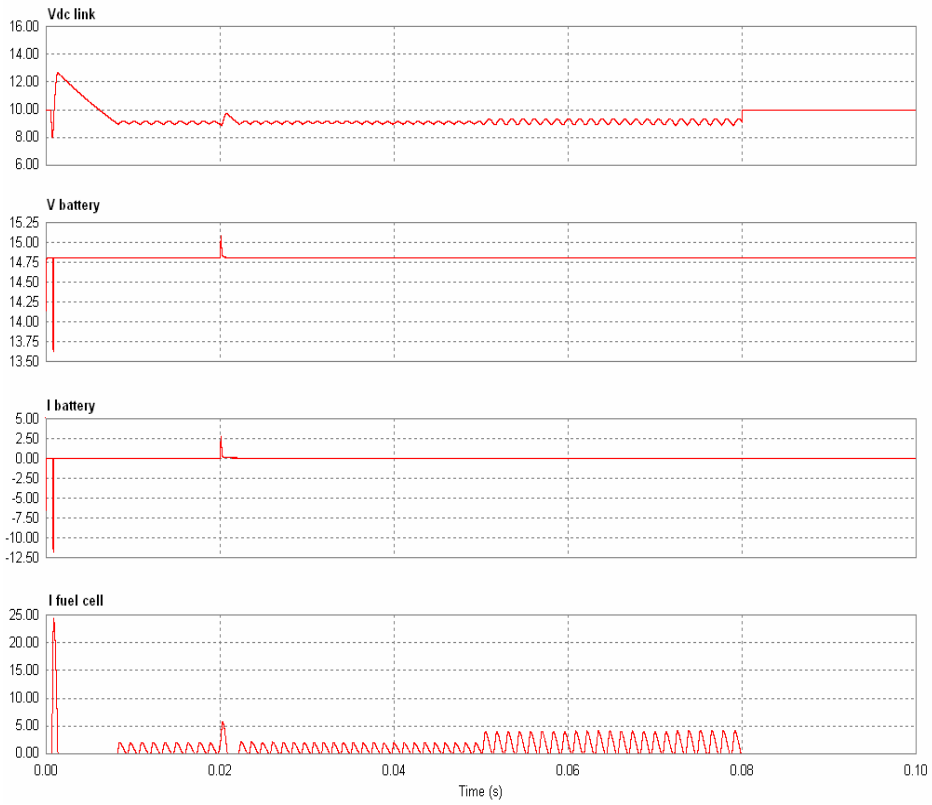

Fig. 33. Simulation results

To design the fuel cell system for an AC-DC/fuel cell external adapter, first the load current of a Dell Latitude C600 computer was measured during the peak load (Fig. 34) and standby operation (Fig. 35) [23].

The measured voltage of the AC-DC adapter was 19 V so the standby load of the laptop is approximately 10 W and the peak loads go up to 30 W. Therefore, a 30 W fuel cell (Model 25-10, BCS Fuel Cells, Inc.) would be sufficient to power the normal functions of the laptop. Table VII shows the specifications of the chosen 30 W fuel cell. Li-Ion battery is capable of operating for 2 to 4 hours so the fuel cell should provide the remaining 20 hours to ensure all day computing.

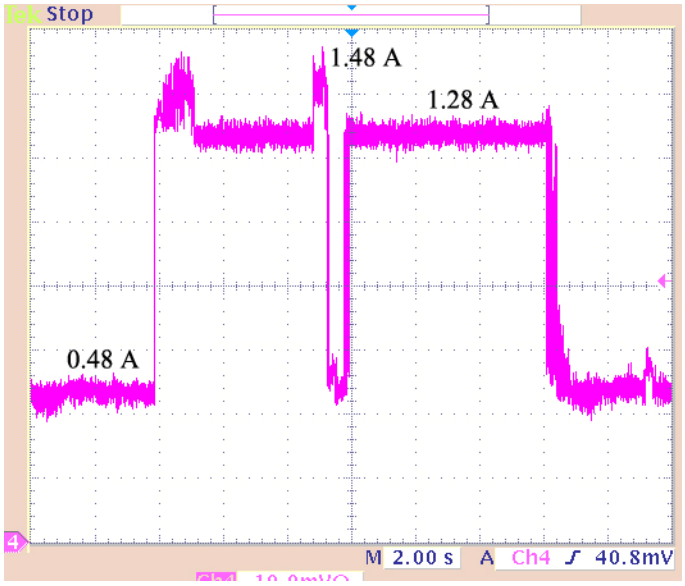

Fig. 34. Load current of Dell Latitude C600 during the saving of a MS Word document

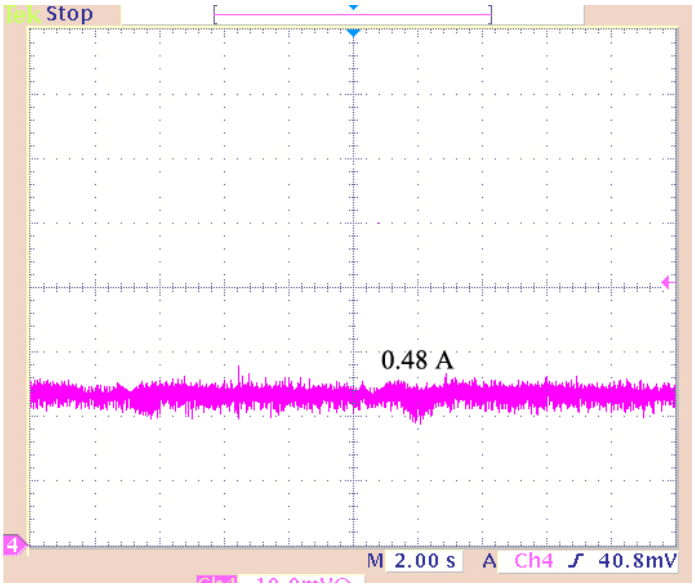

Fig. 35. Load current of Dell Latitude C600 during normal use

TABLE VII
BCS PEM FUEL CELL SPECIFICATIONS

Specifications of the FC	**Value:**
Maximum power	35 W
Cell voltage	0.8 V
Current density	0.24 A/cm^2
Nominal voltage	6 V
Nominal power	30 W
Electrode area	25 cm^2
Operating hydrogen pressure	0-2 psi
Max operating temperature	70 ^{o}C
Conversion efficiency	52% [38]

TABLE VIII
CHARACTERISTICS OF THE DESIGNED SYSTEM

	Li-Ion	**PEMFC**	**AC-adapter**
Max power main system	22 W	35 W	60 W
Max added power sub system		2.5 W	
Voltage	14.8 V	6 V	19.0 V
Total capacity	65 Wh	700 Wh	
Volume of energy system	210 cm^3	150 cm^3	102.125 cm^3
Use time	3 h	20 h	
Energy density total system	0.31 $Whcm^{-3}$	4.67 $Whcm^{-3}$	

The average hydrogen flow is 0.4 l/min (liter/minute), which results in needed 480 l for 20 hours of operation. Hydrogen volume can be reduced by using a pressurized hydrogen tank; using a 3500 lbf/in^2 (psi) tank reduces the volume of the required hydrogen tank to 2 l, which is acceptable from the laptop size point of view. Dimensions of such hydrogen tank could be 30 cm X 5 cm X 13 cm (width X height X depth). Table VIII shows the characteristic parameters of the designed system.

3.6 Experimental results for proposed power distribution architecture # 2

In order to verify the feasibility of the concept, the proposed hybrid multi input DC-DC converter was built. Experiments were carried out on commercially available four cell Li-Ion batteries, Maxwell supercapacitors and a 30 W PEM fuel cell (Model 25-10, BCS Fuel Cells, Inc.). The synchronous boost converter connecting the fuel cell to the DC link was designed to sustain the 9 V output voltage and it is rated for 30 W, which is suitable to supply the laptop computer. The Maxwell supercapacitors have been parallel-connected to the fuel cell to improve the dynamic response during sudden load changes.

The Li-Ion batteries were connected through the 30 W bi-directional buck/boost converter to the DC link. Experimental waveforms are shown in Fig. 36 and Fig. 37.

Fig. 36 shows the DC bus voltage and bi-directional inductor current in a setting when first the battery is supporting the DC link (8 V) and then after the fuel cell completes the start-up procedure and starts to power the DC link with the increased voltage of 9 V. While the battery is supporting the DC bus, the bi-directional converter is working in the buck mode regulating the DC-bus voltage to 8 V, discharging the battery with a constant positive current of 0.5 A. After the fuel cell voltage is raised over the threshold of 8.8 V, the fuel cell is connected to the DC link. During this time interval the controller changes the current reference slowly to its negative charging value to avoid current overshoots. The fuel cell first charges the battery with constant (negative) current through the bi-directional converter working in the boost mode. After charging the battery the bi-directional converter maintains the average battery current at zero, waiting for the possible return of AC power.

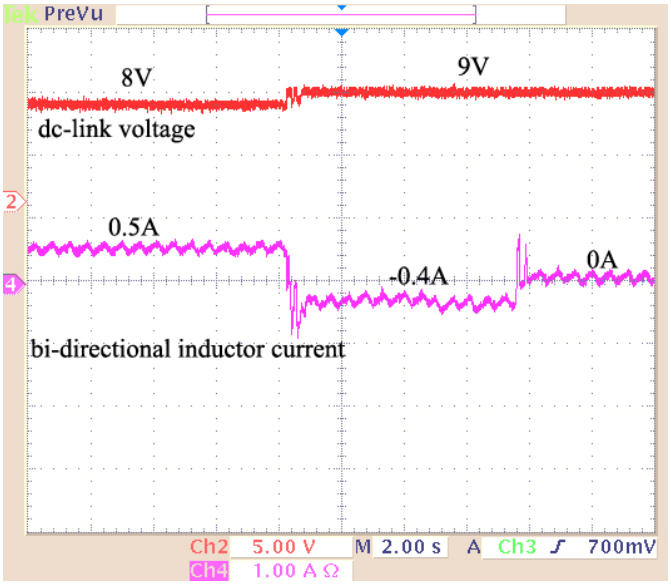

Fig. 36. DC bus voltage and bi-directional inductor current with the fuel cell connected

Fig. 37 shows the transient response of the synchronous boost converter connecting the fuel cell to the DC link. While the fuel cell was supporting the DC link, the load was changed from no load to full load and then back to no load again.

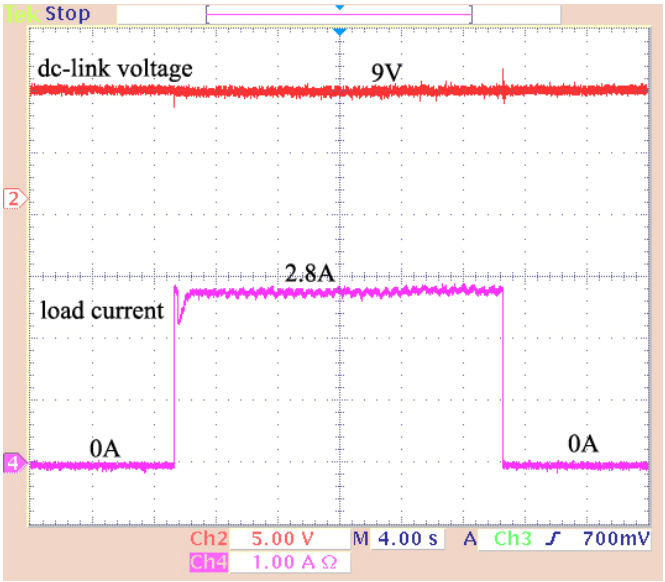

Fig. 37. DC bus voltage and fuel cell current during load switching

From Fig. 37 it can be seen that the DC link voltage is constant with no oscillations. The load current is shown in the lower trace in Fig. 37 and changes between 0 A and 2.8 A.

3.7 Conclusion

This chapter discusses in detail the conceptual design behind the four proposed power distribution architectures for fuel cell powered laptop computers. For each architecture advantages/disadvantages are highlighted. The power consumption of two different laptop computers is measured for different types of loads to determine transient and steady state needs of the system.

Furthermore, a hybrid multi-input bi-directional DC-DC converter for applications in fuel cell powered laptop computers has been proposed. The purpose of this multi-input converter is to suitably control the energy flow from multiple energy sources to enable all day computing. The AC-DC adapter and the fuel cell and its components are integrated with the converter in an external unit while the conventional Li-Ion battery is placed within the laptop casing. A design example highlighting the parameters of the fuel cell stack, Li-Ion battery, and supercapacitor modules appropriately sized for a typical load on a laptop computer is shown. Analysis, design and control aspects of the hybrid DC-DC converter are presented to meet performance requirements for all day computing. Simulation results verified the performance of the system under various input and output power conditions. Experimental results show that the bi-directional converter is working as expected in both operating modes, bucking the voltage down to usable levels when the

battery is supporting the DC link and boosting the fuel cell voltage to charge the batteries and sustain the DC link when the fuel cell is maintaining the DC link voltage. Transient behavior of the DC link during the sudden load change is excellent due to the presence of supercapacitors. This topology stores and delivers energy more efficiently than conventional systems. Therefore this proposed hybrid DC-DC converter system can also be used for energy storage for other portable applications.

CHAPTER IV

DESIGN CONSIDERATIONS FOR FUEL CELL POWERED UPS

4.1 Introduction

Uninterruptible power supplies (UPS) provide electric power for critical applications when the quality of the energy source, i.e. utility power, is not adequate or fails entirely. Generally, there are three basic types of UPS systems – Standby UPS, Line-Interactive UPS and Double Conversion UPS [39-40]. Regardless of the type, conventional UPS employ batteries and/or engine generators as their main power sources. Typical UPS systems are built around rechargeable batteries such as sealed lead-acid (SSLA) or nickel cadmium (Ni-Cd) batteries. However, these contain toxic heavy metals such as cadmium, mercury, and lead and may cause serious environmental problems if they are discarded without special care; furthermore, these batteries suffer from life expectancy, footprint and weight issues. Similarly, engine generators have issues with startup, maintenance, noise and emission. Recently other methods of energy storage such as fuel cells, flywheels, supercapacitors and combinations of the above have come into use.

The UPS market can help fuel cell technology to become a commercial solution. The end of life of a fuel cell can be extended by the intermittent operation of UPS systems and the per kilowatt price associated with UPS operation, although currently one of the highest on the market, can be driven down in the long run by fuel cell technology [1]. Among various kinds of fuel cells, Proton Exchange Membrane Fuel Cells (PEMFC) are compact and lightweight, provide a high output power density at room temperature,

as well as ease of start-up and shut down operations [8]. Further, unlike batteries, fuel cells can continuously provide power as long as the reactants are supplied. This feature is especially useful when the duration of the power outage is uncertain.

It is important for the UPS system to be able to immediately take over the full load at the inception of the power outage or out-of-tolerance situation to avoid any data or production loss, uncontrolled system shutdown or malfunctioning of the devices. Some critical applications do not allow even several tens of millisecond power interruption. As is well known, fuel processors have a delay as long as several tens of seconds, and the fuel cell cannot take over the full load if its membrane is not properly humidified [2]. For this reason, a supercapacitor module is employed to compensate for these response delays by supplying the required instantaneous energy, which is stored during the normal operation. This energy can be used to handle overload conditions as well.

Motivated by the situation described above, this chapter deals with the design considerations for a 1.5 kVA single–phase fuel cell-powered passive stand-by UPS system with one hour of backup power employing modular (fuel cell & power converter) blocks. Interactions between the internal impedance of the fuel cell and steady state and transient stability are investigated. A design example for the DC-DC full bridge converter and sizing of commercially available supercapacitors as well as fuel calculations are presented.

4.2 Classification of UPS systems

Static (or Solid State) UPS systems are classified into three different categories: (a) Online UPS, (b) Offline UPS and (c) Line interactive UPS. Static UPS systems have a broad variety of applications from low power personal computers and telecommunication systems, to medium power medical systems, to high power utility systems. Their main advantages are high efficiency, increased reliability and low THD.

4.2.1 Offline UPS topology

Offline UPS configuration is also known as "standby UPS". Fig. 38 shows the offline UPS configuration. It consists of a battery charger, a battery bank, a DC-AC inverter, and a static transfer switch. The static transfer switch enables the load to be connected to the input AC power supply, while the battery charger ensures the battery bank is adequately charged. In the event of a power loss and/or a disturbance, the static transfer switch switches to the DC-AC inverter and powers the load from the battery bank. When the input AC power is restored, the transfer switch transfers the load back to the AC line, typically within $1/4^{th}$ of a cycle.

The main advantages of this configuration are its simple design, low cost, and small size. On the other hand, lack of real isolation of the load from the AC line and no output voltage/frequency regulation are the main disadvantages.

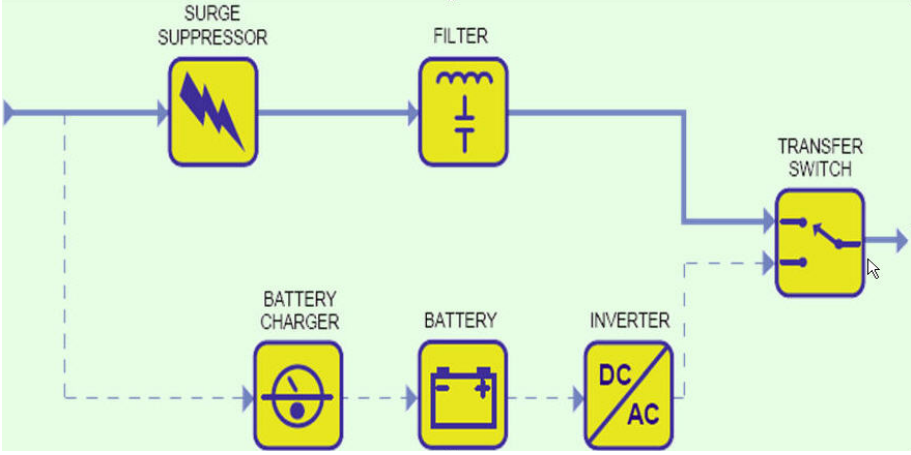

Fig. 38. Offline UPS Configuration

4.2.2 Online UPS topology

The online UPS configuration is also known as “double-conversion UPS”. Fig. 39 shows the block diagram of a typical online UPS. The rectifier/charger continuously supplies the DC bus and the DC-AC inverter powers the load. The UPS system therefore is in continuous operation and supplies the load with regulated voltage and frequency irrespective of the condition of the input AC line. In the event that the input AC is unavailable, the power from the battery bank is utilized. The function of the static switch (Fig. 39) is to provide redundancy in case the UPS malfunctions and/or overload. The main disadvantage of this configuration is its high cost and continuous operation and system losses.

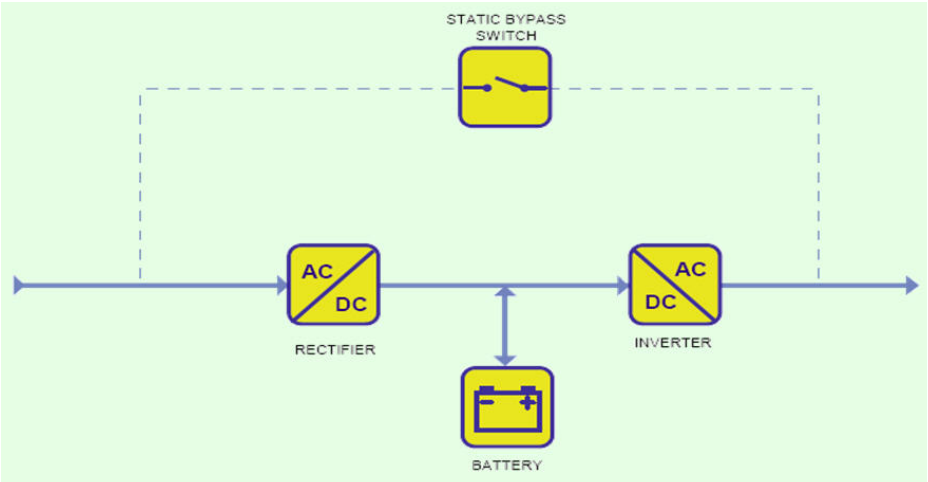

Fig. 39. Online UPS configuration

4.2.3 Line interactive UPS topology

A typical Line-interactive UPS system topology is shown in Fig. 40 and consist of a static switch, a bi-directional converter, and a battery bank. A line interactive UPS can operate either as an online UPS or as an offline UPS. When the AC line is within the preset tolerance, it feeds the load directly.

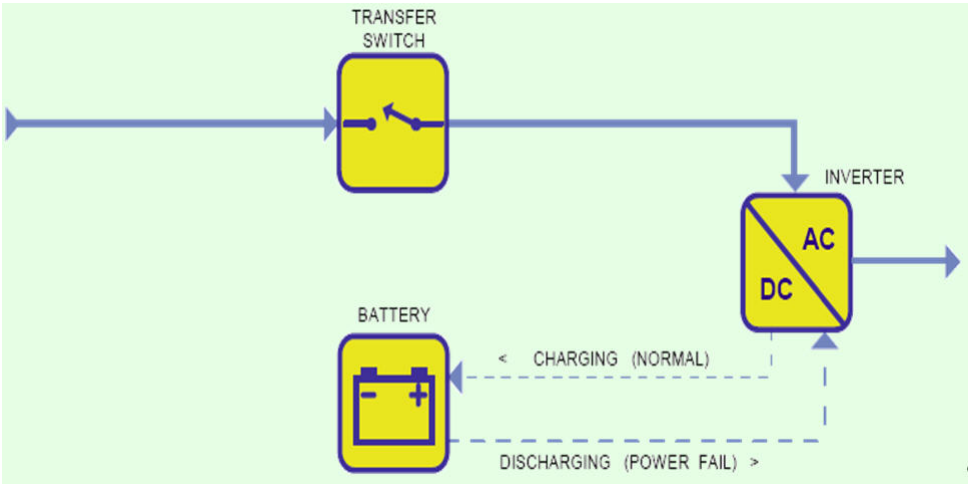

Fig. 40. Line interactive UPS topology

The AC-DC converter is connected in parallel with the load and charges the battery. It may also supply the reactive power required to keep the power factor close to unity or to regulate the output voltage. In the event of a power loss, the DC-AC supplies the load from the battery bank and the static switch disconnects the AC line. The main advantages of the line interactive UPS is its simplicity in design, high reliability and lower cost compared to an online UPS system. The main disadvantage is the lack of effective isolation of the load from the AC line and lack of regulation of the output frequency.

4.3 Proposed fuel cell powered UPS system architecture

Fig. 41 shows the block diagram of a proposed fuel cell powered line interactive UPS system configuration. The approach consists of a fuel cell stack supplied by a fuel processor and/or hydrogen storage, a supercapacitor module for energy storage, a DC-DC converter and a DC-AC inverter along with static transfer switches. Normally, the utility power is transferred to the load through the static switch module (SSM). The proposed system is designed to be battery-less.

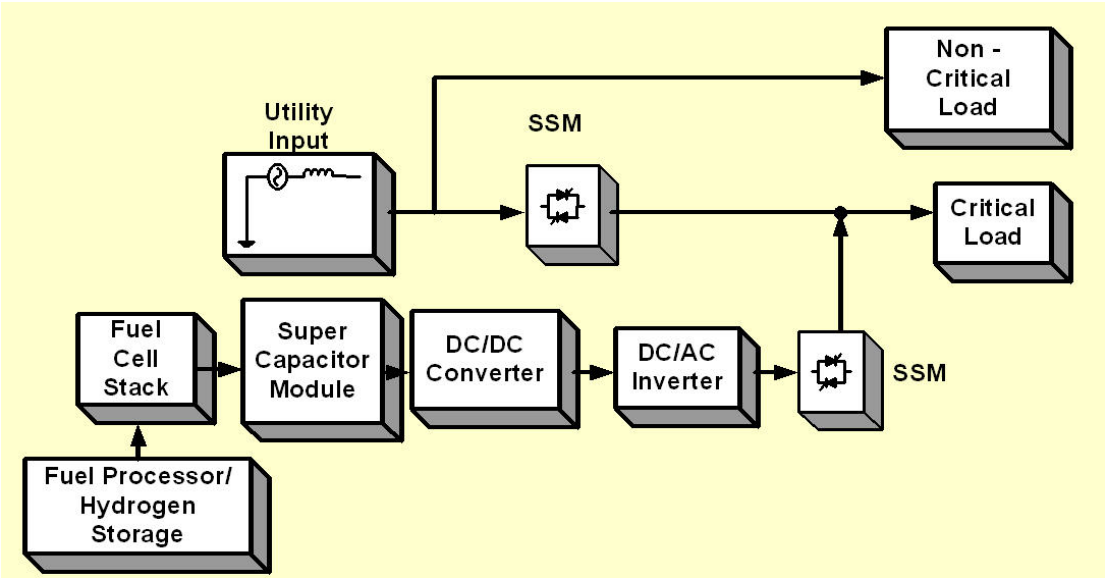

Fig. 41. Proposed fuel cell powered passive stand-by UPS system

At the initial start, the fuel cell charges the supercapacitor, and then supplies 10% of the rated load along with the utility. In the event of a power outage or out-of-tolerance situation the controller turns the SSM off, thereby the fuel cell and its power converter module start to supply the full load alone. At the moment of the transition from the normal mode to fuel cell powered mode, the system is not able to take over the full load due to the slow dynamics of the fuel processor. The fuel processor is a system which cleans and then converts conventional fuels (natural gas, other gaseous hydrocarbons, methanol, naphtha, or coal) into a gas containing hydrogen. This proposed topology overcomes this drawback by placing the supercapacitor in parallel with the fuel cell. This module transfers the energy that was stored in the supercapacitor during the normal mode operation to the load at the initial start to make up the instantaneous power shortage. Stored energy can also be used to handle the transient power shortage due to load step changes and/or overload conditions for a short time. When the transient

situation is over, the fuel cell supplies the minimum power to the load and at the same time recharges the supercapacitor. The control circuit monitors the utility and the fuel cells status continuously. When the system detects a utility disturbance condition, it controls the fuel cell and power converter modules to supply more power. After the disturbance, the controller connects the utility to the load through a synchronization process.

The advantages of the proposed approach over conventional UPS systems are as follows:

1) Due to the absence of batteries and an engine generator, it is environmentally friendly, clean and quiet.
2) In the proposed fuel cell powered UPS the amount of available power is a function of hydrogen availability. This is an advantage compared to the battery based UPS whose state-of-charge (SOC) is not always precisely known.
3) No delay time is required to take over the full load when the power disturbance occurs due to fast discharging characteristics of the supercapacitor.
4) The system possesses good overload handling capability due to the supercapacitor.
5) Continuous power generation is possible as long as the reactant gases are supplied to the fuel cell.

Fig. 42 shows the detailed circuit schematic of the proposed architecture. The DC-DC conversion stage of this architecture consists of the parallel connection of the Ballard Nexa fuel cell and the supercapacitor followed by the full-bridge two-inductor converter.

The need for a transformer with very low and controllable leakage inductance makes the coaxial winding transformer (CWT) the preferred structure [41].

At initial startup of the system the fuel cell is used to charge the supercapacitor. After the startup process is finished, and in order to keep the fuel cell at working temperature, the full bridge DC-DC converter is used to supply 10% of the load rated power. Additionally, when the load changes suddenly, the UPS system is now able to respond promptly to the power demand change due to the supercapacitor. This UPS topology is also useful for handling the instantaneous overload situation. If the load demands more than the rated power momentarily, the energy stored in the supercapacitor can be utilized to supply the load thereby preventing the fuel cell from being overloaded. It is obvious that system delay or voltage drop is unavoidable without this auxiliary energy storage system in the case of sudden load change and/or overload. The DC-AC conversion stage of this architecture consists of a DC-AC IGBT inverter and produces the high quality sinusoidal 120 V output voltage.

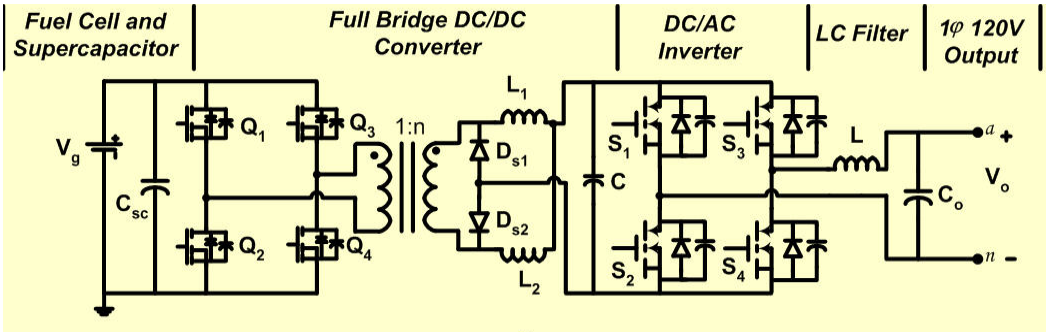

Fig. 42. Circuit topology of the proposed fuel cell powered UPS system

An important variable in the design of the fuel cell power conditioner is the amount of current ripple that the fuel cell can withstand. Since the reactant utilization is known to impact the mechanical nature of a fuel cell, it is suggested in [42] that the varying reactant conditions surrounding the cell (due to current ripple) govern, at least in part, the lifetime of the cells. Both the magnitude and the frequency of the current ripple are important. For fuel cells powering single phase loads (60 Hz), the current ripple of concern is twice the output frequency i.e. 120 Hz. A limit of 0.15 pu (per-unit) (i.e. 15% of its rated current) from 10% to 100% load is specified [24]. In case of single phase inverters with dual output voltage (120 V/240 V) there is a possibility of 60 Hz current ripple injection into the fuel cell under unbalanced loading conditions (i.e. one output phase loaded and the other unloaded). A limit of 0.1 pu is specified for 60 Hz current ripple from 10% to 100% load [24]. Further, the magnitude of the low frequency current ripple drawn from the fuel cell by the DC-DC converter is largely dependent on the voltage loop response characteristics. Also the DC-link capacitor size determines the 120 Hz voltage ripple on DC-link, which in turn has an impact on the input current drawn from the fuel cell. It should be noted that switching frequency components in the DC-DC converter can be easily filtered via a small, high frequency capacitive filter. Measures that are suggested for limiting the fuel cell current ripple are:

1) Installing an input filter to reduce the 120 Hz component of the current ripple to 0.15 pu; however, this approach contributes to additional size, weight and cost of the unit.

2) Increase the size of DC-link capacitor in the DC-AC inverter. Similarly, the size, weight, and cost are of concern.
3) Reduce the response time of the voltage loop of the DC-DC converter which will affect the regulation of the DC-link and impact the quality of inverter AC output, and possibly increase the size of output AC filter.

4.4 Full bridge two-inductor rectifier

At the power level of 1200 W, the preferred topology is full-bridge DC-DC converter with isolation on the intermediate high frequency AC link. The main advantages of this topology include constant frequency operation, which allows for optimum design of the magnetic filter components, PWM control, minimum VA stresses, and good control range and controllability. Major drawbacks of this topology are high-voltage stress induced by the parasitic inductances following diode reverse recovery and increase in device switching losses as the switching frequency is increasing.

Various soft switching schemes (zero voltage switching (ZVS)) and (zero current switching (ZCS)) have been proposed to improve the performance of hard switching converters.[43-44] Most topologies are subject to diode recovery problems. A solution for this problem is a full-bridge DC-DC converter with two-inductor rectifier shown in Fig. 42, which was proposed in [45]. For this topology, ZVS is achieved using the energy stored in the output filter inductors instead of the leakage inductance energy. In fact, the transformer leakage inductance is reduced drastically to allow output diode

commutation prior to switching the primary voltage to the other rail. This, in turn, results in elimination of secondary voltage spikes. The advantages of the proposed topology include the following:

1) Fixed frequency operation with PWM control and minimum VA ratings.
2) ZVS for the main devices is achieved using the energy stored in the secondary filter inductors.
3) Wide load range with ZVS**.**
4) Utilizes the low leakage inductance of a coaxial winding transformer to achieve soft switching for the secondary diodes.
5) No lost duty cycle since the secondary diodes commutate under zero voltage.
6) No voltage spike in the secondary circuit due to the soft switching of the secondary diodes.
7) Utilizes the circuit parasitic elements effectively.

4.5 Fuel cell equivalent circuit

Since fuel cells have internal impedance, the starting point to properly design a fuel cell powered UPS is to obtain an equivalent electrical circuit model. Section 2.1 explains in detail how the equivalent model of the fuel cell was obtained. That same approach was repeated for Ballard Nexa fuel cell. The resistance and reactance of the fuel cell stack for light load, medium load, and full load for frequencies ranging from 0.2 Hz to 20 kHz are shown in Fig. 43. The equivalent circuit parameters of the fuel cell whose response is shown in Fig. 43 are listed in Table IX.

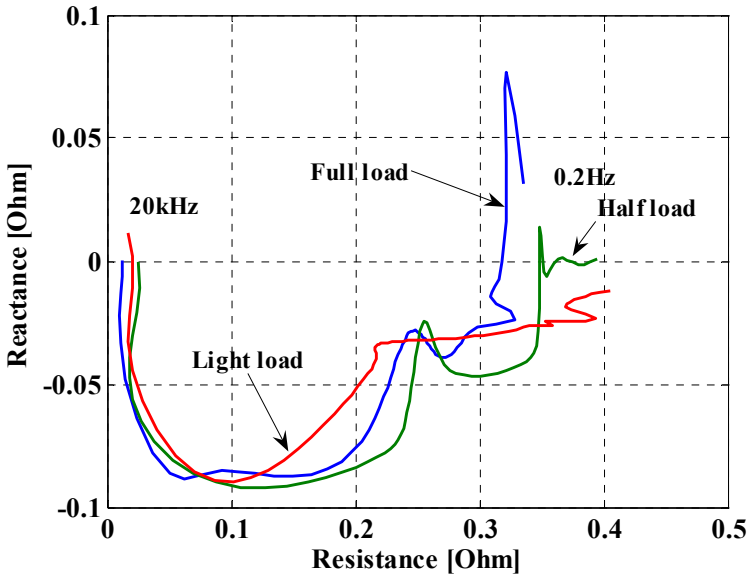

Fig. 43. Nyquist plot for a 1200W fuel cell stack

It can be observed from Table IX and from the Nyquist plot in Fig. 43 that the fuel cell equivalent circuit parameters are a function of the output load. Also from the parameters in Table IX it can be calculated that the dominant time constant of the stack, given by R_{p2} and C_2 is also load dependent and varies from 8.97 ms (light load) to 20.37 ms (full load).

TABLE IX
EQUIVALENT CIRCUIT PARAMETERS

Load Condition	R_m[mΩ]	R_{p1}[mΩ]	C_1[mF]	R_{p2}[mΩ]	C_2[uF]
Light Load	16.8	139.03	64.54	188.28	475.36
Half Load	16.8	111.41	95.44	229.05	376.92
Full Load	16.8	78.65	258.96	218.75	556.85

Therefore from the electrical point of view the fuel cell as a power source exhibits a relatively slow dynamic response. In other words, the fuel cell takes time to respond to load changes (load increases or decreases). This dynamic characteristic needs to be taken into consideration when designing a DC-DC converter stage of a UPS.

4.6 Steady state stability

From the fuel cell terminals point of view any DC-DC converter operating in closed loop can be considered as a constant power load. This is because regardless of the voltage being produced by the fuel cell stack the output voltage of the DC-DC converter is maintained at a constant voltage. In particular for the case of a step-up converter, if there are variations in the voltage produced by the fuel cell stack the converter increases or reduces its input current in order to maintain its output voltage constant. In general for a fuel cell powered DC-DC converter system to be stable in steady state the V-I characteristic of the fuel cell and the constant power locus of the DC-DC converter have

to intersect at one point, which sets the operating condition of the system. If the two curves do not intersect the source is not able to meet the power demanded by the load.

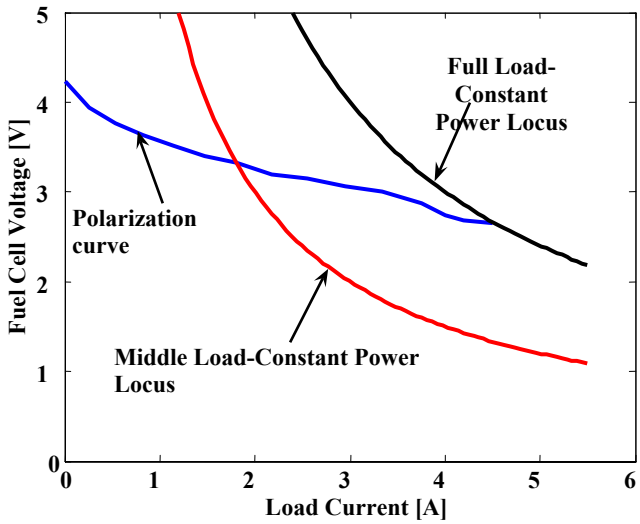

Fig. 44. Fuel cell polarization curve and load constant power locus

Fig. 44 shows the V-I characteristic of the commercial 1200 W fuel cell whose parameters were obtained in the previous section. This figure also shows the constant power locus of a 1200 W DC-DC converter operating at full and half load. As can be observed from Fig. 44 the constant power locus intersects the V-I characteristic of the fuel cell, and therefore the power requirements of the load are met. However, if the voltage produced by the stack experiences variations due to a reduction in its fuel pressure the curves may not intersect, especially for loads close to full power where voltage characteristic of the fuel cell drops quickly as the load current increases. If the curves do not intersect there is a mismatch between the power demanded by the load and the power that the stack can produce. Moreover, if the voltage at the input of the DC-DC converter drops its controller will increase the input current which results in an

additional drop in the fuel cell voltage. In other words, a positive feedback takes place which leads to system instability.

To avoid this problem an energy buffer such as a supercapacitor is required to ride through transient voltage disruptions in the fuel cell output as explained in detail in Chapter II.

4.7 Transient stability

The characteristics of the internal impedance of the fuel cell affect the dynamics of the DC-DC converter, as was explained in detail in Section 2.4.2. The DC-DC converter used for proposed UPS system is a full bridge with two-inductor converter, which is completely different from the boost converter for portable applications. All converter transfer functions need to be checked and the fuel cell impedance influence, which determine the transient stability, needs to be reexamined in this case. A fuel cell connected to the input terminals of the full bridge converter is shown in Fig. 45.

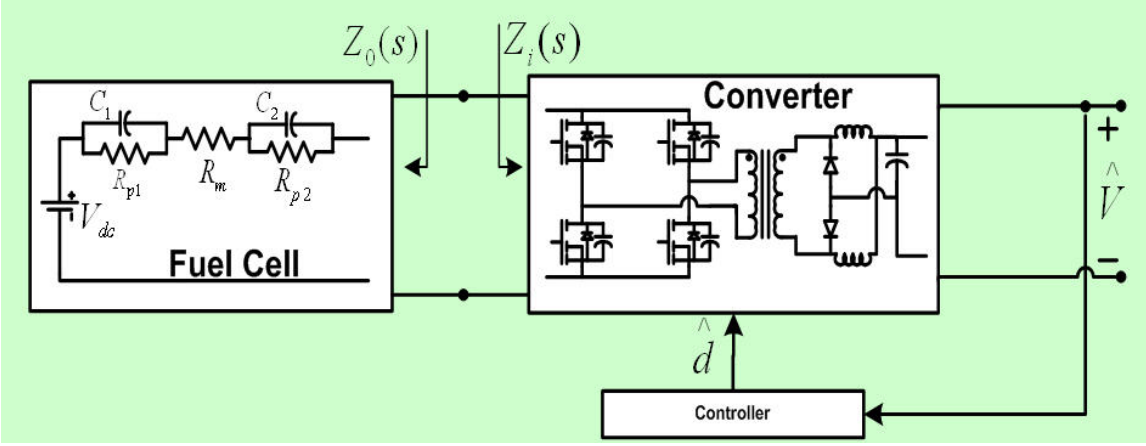

Fig. 45. Fuel cell DC-DC converter system

If the internal impedance of the fuel cell is considered, Middlebrook's extra element theorem [21] can be used to analyze the effect of the fuel cell onto the dynamics of the converter. Application of the theorem results in the system shown in Fig. 46, where the fuel cell output impedance is modeled as an extra element in the system.

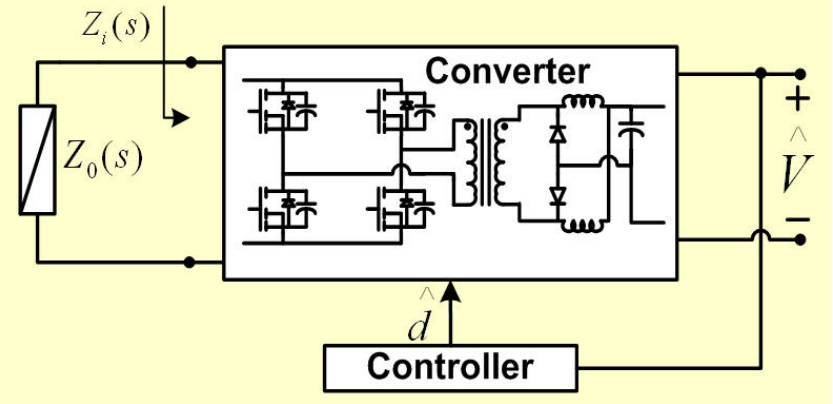

Fig. 46. Modeling of the fuel cell impedance effect

It can be found that the control-to-output transfer function of the converter when the fuel cell is considered is given by (5)

$$G_{vd}(s) = \left(G_{vd}(s)\big|_{Z_o=0} \right) \frac{1 + \dfrac{Z_o(s)}{Z_N(s)}}{1 + \dfrac{Z_o(s)}{Z_D(s)}} \tag{5}$$

where $G_{vd}(s)\big|_{Z_o=0}$ is the converter transfer function when the supply is an ideal voltage source, $Z_N(s)$ is the input impedance of the converter under the condition that the feedback controller operates ideally, $Z_D(s)$ is the input impedance of the converter under the assumption that $\hat{d}(s)=0$, and $Z_o(s)$ is the output impedance of the fuel cell. The small signal model for a full bridge converter is shown in Fig. 47a. If the fuel cell

equivalent circuit model is added to the circuit the small signal equivalent shown in Fig. 47b is obtained. From Fig. 47a the converter transfer function when the supply is an ideal voltage source $G_{vd}(s)$, and input impedances of the system, $Z_N(s)$ and $Z_D(s)$, are given by:

$$G_{vd}(s) = G_{do}\frac{1}{1+\frac{s}{Q\omega_o}+\frac{s^2}{\omega_o^2}} \qquad (15)$$

$$G_{do} = nV_{in},\quad \omega_o = \sqrt{\frac{2}{CL_s}},\ Q = R\sqrt{\frac{2C}{L_s}}$$

$$Z_D(s) = \frac{2R + sL_s + s^2 L_s CR}{2n^2 D^2 (1 + sCR)} \qquad (16)$$

$$Z_N(s) = -\frac{2R}{n^2 D^2} \qquad (17)$$

where V_{in} is the nominal input voltage, D is the converter duty cycle, L_s and C are the inductor and capacitor of the converter, n is the a turns ratio of the transformer and R is a load resistance.

a)

b)

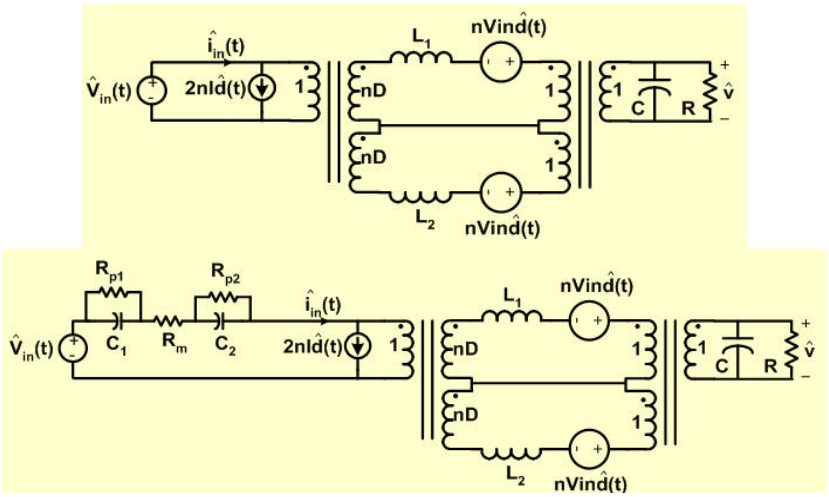

Fig. 47. a) Small-signal models for full bridge converter; b) When connected to a fuel cell

From Fig. 47, the output impedance of the fuel cell equivalent circuit is given by (13).

$$Z_o = \frac{s^2(R_m R_{p1} R_{p2} C_1 C_2) + s(R_m(R_{p1}C_1 + R_{p2}C_2) + R_{p1}R_{p2}(C_1 + C_2)) + R_m + R_{p1} + R_{p2}}{s^2(R_{p1} R_{p2} C_1 C_2) + s(R_{p1}C_1 + R_{p2}C_2) + 1} \quad (13)$$

By plotting the magnitudes of the converter input impedances and fuel cell output impedance (16,17,13) for the fuel cell parameters shown in Table IX and for a 1200 W full bridge converter designed to operate in continuous conduction mode with the 296 mH inductance and 10 mF output capacitance, the graph in Fig. 48 is obtained.

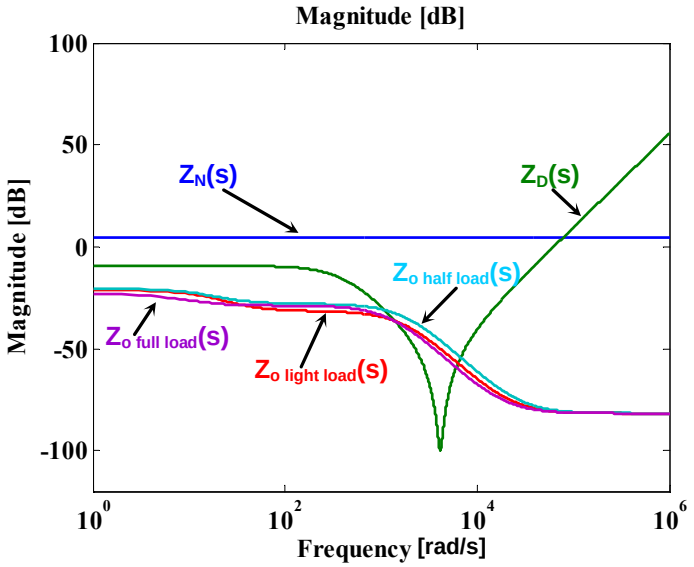

Fig. 48. Impedances for fuel cell full bridge converter system

It was shown in Chapter II that the internal impedance of the fuel cell has an effect on the control-to-output characteristic of the DC-DC converter stage. Because of the internal impedance of the fuel cell the gain of the converter at low frequencies is reduced, and the gain margin of the converter drops. This is depicted in Fig. 49 which

shows the open loop control-to-output characteristic of a step-up DC-DC converter operating from an ideal source and from a Ballard Nexa fuel cell. As can be seen from this figure, when this particular fuel cell is used as a power source there is a significant difference in the gain margin and phase margin between two cases.

This can be also inferred from the impedance plot shown in Fig. 48, since the fuel cell impedance and DC-DC converter impedance curves intersect. In order to meet the design criteria (6-9) in Section 2.4.2 either the converter or the fuel cell impedance have to be modified. A method of modifying the output impedance of the fuel cell by connecting a supercapacitor in parallel was shown in Section 2.4. This will generate displacement of the output impedance of the fuel cell to the left as shown in Fig. 50 and increase the distance between the output impedance of the fuel cell and the input impedance of the DC-DC converter.

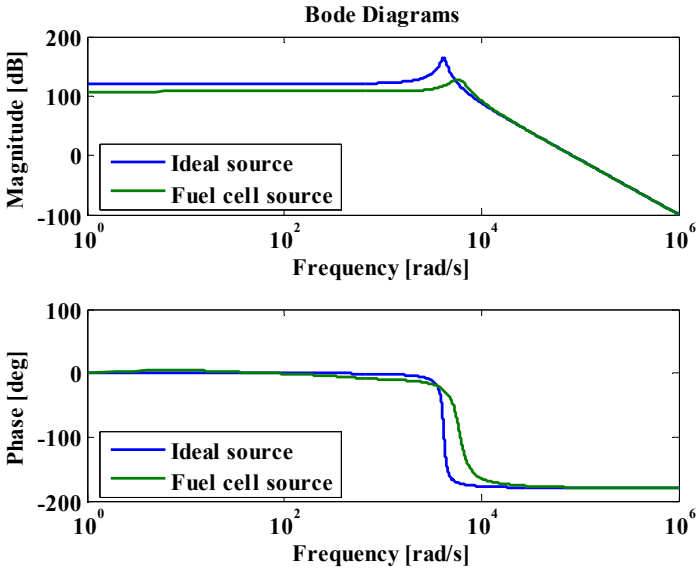

Fig. 49. Control-to-output characteristic for DC-DC converter stage supplied from ideal source and fuel cell

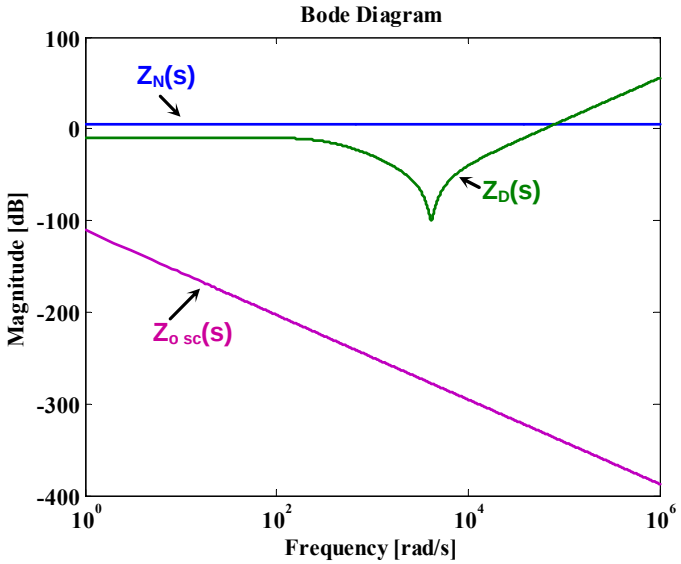

Fig. 50. Impedances for fuel cell full bridge converter with supercapacitor

4.8 Design example

4.8.1 Specifications of the proposed fuel cell powered UPS

Table X shows a typical specification of the proposed fuel cell powered UPS system. The fuel and emission specifications correspond to Ballad-Nexa fuel cell stack [46] shown in Fig. 51. Table XI shows the specifications of the Ballard-Nexa fuel cell stack. Performance ratings are largely determined by the power conditioning unit design along with the associated size of the energy storage.

TABLE X
SPECIFICATION OF PROPOSED FUEL CELL POWERED UPS

Performances	
Power Rating VA/W	1500 VA/1080 W
Technology	Passive stand-by
Output Voltage/Frequency	120V± 3%, 50/60 Hz ± 0.5 %
Overload Capacity	>110% <130% : 12s then on by-pass, >130% : 1.5s then on by-pass
Current Ripple	120 Hz, 24.7% RMS 35% peak-peak
Fuel	
Composition	99.99% dry gaseous hydrogen
Consumption Rate	900 standard liters of hydrogen/kWhr
Supply Pressure	75 PSIG
Emissions (Water and Heat)	
Water Exhaust Rate	750 ml/kWhr
Heat Exhaust Rate	1.5 kW/1 kW electricity produced

TABLE XI
SPECIFICATIONS OF THE BALLARD-NEXA FUEL CELL STACK

Performance :	Rated net power Rated current DC voltage range Operating lifetime	1200 watts 46 Amps 26 to 50 Volts 1500 hours
Fuel :	Composition Supply pressure Consumption	99.99% dry gaseous hydrogen 10 to 250 PSIG ≤ 18.5 SLPM
Operating Environment :	Ambient temperature Relative humidity Location	3°C to 30°C *(37°F to 86°F)* 0% to 95% Indoors and outdoors
Physical :	Length x width x height Weight	56 x 25 x 33 cm *(22 x 10 x 13 in)* 13 kg *(29 lbs)*
Certification :		CSA, UL
Emissions :	Liquid water Noise	0.87 liters *(30 fluid oz.)* maximum per hour2 ≤ 72 dBA @ 1 meter
Integration :	Fuel interface Electrical interface Control interface	45° flared tube fitting for 1/4" OD tubing – metallic #8 AWG electrical wire Full duplex RS 485

4.8.2 Fuel capacity

In this section a method to calculate the amount of hydrogen required to supply 1 kWh is shown. The [47-49] detail an approach from the chemical engineering point of view. However, a more simplistic approach is presented here with some assumptions.

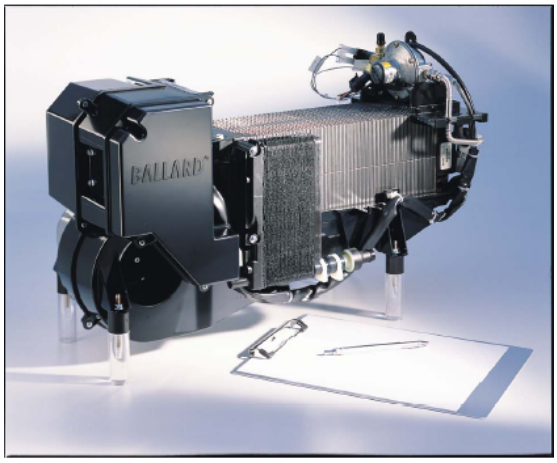

Fig. 51. Ballard Nexa fuel cell

The required output power = *1 kW*

The hydrogen density is = *0.09 kg/m^3*

Specific heating value of hydrogen is = *120 MJ/kg*

This is the energy that we can get by burning the hydrogen, which is its theoretical maximum. Only part of this energy can be utilized to produce the electricity via fuel cell due to other losses as explained below. A typical PEM fuel cell efficiency can be calculated as follows:

$$PEM\,Fuelcell\,efficiency =$$

$$= \frac{Actual\ fuel\ cell\ output\ voltage}{Theoretical\ output\ voltage} * (Fuel\,utilization) * (\frac{Net\ power\ produced}{Total\ power\ produced}) * 100$$

Assuming:

The actual fuel cell voltage = *0.7 V/per-cell*

Theoretical fuel cell voltage = *1.25 V/per-cell*

Hydrogen fuel utilization = *95%*

(i.e. 5% of hydrogen fuel is wasted during purging)

$$\frac{Net\ power\ produced}{Total\ power\ produced} = 0.9$$

(i.e. 10% of the energy is used to power the balancing plant)

$$PEM\,Fuelcell\,efficiency = \frac{0.7}{1.25} * (0.95) * (0.9) * 100 = 48\%$$

Since,

*1 kWh = 1000 Wh = 1000*3600 Ws = 3.6 MJ (mega-joules)*

Weight of the required hydrogen =

$$\frac{3.6\ MJ}{Specific\ heating\ value\ of\ hydrogen} * \frac{1}{PEM\ \ Fuel\ cell\ efficiency}$$

$$= \frac{3.6\ MJ}{(120\ MJ) * (0.48)} = 0.0625\ Kg \qquad (18)$$

Since 0.09 kg of hydrogen needs 1000 liters,

Now, 0.0625 kg of hydrogen needs = 1*000*0.0625/0.09 = 694.5* liters at 1 bar or 14.5 lbf/in^2

At 150 bar, the volume of hydrogen is: 694.5/150 = 4.63 liters

Therefore, 4.63 liters of hydrogen fuel at 150 bar is required for powering a 1 kWh load.

4.8.3 Supercapacitor sizing

The energy stored in a supercapacitor is given by:

$$W_j = \frac{1}{2} CV^2 \tag{19}$$

Since the energy stored in the supercapacitor is directly proportional to the square of the voltage, a drop of 30% in its voltage (1 pu to 0.7 pu) represents the release of 50% of the stored energy. The internal losses due to the equivalent series resistance (ESR) also need to be accounted for. Adopting this discharge strategy, the following equation can be written as:

$$\frac{1}{2}\left[CV^2 - C(0.7V)^2\right] \cdot k = P_{shortage} \cdot t \tag{20}$$

where, C is the required capacitance of the supercapacitor, k is the efficiency, which is less than 1 due to ESR loss. $P_{shortage}$ is the amount of power shortage in Watts due to the system delay or overload and t is the specified duration for those events. The proposed UPS system should be capable of supplying the 130% of the rated power for 12 s and 140% of the rated power for 1.5 s seconds. For the proposed system, more limiting constraint is the 130% rated power for 12 s, therefore we will size the supecapacitor according to this. Assuming that the maximum voltage that a supercapacitor needs to sustain is 43 V, $P_{shortage}=130\% P_{rated}W$; $t=12$ *s* and $k=0.9$; the required capacitance value can be calculated by substituting these values in (20).

$$C = \frac{4 \cdot P_{shortage} \cdot t}{k \cdot V^2} = \frac{4 \cdot 1.3 \cdot 1080 \cdot 12}{0.9 \cdot 43^2} = 40.5\ F \tag{21}$$

One way this can be achieved is by connecting sixteen of commercially available supercapacitors (650 F, 2.7 V) in series. Detailed specification for the supercapacitor is presented in the Table XII. The amount of capacitance calculated to provide power during overload conditions is sufficient to ensure that the impedance inequalities (6-9) are met as can be seen from Fig. 50.

TABLE XII
SPECIFICATION OF SUPERCAPACITOR, BCAP0650 P270 (MAXWELL TECHNOLOGIES)

Capacitance	650 Farads (±20%)
Maximum ESR(25°C)	0.8 mOhms
Specific Power Density	5400 (W/kg)
Voltage(Cont.)	2.7 V
Maximum Current	3500 A
Dimensions	51.5 x 60.0 mm
Weight	1200 g
Volume	0.211 l
Temperature (Operating & Storage)	-40°C to 65°C
Leakage Current (12 hours, 25°C)	1.5 mA

4.8.4 Full bridge converter design

The objective of the design example is to outline step by step calculations of switch voltage/current ratings, DC-link capacitor values, and L-C output filter values to meet the specifications.

Fuel cell power output $P_{out} = 1200\ W$. A nominal fuel cell input voltage, $V_{in} = 26\ V$, is assumed. An output voltage, $V_o = 200\ V$ is generated using the phase shift control. The

switching frequency is set at 50 kHz. The fuel cell current is calculated for its lowest voltage condition ($V_{in} = 26\ V$) as

$$I_{in} = \frac{1200}{26} = 46.15\ A \tag{22}$$

The full bridge DC-DC converter shown in Fig. 39 uses four switches, Q_1 to Q_4. To obtain the output voltage of 200 V for the full bridge converter, a turns ratio of $n = 16$ is selected for the transformer. The duty ratio is defined as the time when the energy is transferred from the primary to the secondary circuit, or when the pairs Q_1, Q_4 or Q_2, Q_3 are conducting. For the full loading condition duty cycle is 0.48 which causes the switch rms current to be:

$$\begin{aligned} I_{Q1,2-rms} &= nI_o\sqrt{\frac{D_t(2+d)}{24} + \frac{(1-2D)}{8}\left[\frac{1}{3} + (1+d)^2\right]} = 37.6\ A \\ I_{Q3,4-rms} &= nI_o\sqrt{\frac{D_t(2+d)^2}{24}} = 36.6\ A \quad and \\ D_t &= \frac{2+d}{1+d}D = 0.814 \end{aligned} \tag{23}$$

where d is defined as secondary current undershoot ratio [45] and is assumed to have value of 0.3.

For the secondary diodes, the average current in each diode is equal to the half of the output current and the maximum and the minimum values are given by:

$$\begin{aligned} I_{Ds1,2-max} &= I_o + \frac{dI_o}{2} = 6.21\ A \\ I_{Ds1,2-min} &= -\frac{dI_o}{2} = 0.81\ A \end{aligned} \tag{24}$$

The reverse blocking voltage is equal to the transformer secondary voltage,

$$V_{reverse} = nV_{in} = 416\,V \tag{25}$$

Voltage and current ratings of the transformer are:

Primary voltage, $V_p = V_{in}\sqrt{2D} = 25.5V$

Secondary voltage $V_s = nV_{in}\sqrt{2D} = 408\,V$

Primary current, $I_p = 54.68\ A$

Secondary current $I_s = 3.42\ A$

The VA rating of the transformer is defined as the sum of the total primary and secondary winding VA divided by two,

$$VA_{tr} = \frac{1}{2}\left(V_{in}\sqrt{2D}I_p + nV_{in}\sqrt{2D}I_s\right) = 1.395\,kVA \tag{26}$$

4.8.5 Inverter output filter design considerations

Fig. 52 below shows the topology for the inverter output filter. A transfer function is derived using the schematic in Fig. 52. The assumptions used in the analysis are: the output filter is lossless and the third current harmonic current is 80% of the fundamental current rms value.

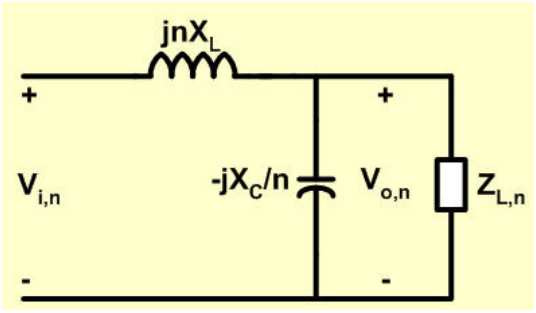

Fig. 52. Topology of a DC-AC output filter

The transfer function for this type of L-C filter is described by the equation:

$$H_n = \frac{V_{o,n}}{V_{i,n}} = -\frac{jX_C \cdot Z_{L,n}}{nX_L X_C + jZ_{L,n}(n^2 X_L - X_C)}, \tag{27}$$

where:

H_n - transfer function

$V_{o,n}$ - output voltage harmonic

$V_{i,n}$ - input voltage harmonic

X_C - capacitive impedance component

X_L - inductive impedance component

$Z_{L,n}$ - load impedance

n - harmonic

For first harmonic $H_1 \to 1$; or $X_L << X_C$, then

$$H_1 \leq \frac{-jX_C \cdot Z_{L,1}}{-jZ_{L,1} \cdot X_C} \cong 1 \tag{28}$$

Also, for a no load condition, $Z_{L,1} \to \infty$, therefore equation (27) is:

$$|H_n| = -\frac{X_C}{n^2 X_L - X_C} = \frac{1}{n^2 \cdot \frac{X_L}{X_C} - 1} \tag{29}$$

To satisfy a THD requirement of less than 5%

$$\frac{1}{n^2 \cdot \frac{X_L}{X_C} - 1} \leq 0.045 = \frac{X_L}{X_C} \geq \frac{23.222}{n^2} \tag{30}$$

An equivalent circuit model used in finding the filter characteristics for a non-linear load is shown in Fig. 53.

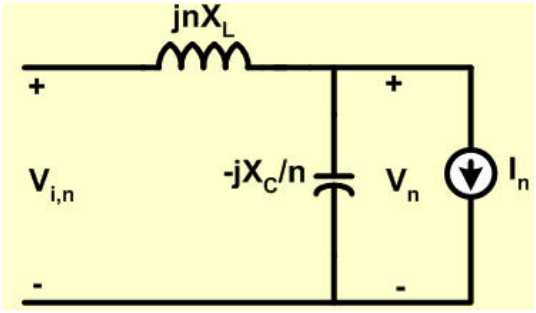

Fig. 53. Equivalent circuit for a non-linear load

The transfer function for this schematic is described by equation

$$V_n = \frac{jnX_L \cdot X_C}{X_C - n^2 X_L} \cdot I_n , \tag{31}$$

where:

V_n - equivalent output voltage at nth harmonic

n - harmonic

I_n - load current at nth harmonic

X_C - capacitive impedance component

X_L - inductive impedance component

Equation (31) can then be shown as:

$$|V_n| = \frac{nX_L}{1 - n^2 \frac{X_L}{X_C}} \cdot I_n . \tag{32}$$

Here $\frac{X_L}{X_C}$ is very small making $n^2 \frac{X_L}{X_C} << 1$

$$|V_n| \le nX_L \cdot I_n \tag{33}$$

For the third harmonic $n = 3 \therefore$

$\frac{|V_3|}{V_1} = \frac{3X_L \cdot I_3}{V_1}$, where THD is $\frac{|V_3|}{V_1} = 0.03$ or 3%. Inductor impedance can be found by:

$$X_L = \frac{0.03 \cdot V_1}{3 * I_3} \tag{34}$$

Let f_s be defined as the switching frequency and f_1 be defined as the fundamental frequency. Then for $f_s = 20\,kHz$, $f_1 = 60\,Hz$, and $n = \frac{f_s}{f_1} = 333.33$, $\frac{X_L}{X_C} \ge 2.09x10^{-4}$ the filter resonant frequency f_r can be found with

$$\frac{f_r}{f_1} = \sqrt{\frac{X_C}{X_L}} \le \sqrt{\frac{n^2}{23.222}} \le 69.17 \tag{35}$$
$$f_r \approx 4150.3Hz$$

The 1kW inverter with $V_1 = 120\,V$, produces $I_1 = 8.33\,A$, $I_3 = 0.8 \cdot I_1 = 6.67\,A$. Using (34) X_L is found to be $X_L = 0.18$. Then, using

$$L = \frac{X_L}{2\pi f_1}, \tag{36}$$

where

L - inductance

f_1 - fundamental frequency

X_L - inductive impedance component

where $f_1 = 60Hz$, the inductance will be $L = 477.46\,\mu H$.

To find the capacitor impedance we use (30), and get $X_C = 861.24$, then using

$$C = \frac{1}{2\pi f_1 \cdot X_C} \tag{37}$$

where

C - capacitance

X_C - capacitive impedance component

f_1 - fundamental frequency

and $f_1 = 60\,Hz$, capacitance turns out to be $C = 3.08\,\mu F$.

4.9 Conclusion

In this chapter, a fuel cell powered, passive stand-by single-phase UPS system has been discussed in detail. It has been shown that the proposed topology provides stable power to the load when the utility is interrupted. A mathematical approach to analyze the interactions between the internal impedance of the fuel cell and the DC/DC converter closed loop control to verify steady state and transient stability has been presented. It has been shown that the fuel cell's dominant time constant is load dependent and varies from 8.97ms (light load) to 20.37ms (full load) resulting in fuel cell's relatively slow dynamic response. Design inequalities have been reviewed to better understand the interaction between the DC/DC converter and fuel cell during potential instability conditions. A method to size the supercapacitor module was incorporated to overcome the load transients such as instantaneous power fluctuations, slow dynamics of the fuel

preprocessor and overload conditions. It has been shown that the supercapacitor values calculated for overload conditions were sufficient to enhance stability and improve dynamic response of the fuel cell. A complete design example illustrating the amount of hydrogen storage required for 1 hour power outage and sizing of supercapacitors for transient load demand has been presented for a 1.5kVA UPS. In conclusion, an environmentally friendly and clean power back-up system has been proposed.

CHAPTER V

HIGH MEGAWATT CONVERTER TOPOLOGIES FOR FUEL CELL BASED POWER PLANTS

5.1 Introduction

Fuel cells have been recognized as one of the most promising energy sources for power generation in the near future. In particular, high temperature fuel cells such as solid oxide fuel cell (SOFC) and molten carbonate fuel cell (MCFC) have sufficient potential in terms of overall system efficiency and operation costs to compete with conventional power plants in the mega watt (MW) power range [9]. Typical efficiency of conventional power plants ranges from 38% to 40%, whereas the efficiency of a SOFC is in the range of 55-60%; consequently, fuel cell based plants have efficiency around 20% higher that conventional systems. On the other hand the cost of generating power in a fuel cell based plant is slightly higher than in conventional systems (0.12 $/kWh) [9].

The fuel cell stack is interfaced with the AC grid, usually at the medium voltage distribution level, via a converter transformer unit [10]. Since each individual cell produces only 0.6 V, there is a maximum number of cells that one can stack before thermal/water management issues arise. Additionally, electrostatic potential to ground within the fuel cell stack needs to be limited for safe operation. Considering the above limitations the maximum voltage that a fuel cell stack can safely produce is around 350

V [11]. To achieve a higher DC link voltage, two stacks can be connected in series and their mid points tied to ground.

The power converter is usually constructed using a two stage approach (Fig. 54) having a DC-DC converter connected in series with a DC-AC inverter. Fig. 54 and Fig. 55 show the conventional approach in which each fuel cell stack is connected to a dedicated power electronic converter (DC-DC and DC-AC) interfaced to electric utility. Section 5.3 shows several other possible power electronics topology configurations. The aim of this Chapter is to study the various possible ways in which fuel cell stack and power electronics can be interfaced with utility and ways of converting the available DC power to AC power. The various topologies are then compared for performance, component count, cost, usage of magnetics, etc.

The switching mode nature of the power converters generates common mode voltage with respect to ground. The presence of high frequency common mode voltage contributes to circulating ground currents which can interfere with ground fault protection system and also contribute to neutral shift and electro magnetic interference (EMI). Another aim of this chapter is to present an analysis of common mode voltage in the converter topologies and discuss several mitigation methods.

5.2 Conventional approach

Fuel cell mega watt power systems can be configured to directly connect to the utility to supply power as shown in Fig.54. Similar to the low-power case, fuel cell stacks in this power range have relatively low voltage (less than 1 kV DC) and high

current output characteristics (around 1000 A). On the other hand, the desired output voltage is much higher (2.3, 3.3, 4.16, 6.9 or 18 kV AC) which generates the huge gap between these two values and makes the design of power electronics inverters, which should have high input current and high output voltage handling capabilities, a challenge.

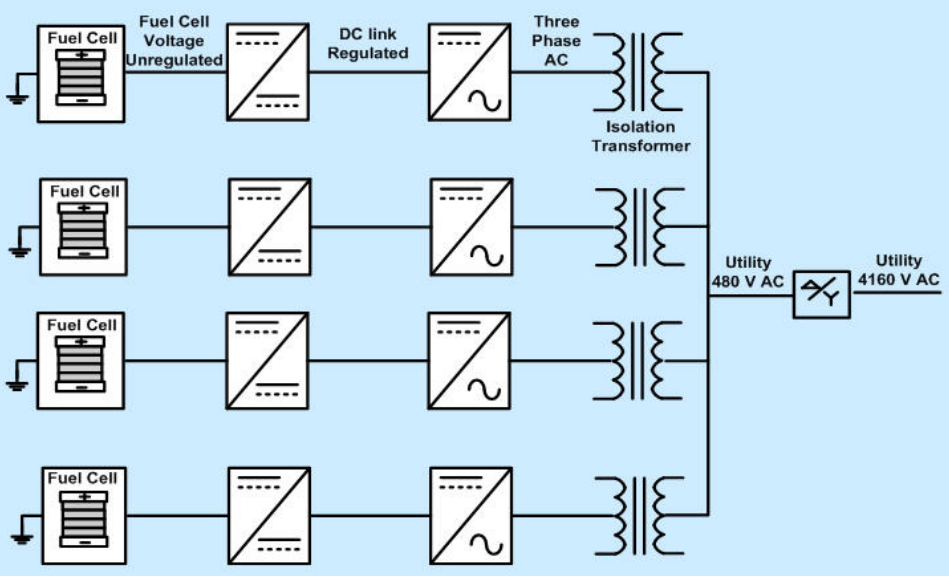

Fig. 54. Conventional multi stack fuel cell system with line-frequency transformer

Fig. 54 shows the conventional multi stack fuel cell system with line-frequency transformer and low-voltage (LV) inverters for supplying power to the utility. Each fuel cell stack rated for 350 V, 0.35 MW is followed by a non-isolated DC-DC converter that increases and regulates the voltage to the DC-AC inverter to 800 V level (minimum DC-link voltage to generate 480 V AC output from a three phase inverter). Inverters with constant DC inputs are easier to control and are not limited by the minimum voltage of the fuel cell. Inverter uses commercially available, low cost 1200 V IGBTs as switching

devices which are very efficient in this voltage range and could switch at high frequencies (tens of kHz).

Fig. 55 shows a conventional multi stack fuel cell system with the isolated DC-DC converter which is a variation of the previous topology. The weight and size disadvantage of the line-frequency transformer (50/60 Hz) is surpassed by using the high frequency transformer.

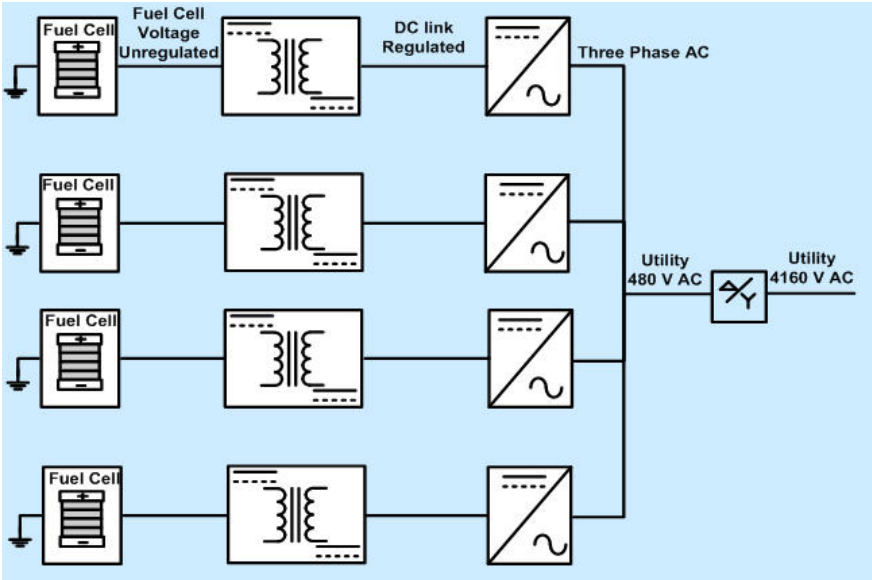

Fig. 55. Conventional multi stack fuel cell system without line-frequency transformer

Inductors and capacitors are required for these inverters to stabilize the DC bus and sink the current if diode rectifiers are used at the front [50]. Inductors and capacitors on the DC bus not only increase the cost but, due to their relatively short life span, reduce the system's reliability.

Single-stage power conversion topology shown in Fig. 56 connects the DC-AC inverter directly to the fuel cell without the use of DC-DC converter in front resulting in a complex control scheme. The disadvantages of this control strategy are that the AC output voltage is limited by the minimum voltage of the fuel cell and the inverter must be rated for a higher power than it is intended to be used for. The advantages include the relatively low production cost because of lower component count. For all three conventional topologies an output filter creates a smooth sinusoidal voltage before the output is connected to the utility. A disadvantage of the single-stage strategy is that it requires much larger and more expensive filters than the two-stage strategies (Fig. 54 and Fig. 55). The DC-DC stage of the two-stage implementation helps to reduce the ripple seen by the fuel cell, so less filtering is required.

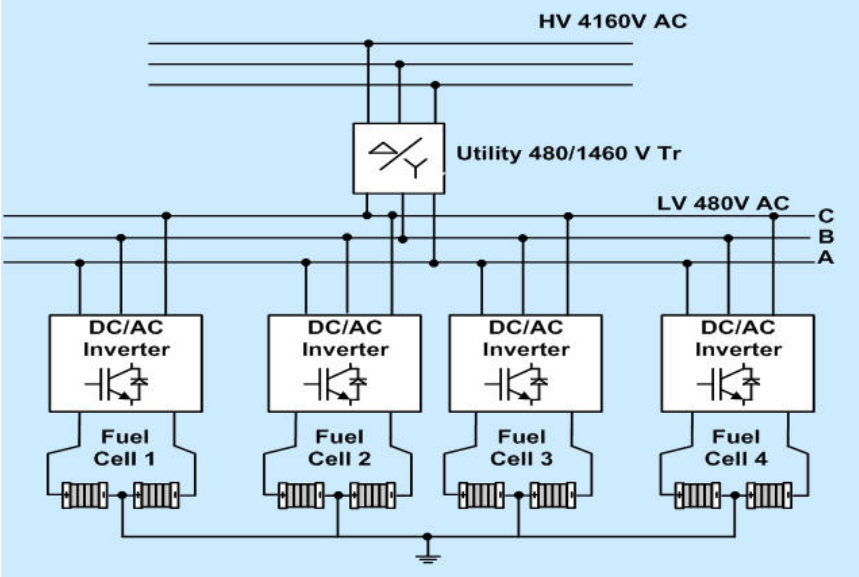

Fig. 56. Single-stage power conversion topology

All of the above presented conventional topologies are modular systems where the failure in power electronics and/or a fuel cell in only one unit does not affect the performance of the entire system. Fuel cells can share a common fuel supply and heat exchangers, which reduces the overall cost. In addition, ability to bias current of individual stack pairs provides compensation mechanism for air and fuel flow asymmetries.

5.3 Novel high mega watt topologies

In recent years, industry has begun to demand higher power equipment, which now reach the mega watt levels. Fuel cell based power plants in the mega watt range could be connected to the medium voltage network. Today, it is hard to connect a single power semiconductor switch directly to medium voltage grids (2.3, 3.3, 4.16, or 6.9 kV). For those reasons, a new family of multilevel inverters has emerged as the solution for working with higher voltage levels [51–54].

5.3.1 Topology #1

Fig. 57 shows a medium voltage topology #1 where two fuel cell stack systems followed by an isolated DC-DC converter and DC-AC inverter are connected to 2.3 KV utility. Output of DC-DC converter is set to 3500 V as shown in Fig. 57.

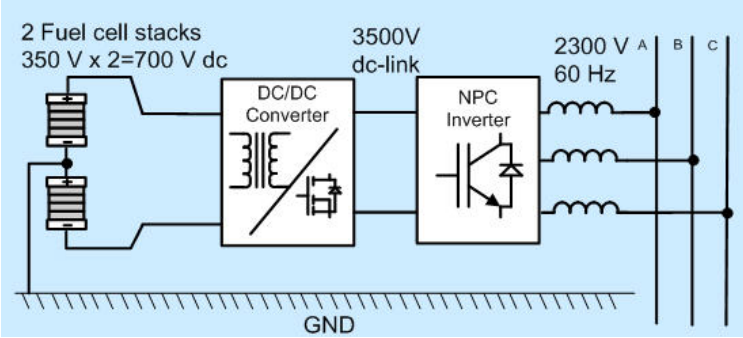

Fig. 57. Medium voltage topology #1

A three-phase neutral-point clamped (NPC) inverter with either IGBT or IGCT devices could be used depending on the level of the inverter (3-level NPC inverter with IGCTs or 7-level NPC with IGBTs to match different semiconductors voltage ratings). Low switching frequency (2 kHz) requires larger filters when IGCTs are used. One of the advantages of using a medium voltage inverter is that the semiconductor switches in the inverter require a lower current, therefore resulting in higher efficiencies.

5.3.2 Topology #2

The medium voltage topology #2 shown in Fig. 58 employs four fuel cell stacks with two cascaded isolated DC-DC converters and one DC-AC inverter and is connected to 4.16 kV utility. This topology offers flexibility in control of fuel cell stack pairs. Independent control of DC-DC converters is possible to allow each pair of fuel cell stacks to supply different output power if needed. Higher voltage and current rating IGCT/IGBT devices are used in this DC-AC inverter, which decreases the number of devices used in the system.

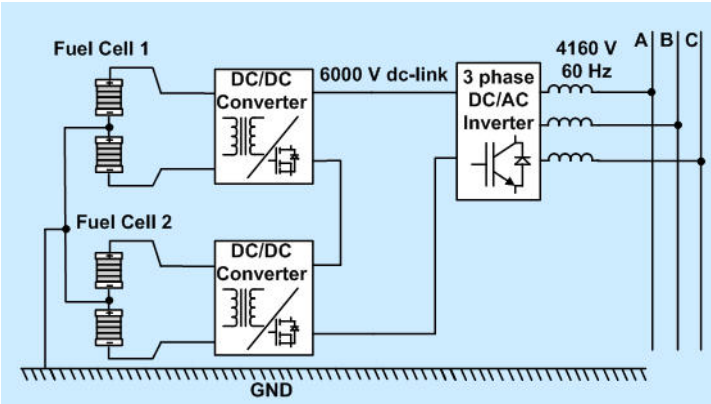

Fig. 58. Medium voltage topology #2

5.3.3 Topology #3

The medium voltage topology #3 shown in Fig. 59 is a variation of the previous topology with an 11-level NPC inverter designed with low-voltage IGBTs instead of previous high-voltage (HV) devices. An 11-level PWM output voltage is high quality and suitable for 4.16 kV, 60 Hz utility interface eliminating the need for output filters.

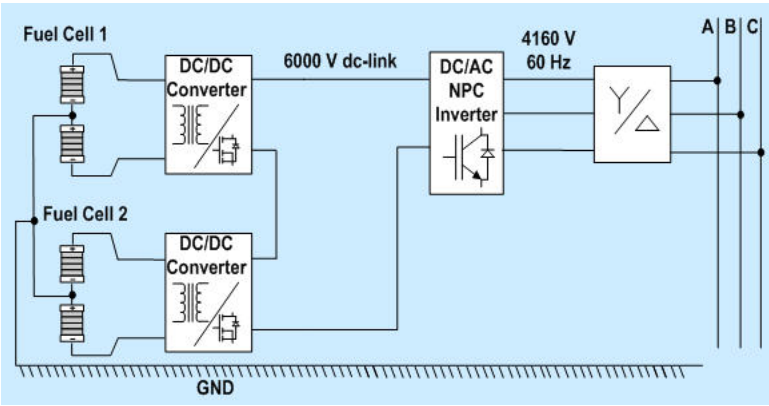

Fig. 59. Medium voltage topology #3

5.3.4 Topology #4

A cascaded multilevel inverter topology is shown in Fig. 60. It is based on the series connection of single-phase inverters with separate fuel cell stack systems. Fig. 60 shows the power circuit of a 7-level inverter with three cells ($N_c=3$) in each phase. The resulting phase voltage is synthesized by the addition of the voltages generated by different cells. Each single-phase full-bridge inverter generates three voltages at the output: +Vdc, 0, and –Vdc. The resulting output AC voltage swings from -3Vdc to 3Vdc with seven levels, and the staircase waveform is nearly sinusoidal, even without filtering [54].

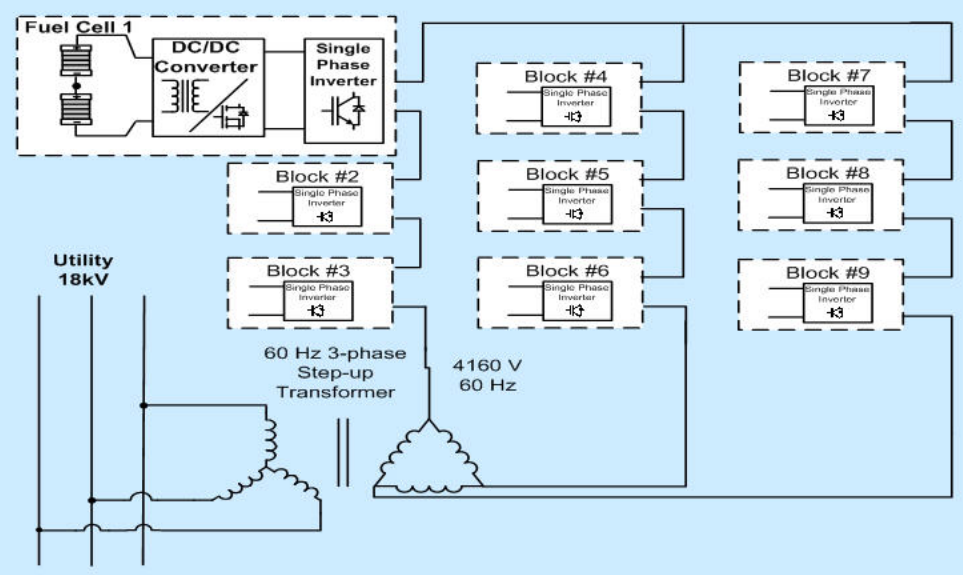

Fig. 60. Cascaded multilevel inverter topology

A classical SPWM with phase shifted (120^o) triangular carriers using either the same control voltage or selective harmonic elimination control produces a voltage with the smallest distortion. Another control option could be the injection of a third harmonic in

each cell, which is a very common practice in industrial applications to increase the output voltage for the multilevel inverters [55], [56]. An additional advantageous feature of multilevel SPWM is that the effective switching frequency of the output voltage is N_c times the switching frequency of each cell, as determined by its carrier signal. This property allows a reduction in the switching frequency of each cell, thus reducing the switching losses.

5.3.5 Topology #5

A hybrid multilevel inverter topology combines neutral-point clamped IGCT 3-phase inverter with 2 kV DC-bus and neutral-point clamped IGBT 3-phase inverter with 1 kV DC-bus to obtain higher output voltage, as shown in Fig. 61.

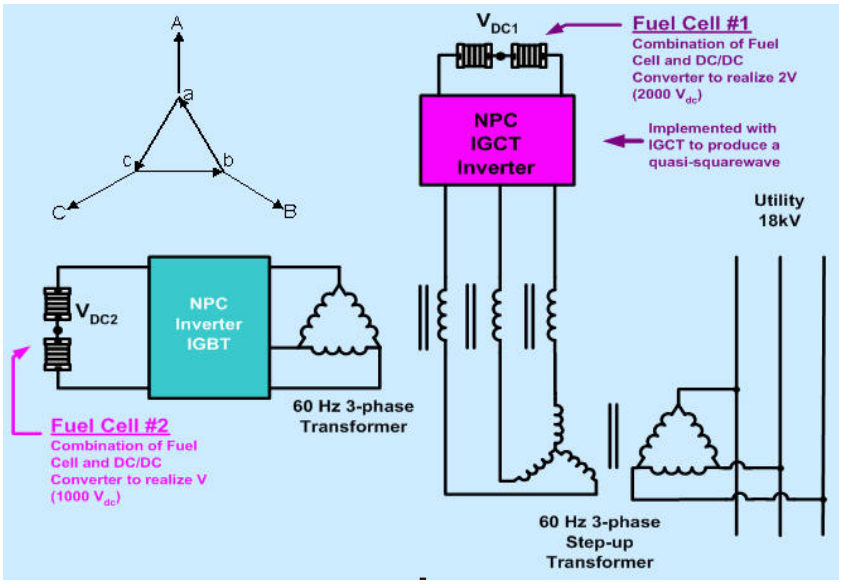

Fig. 61. Hybrid multilevel inverter topology

This topology uses an output transformer to add the output voltages of each inverter. In order for the inverter output voltages to be added up, the inverter outputs must be synchronized with a separation of 120^{o} between each phase as shown in Fig. 61. It is well known that the switching capability of IGCT devices is limited at higher frequencies [57]. Hence, a hybrid modulation strategy which incorporates stepped synthesis in conjunction with variable pulse width of consecutive steps has been presented in [58]. Under this modulation strategy, the IGCT inverter is modulated to switch only at fundamental frequency of the inverter output, while the IGBT inverter is used to switch at a higher frequency [59]. With this hybrid topology and modulation strategy, the high quality PWM output voltage depends on the IGBT switching, while the overall voltage generation is decided by the voltage ratings of the IGCTs.

5.4 Comparison

Conventional multi stack fuel cell systems with/without the line-frequency transformer and single-stage power conversion topology have very high cost because of bulky line-frequency transformers (boost voltage from 480 V level to medium voltage level of 2.3 or 4.16 kV) and reactive components. Further, scaling these topologies to higher power and higher voltage applications would result in high part count which in turn decreases cost effectiveness.

On the other side the most attractive features of multilevel inverters are as follows:

- They can generate output voltages with extremely low distortion and lower dV/dt.

- They draw input current with very low distortion.
- They generate smaller common-mode (CM) voltage and implementation of sophisticated modulation methods can entirely eliminate common-mode voltages [60].
- They can operate at a lower switching frequency, reducing the switching losses and EMI.

Table XIII outlines the summary of key parameters for five mega watt topologies introduced in the previous sub-chapters.

TABLE XIII
MEGA WATT TOPOLOGIES SUMMARY

Topology # 1	2 fuel cell stacks (350 V) series connected and center point grounded, 1 DC-DC converter followed by a 3-level NPC (IGCT) (or 7-level NPC IGBT) inverter to produce 2300 V 3- phase AC
Topology # 2	4 fuel cell stacks (350 V) series connected in pairs and center point grounded, 2 DC-DC converters with outputs connected in series, followed by a 3-level inverter to produce 4160 V 3-phase AC, control flexibility, HV devices
Topology # 3	4 fuel cell stacks (350 V) series connected in pairs and center point grounded, 2 DC-DC converters with outputs connected in series, followed by a 11-level NPC inverter to produce 4160 V 3-phase AC, control flexibility, LV IGBT, no need for output filter
Topology # 4	Each fuel cell stack (350 V) (18 total) connected to isolated DC-DC converters (9 total), followed by a 1-phase LV inverter (9 total). Several such modules are connected in cascade to form one MV AC system, LV power electronics, no need for output filter
Topology # 5	Fuel cell stacks (4 total) followed by DC-DC converter (2 total) and 3- phase inverters (2 total). Several of these modules are combined together via 3-phase transformers to realize a multilevel inverter system for medium voltage. HV and LV devices are combined, no need for output filter

Table XIV compares the topologies with respect to the component count in the DC-DC and DC-AC stages and their ratings, the use of magnetics (filters and transformers), the complexity of the implemented modulation, the switching frequency and roughly estimated cost. In general, the need for output filter and transformer increases the cost of the system because of the large size and price of such devices. Some topologies do not require use of output filters; as a result, the complexity of the modulation schemes in these topologies is higher in order to maintain the quality of the output signal.

TABLE XIV
MEGA WATT POWER TOPOLOGY COMPARISON

Topology	DC-DC component count (rating)	DC-AC component count (rating)	Output filter	Transformer	Modulation complexity	Switching frequency	Roughly estimated cost
# 1a	400 MOSFETS (700 V, 20 A) 192 diodes (8 kV, 4.2 A)	12 IGCT (2.1 kV, 500 A) 6 diodes (2.2 kV, 305 A)	BIG	NO	SIMPLE	2 kHz	$ 725700
# 1b	400 MOSFETS (700 V,20 A) 192 diodes (8 kV, 4.2 A)	252 IGBT (900 V, 75 A) 270 diodes (700 V, 35 A)	SMALL	NO	MEDIUM	20 kHz	$ 554400
# 2	400 MOSFETS (700 V,20 A) 56 diodes (4.8 kV, 10.2 A)	6 IGCT (6.5 kV, 500 A) 0 diodes	MEDIUM	NO	SIMPLE	20 kHz	$ 607300
# 3	400 MOSFETS (700 V,20 A) 56 diodes (4.8 kV, 10.2 A)	420 IGBT (900 V, 75 A) 216 diodes (700 V, 35 A)	NO	NO	MEDIUM	20 kHz	$ 505800
# 4	360 MOSFETS (700 V, 20 A) 108 diodes (1.2 kV, 35 A)	72 IGBT (1.2 kV, 110 A) 0 diodes	NO	NO	MEDIUM	12.6 kHz	$ 363700
# 5	380 MOSFETS (700 V, 20 A) 8 diodes (2 kV, 200 A) 12 diodes (1 kV, 110 A)	36 IGBT (600 V, 400 A) 12 IGCT (1.2 kV, 500 A) 18 diodes (500 V, 300 A) 6 diodes (1 kV, 430 A)	NO	YES	HIGH	2.88 kHz	$ 915100

When it comes to the switching devices, the higher the component count, the higher the cost. This is particularly true for high voltage rated IGCTs and IGBTs as their unit price is in the order of several thousand dollars, whereas the price of low-voltage rated IGBTs is around 10 dollars.

5.5 Common mode analysis

The connection of distributed power sources with the utility grid generally requires an electronic power converter for processing the locally generated power and injecting current into the system. If the source provides a DC voltage, the converter must be able to produce a low-distortion high-power factor AC current. Pulse width-modulated (PWM) converters can be used to produce any voltage or current waveform. This modulation technique has been used in both DC-DC and DC-AC converters. These converters present some drawbacks, especially related to the electromagnetic interference generation, due to the high-frequency commutation [61]. A low-pass filter is necessary to attenuate the high-frequency components due to the switching process [62]. These high-frequency commutations have the effect of inducing large current spikes (due to the dV/dt) thought stray capacitance as shown in Fig. 62.

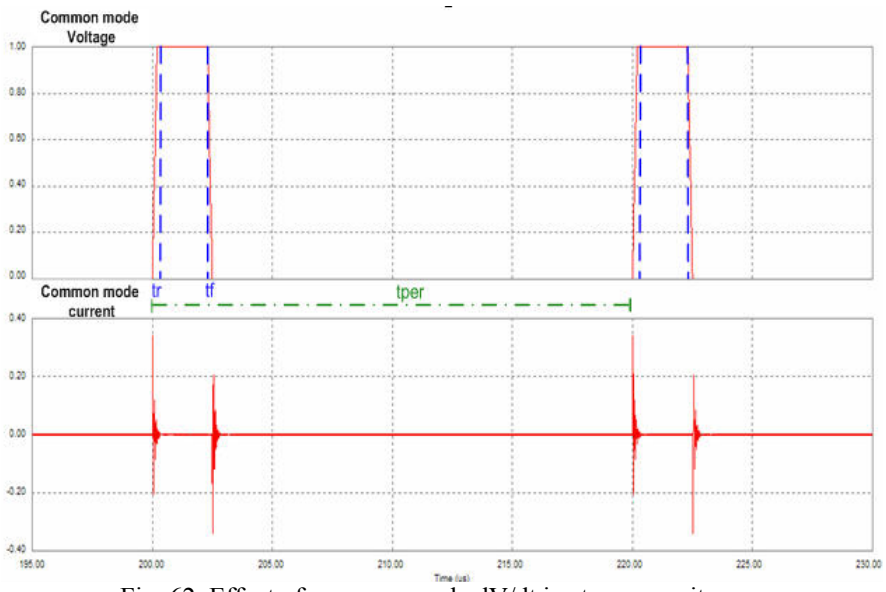

Fig. 62. Effect of common mode dV/dt in stray capacitances

The time it takes the voltage to change from one voltage level to an other is essentially controlled by the semiconductor switching time (rise and fall time). The transition time of a semiconductor is inherent to the technology used for the particular device. For example the transition times for insulated gate bipolar transistors (IGBTs) is in the range from 0.05 to 0.2 μs, and for metal oxide field effect transistors (MOSFETs) it ranges from 50 – 80 ns. As a result the dV/dt produced by the operation of MOSFETs can be 2.5 to 4 times larger than in the case of IGBTs. The time it takes to transition from one voltage level to another (rise time, t_r, and fall time, t_f) determines the equivalent noise coupling frequency which can be calculated as follows [63]:

$$f_n = \frac{0.38}{t_{rise}} \tag{38}$$

Thus MOSFETs generate noise in the frequency range from 4.75 MHz to 7.6 MHz. On the other hand IGBTs have a noise coupling frequency in the range from 1.6 MHz to

6.4 MHz. The coupling frequency of MOSFET devices can be up to 5 times higher than that of IGBTs. Typically a combination of MOSFET and IGBT devices is used for fuel cell applications. The reason for this is that the power conditioning units are normally constructed in a two stage approach composed of a step-up DC-DC converter and a cascaded inverter which are implemented using MOSFETs and IGBTs, respectively. Consequently, both types of noise coupling frequencies exist in these systems.

The effect of the common mode noise induced by stray common mode currents on other equipment is a function of the distance separating the noise generation and reception. Since power converters are enclosed in metal cabinets most of the electro magnetic interference is due to the conducted noise current circulating through ground. Therefore it is important to keep the circulation paths of common mode currents as short as possible.

5.5.1 Topology #1

The analysis of the generation of common-mode voltage and current in power conditioning systems is simplified if an equivalent circuit is used. From the common-mode voltage point of view each of the legs in the three phase inverter can be modeled as a switching mode voltage source from the midpoint of the DC link (denoted by “n”) to one of the output lines of the inverter. The common mode equivalent circuit for medium voltage topology #1 is given by the schematic shown in Fig. 63 regardless of the inverter type (low voltage device inverter or medium voltage neutral-point clamped inverter).

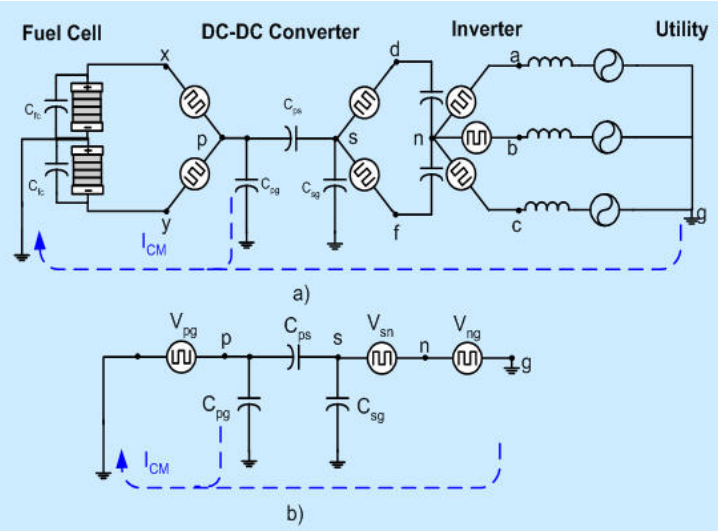

Fig. 63. Common mode equivalent circuit for medium voltage topology #1 a) detailed equivalent b) simplified equivalent

The transformer in the DC-DC converter is modeled by lumped capacitances from primary and secondary to ground, and capacitor from secondary to primary models the parasitic capacitance between two sides of the transformer. From Fig. 63 the voltage from the point "n" to ground can be calculated by:

$$V_{gn} = \frac{V_{an} - V_{ag} + V_{bn} - V_{bg} + V_{cn} - V_{cg}}{3} = \frac{V_{an} + V_{bn} + V_{cn} - (V_{ag} + V_{bg} + V_{cg})}{3} \quad (39)$$

Assuming that the utility voltage is balanced we have that $V_{ag} + V_{bg} + V_{cg} = 0$, thus

$$V_{gn} = \frac{V_{an} + V_{bn} + V_{cn}}{3} \quad (40)$$

In the same way the common mode voltage generated by the DC-DC converter and its rectifier can be calculated by

$$V_{pg} = \frac{V_{px} + V_{py}}{2} \quad (41)$$

$$V_{sn} = \frac{V_{sd} + V_{sf}}{2} \tag{42}$$

Using the equivalent common mode source V_{ng}, V_{pg}, and V_{sn} the equivalent circuit in Fig. 63a can be simplified as shown in Fig. 63b. The common mode current, I_{cm}, then can be calculated using (43) as follows

$$I_{CM\ \#1} = C_{ps}\frac{d(V_{ng} + V_{sn} - V_{pg})}{dt} + C_{pg}\frac{dV_{pg}}{dt} = C_{ps}\frac{d(V_{np} + V_{sn})}{dt} + C_{pg}\frac{dV_{pg}}{dt} \tag{43}$$

The theoretical analysis is verified using computer simulations in PSim software package. The circuit schematic used for simulating a three-phase 3-level NPC inverter with IGCT devices is shown in Fig. 64. Low switching frequency (2 kHz) requires larger filter when IGCT devices are used. The input voltage of the system is 700 V and its output is 2.3 kV (line-to-line rms), 60 Hz.

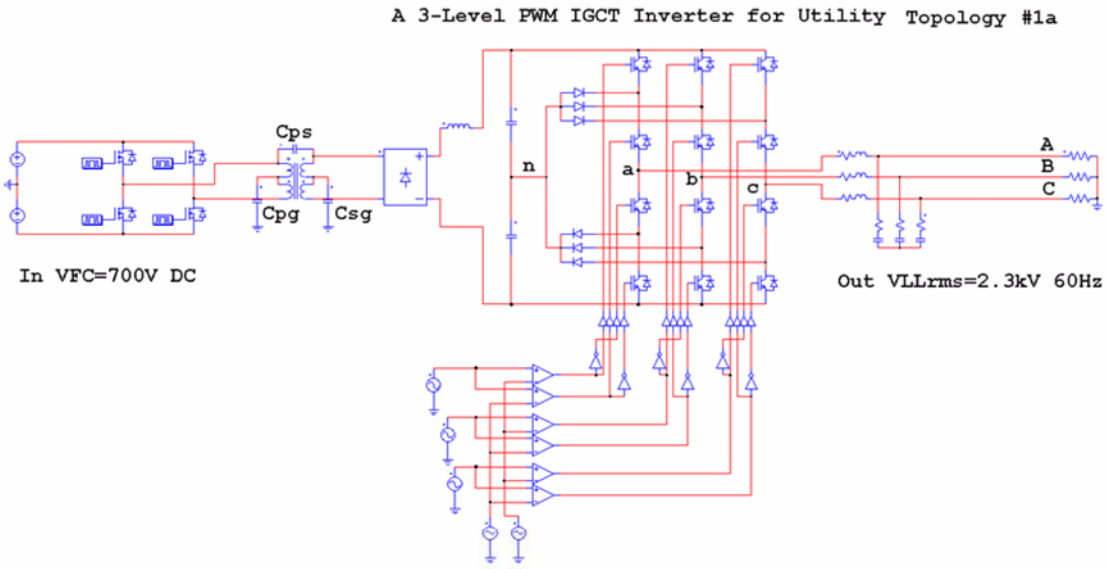

Fig. 64 Circuit schematic of medium voltage topology #1 with IGCT devices

The values used for the parasitic capacitance for the transformer are C_{pg}=200 pf, C_{sg}=200 pF, and C_{ps}=50 pF. Fig. 65 shows the resulting common mode current I_{cm}, voltage V_{an}, voltage V_{ng} and the common mode voltage of the system. From this figure it can be observed that the common mode current is as high as 15.42 A with rms value of 1.81 A.

Also circuit schematic shown in Fig. 66 is used for simulating another variation of the medium voltage topology #1 - the three-phase 7-level NPC inverter with IGBT devices, as a low voltage device case. In this case a higher switching frequency (20 kHz) is used resulting in smaller output filter. The input voltage of the system is the same as before (700 V) and its output is set to 2.3 kV (line-to-line rms), 60 Hz.

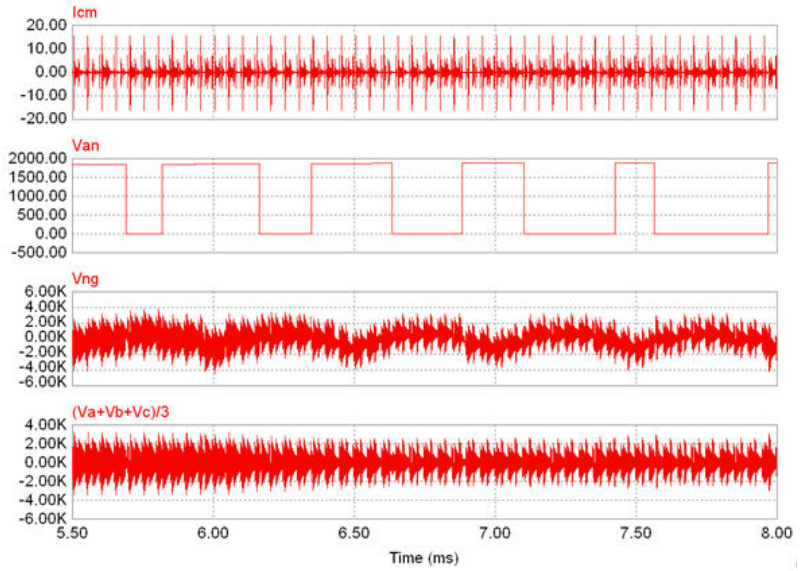

Fig. 65 Simulation result of medium voltage topology #1 with IGCT devices

Values for parasitic capacitance for the transformer stayed the same as before. Fig. 67 shows the resulting common mode current I_{cm}, voltage V_{an}, voltage V_{ng} and the

common mode voltage of the system. As can be seen from Fig. 66 the common mode current is considerably larger in this case. The peak common mode current for this case reaches 52.27 A; with rms value of 1.043 A. This is about three times higher than the previous case because this topology has considerably higher switching frequency. The magnitude of these transitions is a function of the parasitic capacitances, the magnitude of the DC-link voltage and the raise and fall time of the semiconductors as was shown in equations (38) and (43).

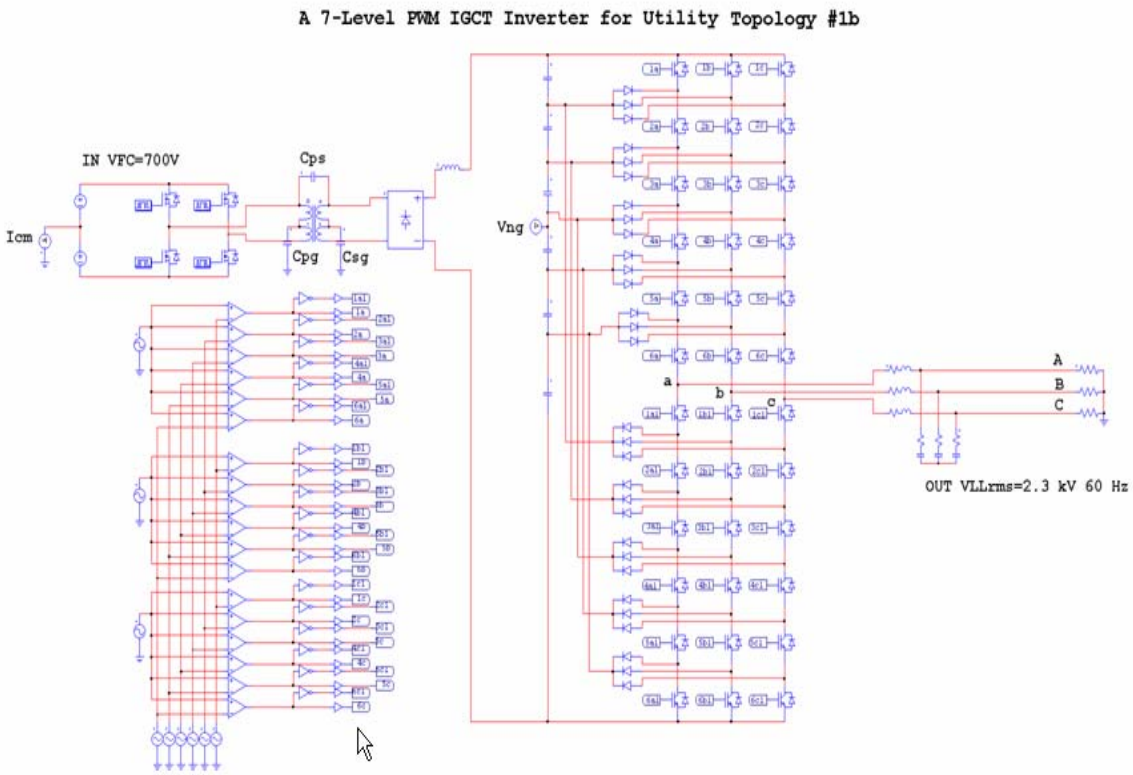

Fig. 66 Circuit schematic of medium voltage topology #1 with IGBT devices

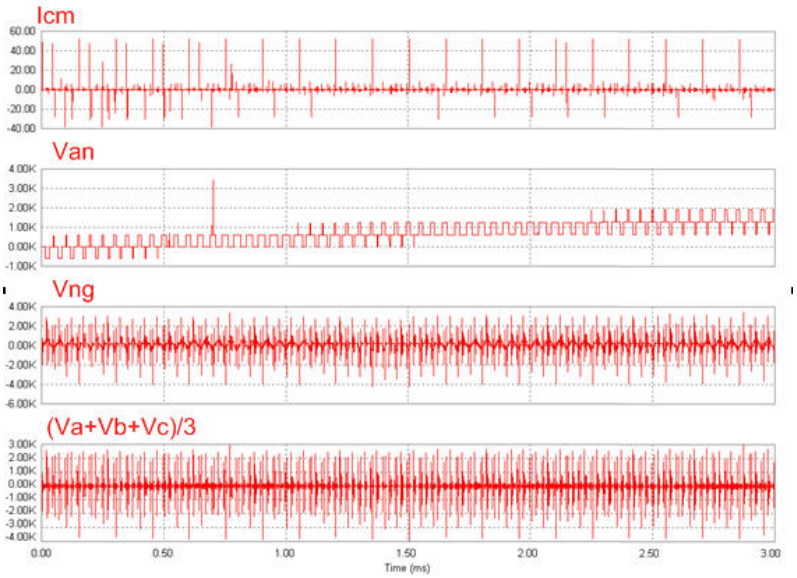

Fig. 67 Simulation result of medium voltage topology #1 with IGBT devices

5.5.2 Topologies #2 and #3

The common mode equivalent circuit for medium voltage topology #2 and topology #3 can be obtained in the same fashion as was done for the previous topology. The resulting equivalent circuit is shown in Fig. 68. From this common mode equivalent circuit one can obtain that the voltage that appears from point "n" to ground is given by (40) and the voltage at mid points of the secondary windings is then calculated using (44) and (45).

$$V_{s1n} = \frac{V_{s1d} + V_{s1f}}{2} \tag{44}$$

$$V_{s2n} = \frac{V_{s1f} + V_{s2d}}{2} \tag{45}$$

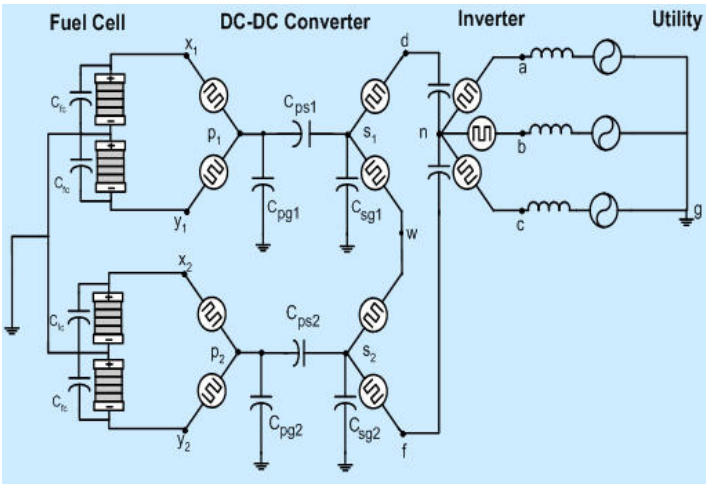

Fig. 68. Common mode equivalent circuit for topology #2

Using these equations the common mode current can be then calculated as follows.

$$I_{CM\#2} = C_{ps1}\frac{d(V_{np1} + V_{s1n})}{dt} + C_{pg1}\frac{dV_{p1g}}{dt} + C_{ps2}\frac{d(V_{np2} + V_{s2n})}{dt} + C_{pg2}\frac{dV_{p2g}}{dt} \quad (46)$$

Equation (46) clearly shows that the magnitude of the common mode current circulating through ground is generated by the operation of both DC-DC converters and the DC-AC inverter.

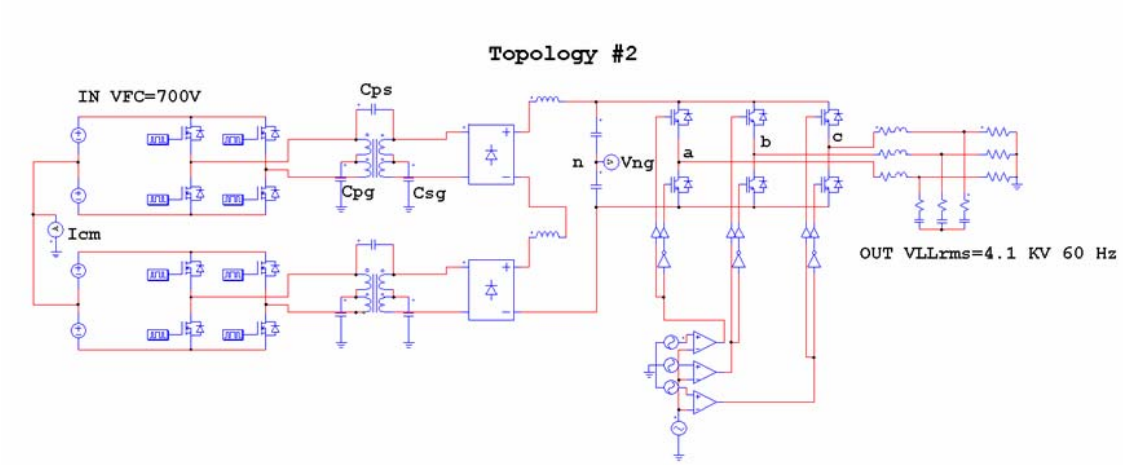

Fig. 69 Circuit schematic of medium voltage topology #2

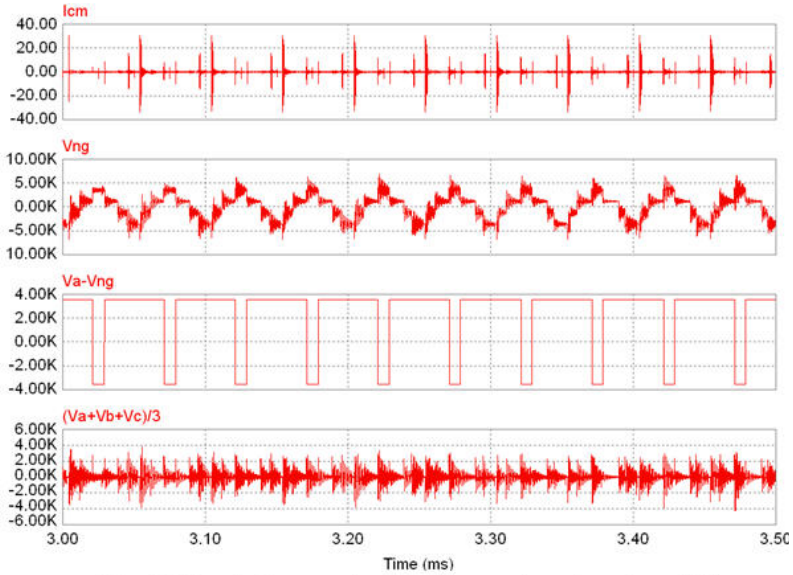

Fig. 70 Simulation result of medium voltage topology #2

A simulation of the medium voltage topology #2 shown in Fig. 69 is run in order to verify the result obtained in equation (46), and the resulting common mode current is shown in Fig. 70. The input voltage of the system is 700 V for each DC-DC converter and system's output is 4.16 kV (line-to-line rms), 60 Hz. Values for parasitic capacitances for the transformer stayed the same as in the previous case. As can be seen from Fig. 70 the common mode current peak is 30.65 A and the rms current is 2.69 A. This is larger than in the case of topology #1 with IGCTs, but smaller than the same topology with IGBT devices. One reason is the higher DC link voltage necessary to generate 4.16 kV instead of 2.3 kV at the output, which also influences the dV/dt also to be higher. Another reason is that this configuration has two DC-DC converters with two transformers which create second common mode voltage source, as was shown in equation (46) which further increases the magnitude of the common mode current.

5.5.3 Topology #4

Fig. 71 shows the equivalent circuit of the cascaded multilevel inverter shown in Fig. 60 suitable for common mode voltage analysis. The points "n_{11}", "n_{12}" and "n_{13}" represent the DC-link mid points of three single-phase inverter cells in phase A. Further, the transformer in the DC-DC converter is modeled by lumped capacitances from primary and secondary to ground, and capacitance from secondary to primary, assuming that they are equal for each DC-DC converter. The voltages $V_{a1a1'}$ to $V_{a3a3'}$ represent the PWM output voltages of single-phase inverter cells 1 to 3 in phase A respectively. From the equivalent circuit shown in Fig. 64 it can be seen that

$$\begin{aligned} V_{AN} &= V_{a1'a1} + V_{a2'a2} + V_{a3'a3} \\ V_{BN} &= V_{b1'b1} + V_{b2'b2} + V_{b3'b3} \\ V_{CN} &= V_{c1'c1} + V_{c2'c2} + V_{c3'c3} \end{aligned} \tag{47}$$

The common mode voltage generated by the cascaded inverter modules is given by

$$V_{CM} = \frac{V_{AN} + V_{BN} + V_{CN}}{3} \tag{48}$$

The instantaneous summation of PWM voltages $V_{AN} + V_{BN} + V_{CN}$ may not be zero and is dependent on the PWM strategy employed. Since each single inverter cell has 0 and $\pm V_d$ switching states, the worst case value for V_{AN}, V_{BN}, V_{CN} and common mode voltage V_{CM} is $\pm 3V_d$.

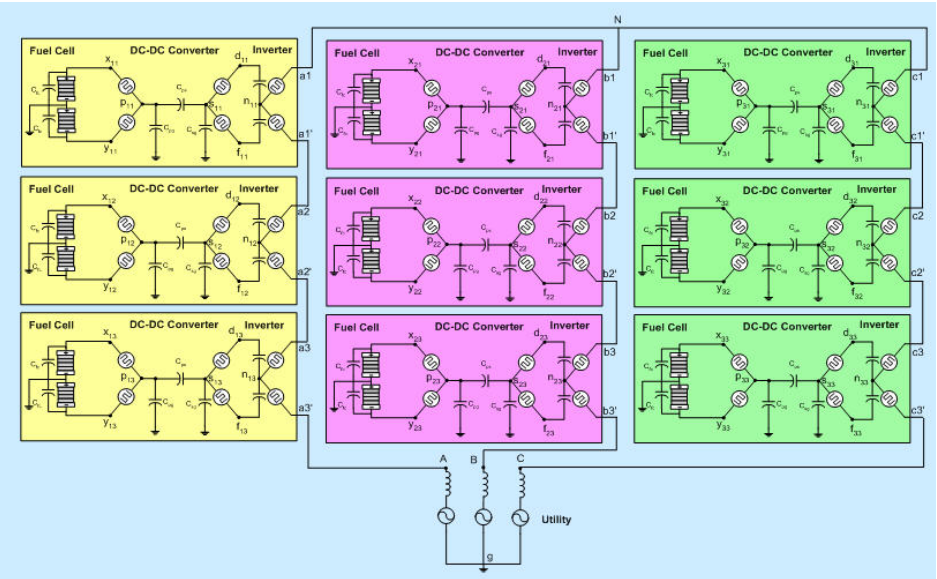

Fig. 71. Common mode equivalent circuit for topology #4

Fig. 72 shows the simulated circuit of cascaded multilevel inverter. The simulation parameters were: inverter DC-link voltage set to 1200 V; switching frequency 12.6 kHz; output voltage 4.16 kV (line-to-line rms); PWM strategy = SPWM - unipolar with 120^{o} phase shift between inverter stages; with the transformer's parasitic capacitances as in previous case. Fig. 73b shows the resulting common mode current I_{cm}, voltage V_{a1n}, voltage V_{ng1} and the common mode voltage of the system. As can be seen from figure the common mode current is considerably larger in this case. The peak common mode current for this case reaches 136.3 A; with rms value of 10.95 A. This topology has many common mode sources (9 DC-DC converters) which results in higher common mode current.

The common mode voltage in this topology is distributed between the line transformer capacitance to ground and the respective DC-DC converter's transformer secondary winding capacitances to ground. The common mode voltage of each

transformer secondary winding is also widely different. From the equivalent circuit in Fig. 71, it is easy to infer that the common mode voltage is maximum for the transformer secondary winding supplying power to the inverter cell which is closest to the load. That is, voltage $V_{n13g} > V_{n11g}$ voltage (Fig. 71). The exact nature of the transformer secondary windings with respect to ground can be determined via simulations and is shown in Fig. 73a.

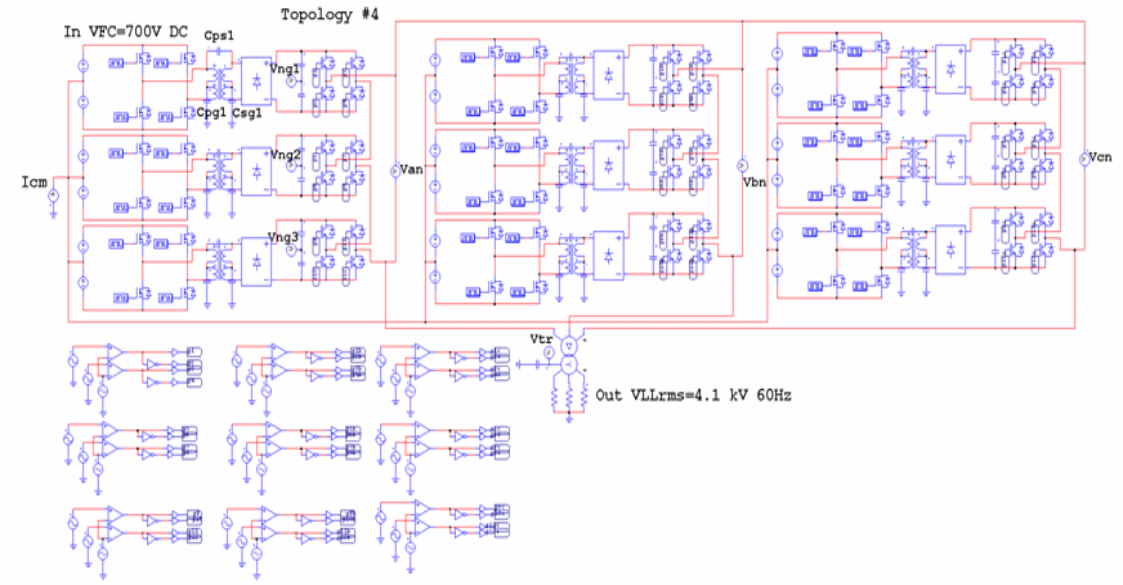

Fig. 72. Circuit schematic of medium voltage topology #4

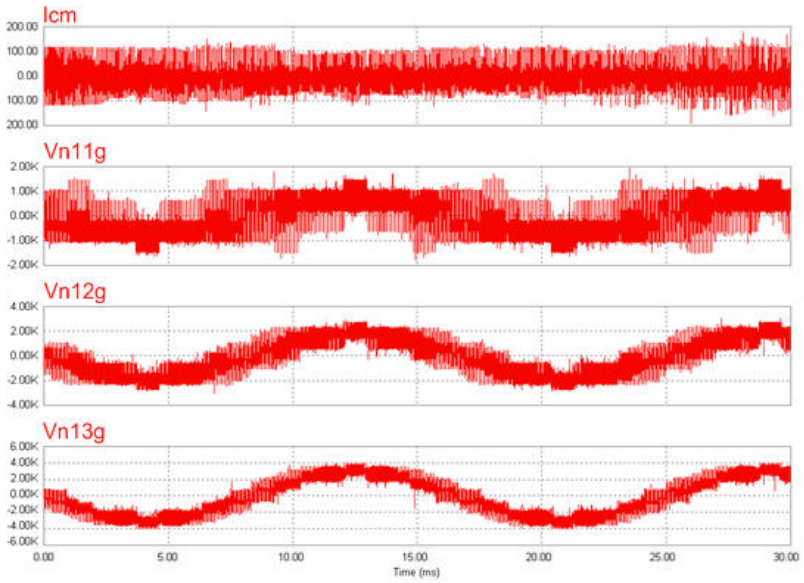

a)

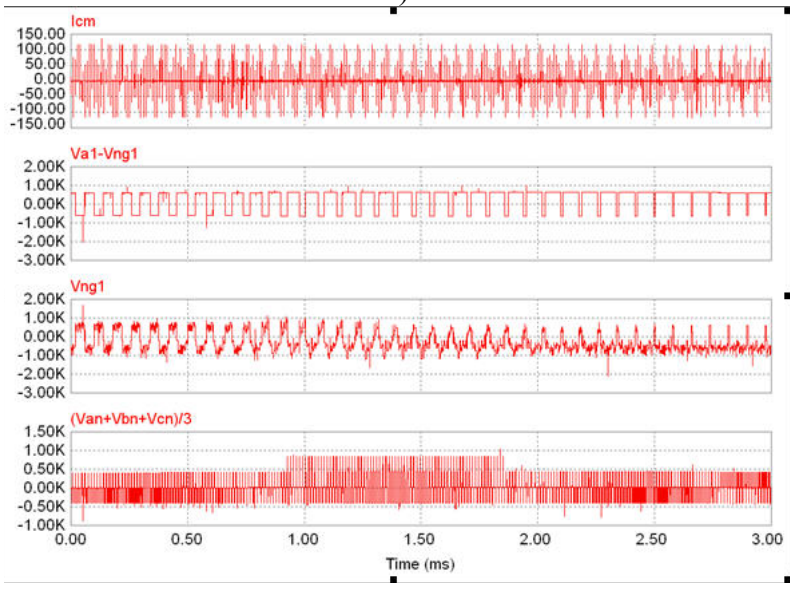

b)

Fig. 73. Simulation result of medium voltage topology #4

5.5.4 Topology #5

Fig. 74 shows the common mode equivalent circuit of the hybrid multilevel inverter shown in Fig. 61 obtained in same fashion as previous topologies. This topology uses an output transformer to add the output voltages of each inverter. Both DC-DC converters

and DC-AC inverters are modeled similar to previous topologies. If we assume that the first inverter system generates three phase voltages with rms V_1 (terminals a_1, b_1, c_1) and that second inverter system is generating the three phase voltages with rms V_2 (terminals a_2, b_2, c_2), then the output voltage at the terminals a_3, b_3, c_3 will be

$$V_3 = V_2 + n_1 \cdot \sqrt{3} \cdot V_1 e^{j\pi/6} \tag{49}$$

where n_1 is transfer ratio of delta to Y transformer T_1. Thus, the final output voltage to the utility side (terminals A, B, C) will be

$$V_{out} = V_3 \cdot n_2 \cdot \frac{1}{\sqrt{3}} \cdot e^{-j\pi/6} \tag{50}$$

where n_2 is transfer ratio of Y to delta transformer T_2. From (49) and (50) we can conclude that the common mode voltage of the inverter system 1 will have bigger influence than the common mode voltage of the inverter system 2.

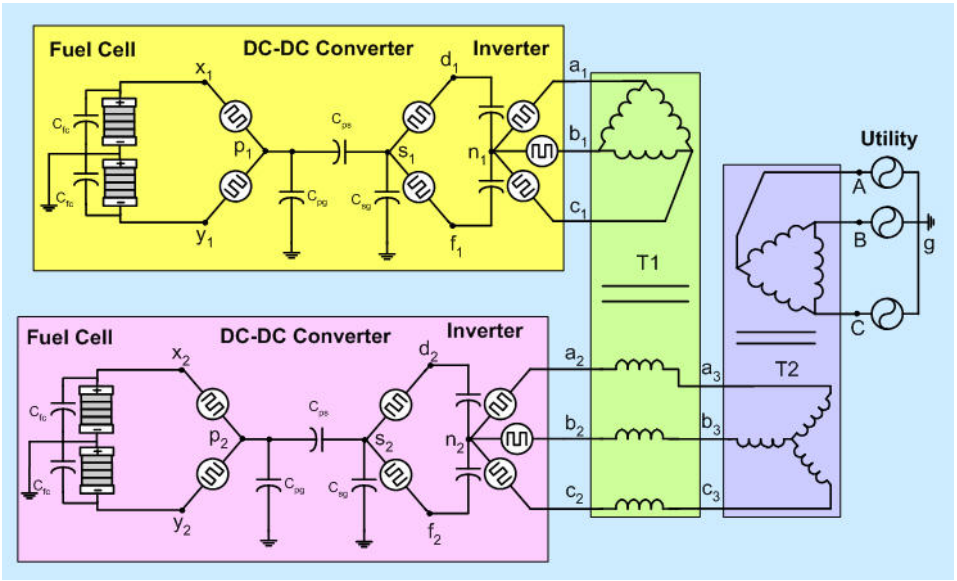

Fig. 74. Common mode equivalent circuit for topology #5

Fig. 75 shows the simulated circuit of hybrid multilevel inverter. DC-link voltage of inverter 1 was set to 1000 V, and inverter 2 DC-link voltage was set to 2000 V, output voltage was 4.16 kV (line-to-line rms), 60Hz.

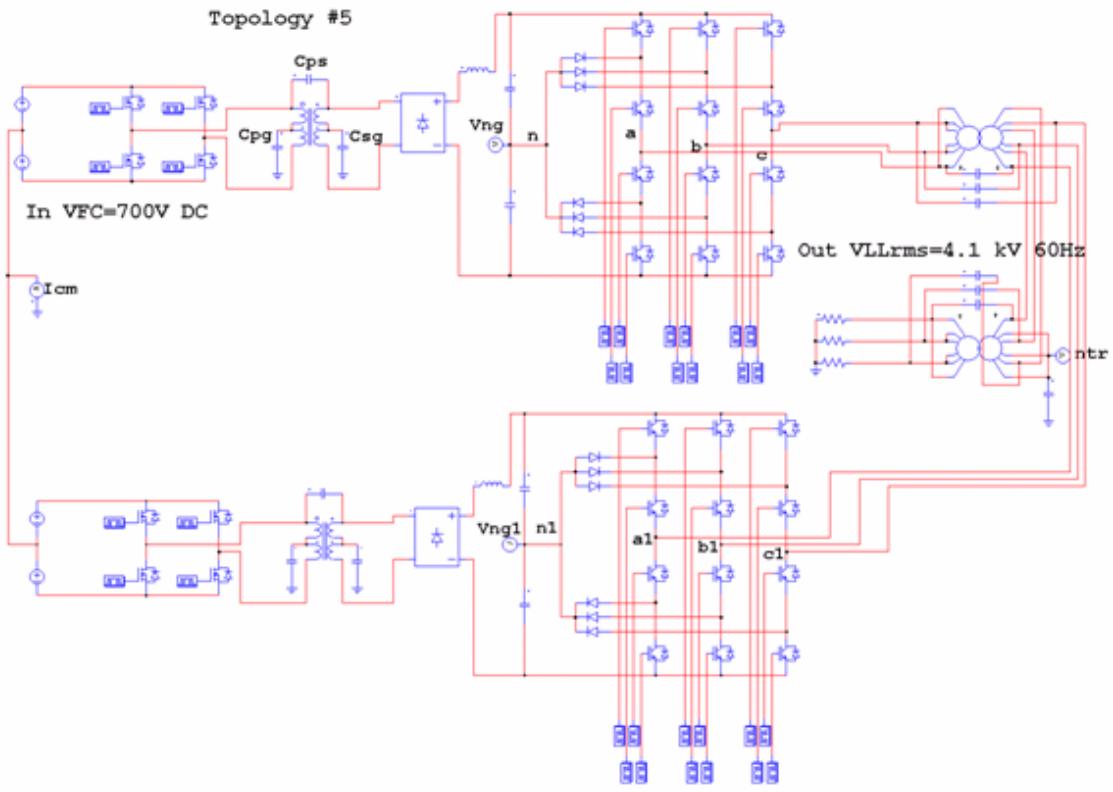

Fig. 75. Circuit schematic of medium voltage topology #5

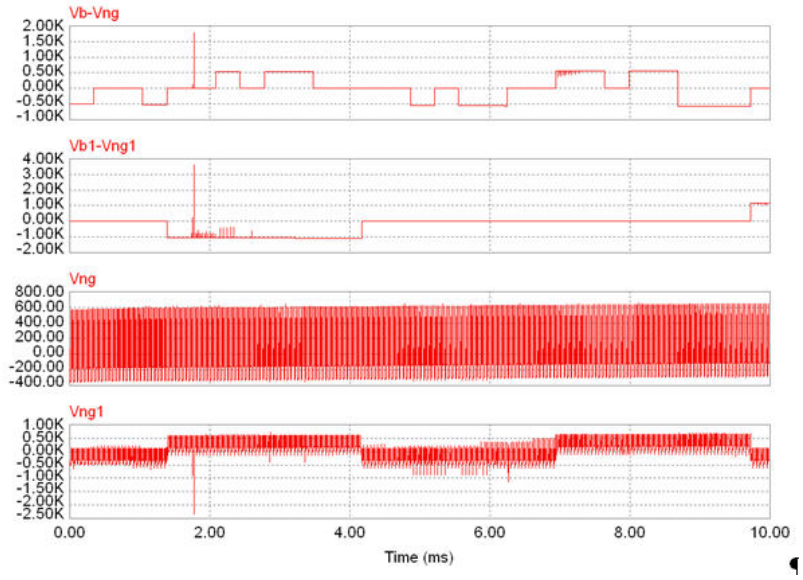

a)

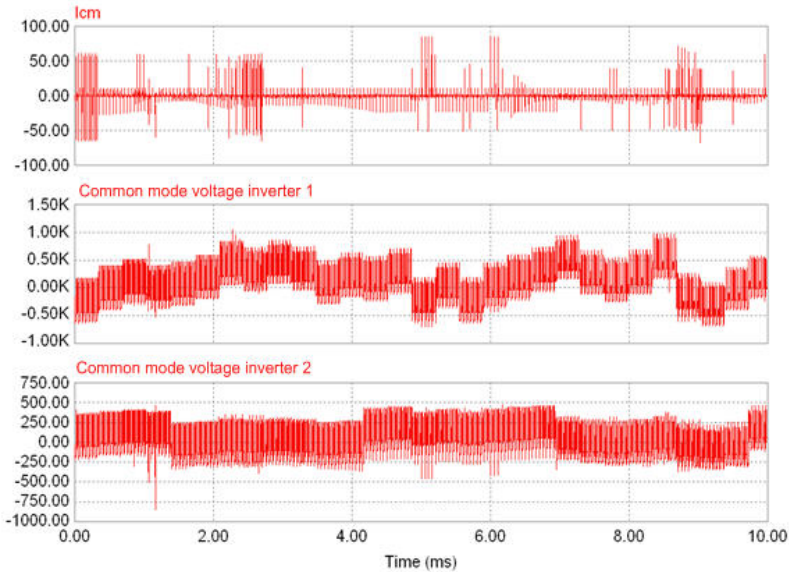

b)

Fig. 76. Simulation results of medium voltage topology #5

Fig. 76a shows the resulting output voltages of phase B for each converter before they are added with transformer T_1, V_{bng} and V_{bng1}, and voltage between point 'n' and ground for both converters. Fig. 76b shows the resulting common mode current I_{cm}, the common mode voltage of the system 1 and common mode voltage of the system 2. The

peak common mode current for this case reaches 85.78 A; with rms value of 1.93 A. The value of the common mode voltage is much smaller than in the cascaded inverter case, but it is still very high if we compare it with results for topologies #1 and #2.

5.5.5 Reduction of common mode current

The short duration and high amplitude of the current spikes in the common mode current contribute to the conducted EMI, which can affect the operation of low power electronic circuitry. The amount of EMI generated is proportional to the magnitude of the current pulses in the common mode current. For this reason it becomes necessary to reduce the magnitude of the current pulses. From equations (43) and (46) it can be seen that the common mode current is generated by the common mode voltage sources of the DC-DC converter and DC-AC inverter. Also since the voltage in the DC link between the DC-DC converter and inverter is several times higher than the voltage produced by the fuel cell; the component of the common mode current generated by the inverter is dominant in the overall common mode current. Further analyzing equations (43) and (46) it becomes clear that to limit the main component of the common mode current the capacitance C_{ps} in the equivalent circuit has to be reduced. In the common mode equivalent circuit this capacitance stands for the parasitic capacitance between the primary and secondary of the high frequency transformer used in the DC-DC converter, as can be seen in Fig. 77a.

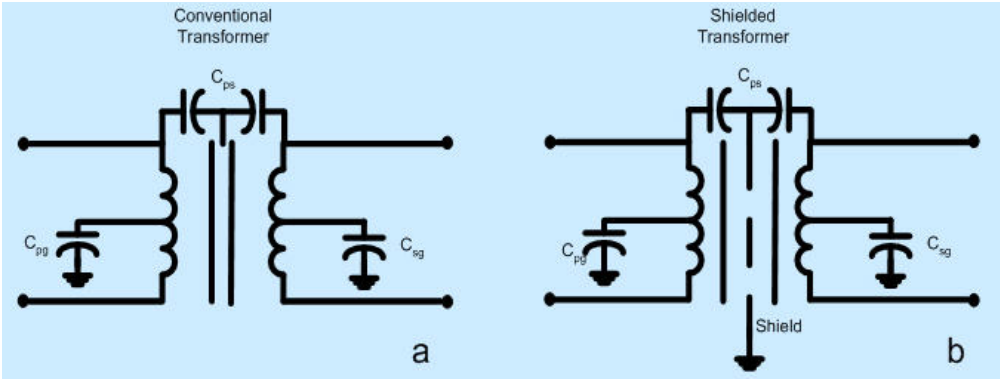

Fig. 77. Conventional and shielded transformer

A practical way of reducing the value of this capacitance is by using a shield in the transformer. The shield is then connected to ground (Fig. 77b), reducing the capacitive coupling between primary and secondary.

To verify the effectiveness of the shielded transformer all medium voltage topologies were simulated in PSim and the common mode current was measured. Fig. 78a shows the common mode current obtained for the medium voltage topology #1 with IGCT devices when a shielded transformer is used, while Fig. 78b shows the common mode current obtained for the medium voltage topology #1 with IGBT devices when a shielded transformer is used.

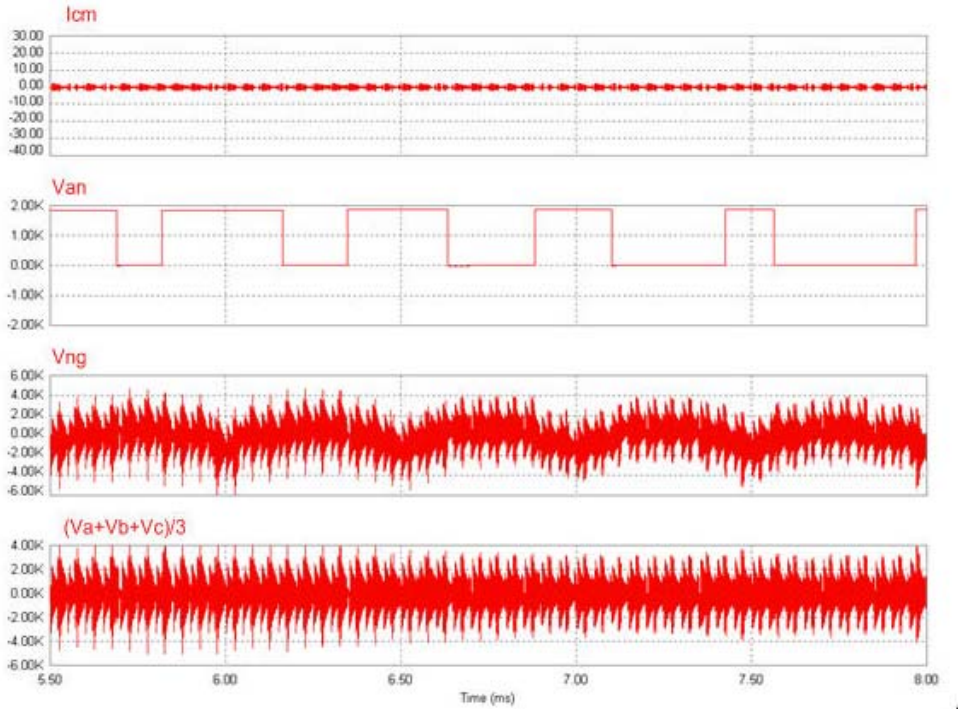

a)

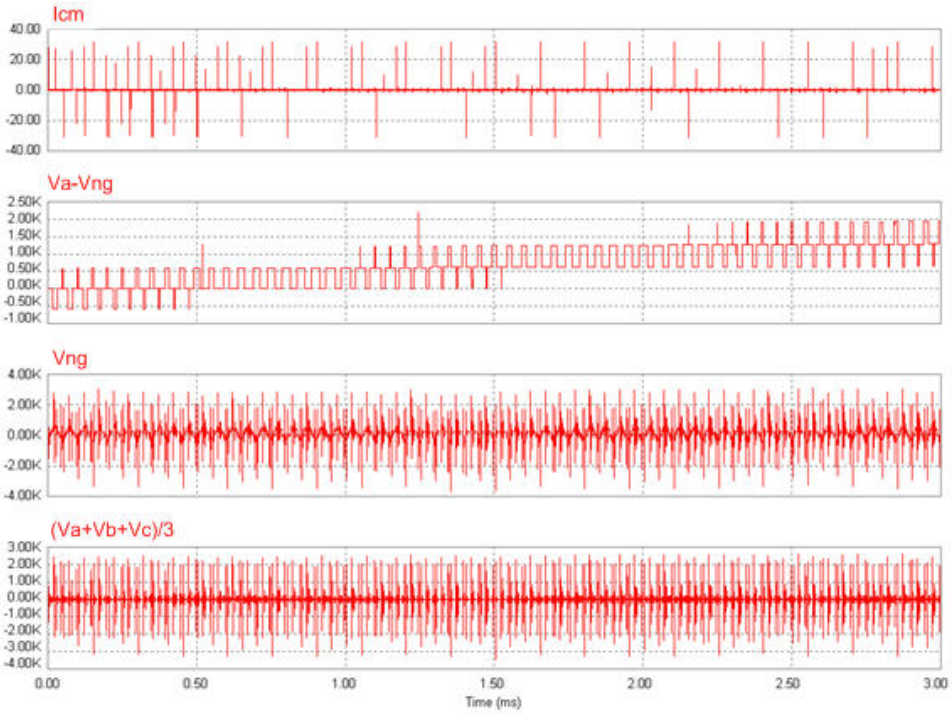

b)

Fig. 78. Simulation result of medium voltage topology #1 with shielded transformer a) IGCT devices b) IGBT devices

As can be seen from Fig. 78 the common mode current is significantly reduced. In this case the peak amplitude of the current is 2.72 A in case IGCT devices were used and 3.2 A in case IGBT devices were used. The common mode current is five orders of magnitude smaller than the current present when a normal transformer is used to implement the DC-DC converter in case when inverter with IGCT devices was used, and sixteen times smaller when inverter with IGBT devices was used.

The case of the medium voltage topology #2 is studied next. The same three phase fuel cell power converter shown in Fig. 69 is simulated. However, in this case the parasitic capacitance from transformer primary to secondary was split into two capacitances of 25 pF as shown in Fig. 77b to account for the shielding in the transformer. Fig. 79 shows results obtained from the simulation. As can be observed from the figure the peak common mode current in this case reaches 4.56 A.

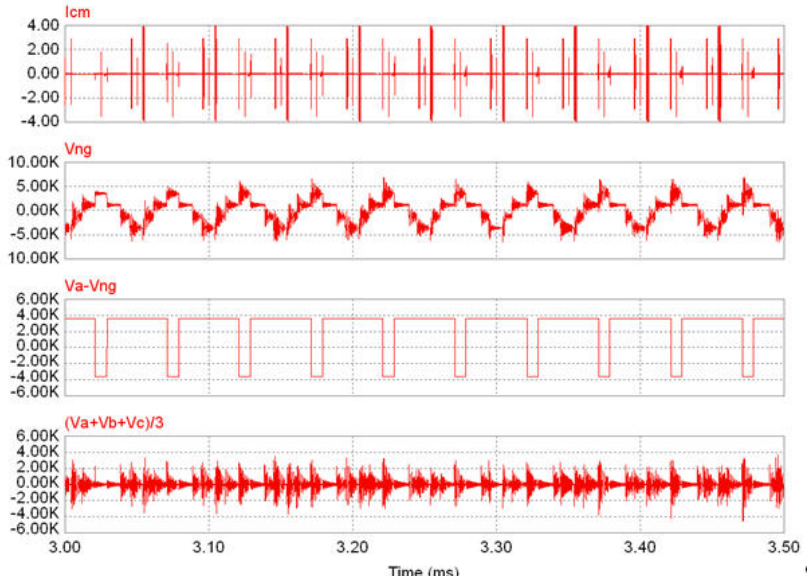

Fig. 79. Simulation result of medium voltage topology #2 with shielded transformer

Next, simulations were repeated for cascaded multilevel inverter from Fig. 72 with all 9 transformers shielded. The parasitic capacitance from transformer primary to secondary was split into two capacitances of 25 pF as explained in previous case. Fig. 80 shows results obtained from the simulation. The peak common mode current in this case reaches 116 A. This is a minor improvement, so this topology needs improvements in PWM modulation strategy. An example approach was explained in [30].

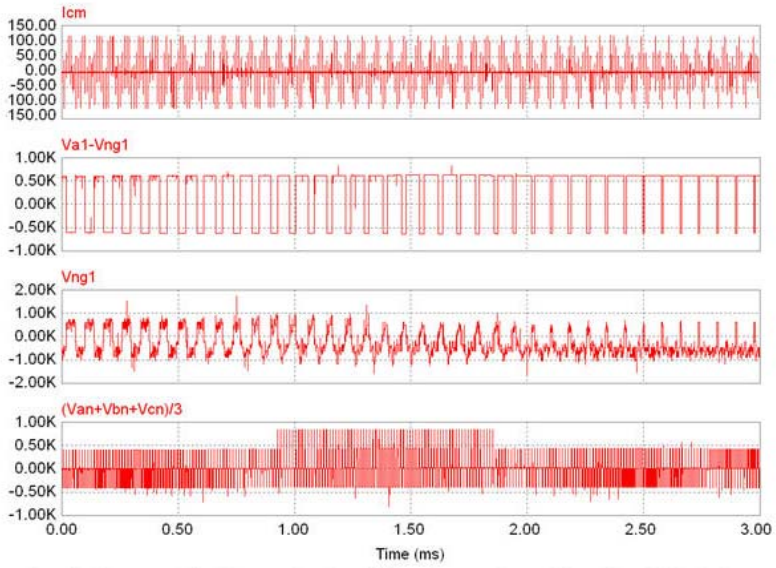

Fig. 80. Simulation result of cascaded multilevel topology #4 with shielded transformer

Finally the case of the hybrid multilevel topology #5 was studied. Fig. 81 shows results obtained from the simulation. As can be observed from the figure the peak common mode current in this case reaches 69 A. This is also a minor improvement and there is a need to change the PWM modulation strategy to fix the common mode voltage and current problems.

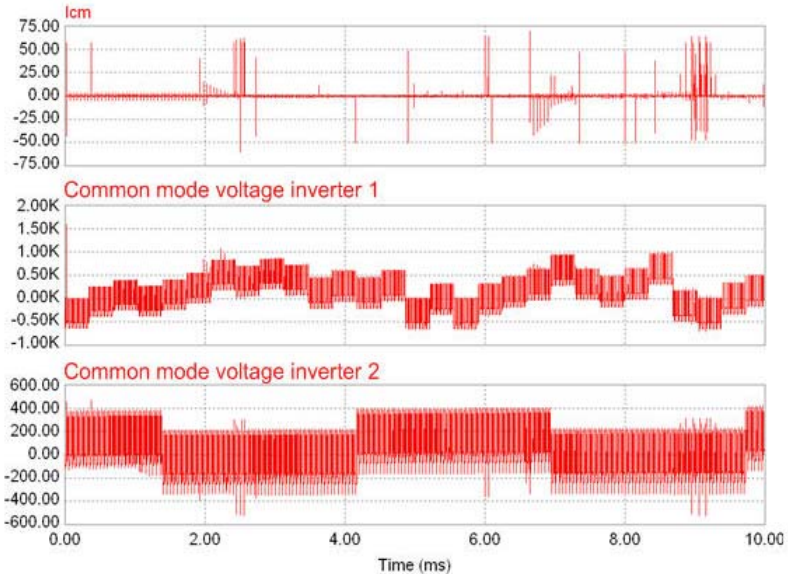

Fig. 81. Simulation result of hybrid multilevel topology #5 with shielded transformer

From the comparison of the results shown in previous figures one can see that the common mode current is greatly reduced by the introduction of a shield in the high frequency transformer in the DC-DC converter. The magnitude of the reduction in the peak value of the common mode current depends on the topology. From these results it is possible to conclude that by using a shielded transformer the common mode current can be minimized, which contributes to a reduction of the conducted EMI.

5.6 Conclusion

Fuel cell stacks produce DC voltage with a 2:1 variation in output voltage from no load to full load. A power conditioner consisting of DC-DC and DC-AC converters is required for utility interface. In this chapter power electronics converter topologies suitable for high megawatt fuel cell based power plants were examined in detail. It was shown that converting DC power produced by fuel cell to AC power suitable for utility

interface can be accomplished by a variety of converter topologies and their interconnections. The aim of this chapter was to study the various possibilities and compare them with respect to performance, component count, cost, usage of magnetics, etc. It was also shown that the switching mode nature of the power converters generates common mode voltage with respect to ground. The presence of high frequency common mode voltage contributes to circulating ground current which can interfere with ground fault protection system and also contribute to neutral shift and electro magnetic interference (EMI). This chapter presented an analysis of common mode voltage in the converter topologies and discussed several mitigation methods. Several possible fuel cell power converter topologies were considered for utility scale generation. This Chapter presents extensive simulations regarding common mode and converter performance for all megawatt topologies.

CHAPTER VI

CONCLUSIONS

A combination of the high cost of fossil fuels and the increased awareness of their negative environmental impact has influenced the development of new cleaner energy sources. Among various viable technologies the fuel cells have emerged as one of the most promising sources for both portable and stationary applications.

Fuel cell stacks produce DC voltage with a 2:1 variation in output voltage from no load to full load conditions. Hence, to increase the utilization efficiency and system stability, a power conditioner consisting of DC-DC and DC-AC converters is required for load interface. The design of power conditioners is driven by the application. This dissertation presented several different solutions for applications ranging from low-power portable sources for small electronics and laptop computers to megawatt-power applications for fuel cell power plants. The design and analysis for each power conditioner was presented in detail and the performance was verified using simulations and prototypes.

Special consideration was given to the role of supercapacitors which act as the additional energy storage elements. Chapter II showed that the supercapacitor connected at the terminals of a fuel cell can contribute to increased steady state stability when powering constant power loads, improved transient stability against load transients, and increased fuel efficiency (i.e. reduced hydrogen or other fuel consumption). Further, it was shown that the electric equivalent circuit of a fuel cell is essential to establishing a

design procedure to size the required supercapacitor. The development of the equivalent circuit model for fuel cells and supercapacitors using frequency analysis was presented and results discussed. Additionally, the benefits obtained in steady state stability of the power conditioner when powered by the hybrid source were analyzed and it was shown that such configuration possesses several advantages from the energy management point of view. For transient stability analysis, the effect of fuel cell internal impedance (extra element) along with the impedance of the nonlinear supercapacitor on the transfer function of the DC-DC converter was analyzed. Finally, experimental evaluation and comparison of fuel consumption in the conventional and hybrid systems was performed, showing that the hybrid source has improved fuel utilization.

Next chapter discussed in detail the conceptual design behind the four proposed power distribution architectures for fuel cell powered laptop computers. For each architecture, advantages/disadvantages were highlighted. Power consumption of two different laptop computers was measured for different types of loads to determine transient and steady state needs of the system.

Furthermore, a hybrid multi-input bi-directional DC-DC converter for applications in fuel cell powered laptop computers has been proposed. The purpose of this multi-input converter is to suitably control the energy flow from multiple energy sources to enable all day computing. The AC-DC adapter and the fuel cell and its components were integrated with the converter in an external unit while the conventional Li-Ion battery was placed within the laptop casing. A design example highlighting the parameters of the fuel cell stack, Li-Ion battery, and supercapacitor modules appropriately sized for a typical load on

a laptop computer was shown. Analysis, design and control aspects of the hybrid DC-DC converter were presented to meet performance requirements for all day computing. Simulation results verified the performance of the system under various input and output power conditions. Experimental results showed that the bi-directional converter is working as expected in both operating modes, bucking the voltage down to the usable levels when the battery is supporting the DC link and boosting the fuel cell voltage to charge the batteries and sustain the DC link when the fuel cell is maintaining the DC link voltage. Transient behavior of the DC link during the sudden load change is excellent due to the presence of supercapacitors. It was shown that this topology stores and delivers energy more efficiently than the conventional systems and hence, can be used for energy storage for other portable applications.

Chapter IV introduced a fuel cell powered, passive stand-by single-phase UPS system. It has been shown that the proposed topology provides stable power to the load when the utility is interrupted. A mathematical approach to analyze the interactions between the internal impedance of the fuel cell and the DC-DC converter closed loop control to verify steady state and transient stability has been presented. It has been shown that the fuel cell's dominant time constant is load dependent and varies from 8.97ms (light load) to 20.37ms (full load) resulting in fuel cell's relatively slow dynamic response. Design inequalities have been reviewed to better understand the interaction between the DC-DC converter and fuel cell and, as well, potential instability conditions. A method to size the supercapacitor module was incorporated to overcome the load transients such as instantaneous power fluctuations, slow dynamics of the fuel

preprocessor and overload conditions. It was shown that the supercapacitor values calculated for overload conditions were sufficient to enhance stability and improve dynamic response of the fuel cell. A complete design example illustrating the amount of hydrogen storage required for 1 hour power outage and sizing of supercapacitors for transient load demand has been presented for a 1.5 kVA UPS.

Finally, Chapter V examined in detail power electronics converter topologies suitable for high mega watt fuel cell based power plants. It was shown that converting DC power produced by fuel cell to AC power suitable for utility interface can be accomplished by a variety of converter topologies and their interconnections. The aim of this chapter was to study the various possibilities and compare them with respect to performance, component count, cost, usage of magnetics, etc. It was also shown that the switching mode nature of the power converters generates common mode voltage with respect to ground. The presence of high frequency common mode voltage contributes to circulating ground current which can interfere with ground fault protection system and also contribute to neutral shift and electro magnetic interference. Chapter V presented an analysis of common mode voltage in the converter topologies and discussed several mitigation methods. Several possible fuel cell power converter topologies were considered for utility scale generation. Extensive simulations regarding common mode and converter performance for all mega watt topologies were presented.

REFERENCES

[1] Y.R. de Novaes, R.R. Zapelini, and I. Barbi, "Design considerations of a long-term single-phase uninterruptible power supply based on fuel cells," in *Proc. IEEE-PESC*, 2005, pp. 628-1634.

[2] M. Pagano, and L. Piegari, "Electrical networks fed by fuel-cells for uninterruptible electrical supply," in *Proc. IEEE-ISIE*, 2002, pp. 953-958.

[3] EG&G Technical Services, Inc., *Fuel Cell Handbook,* 6th ed., Morgantown, WV: US Department of Energy, Office of Fossil Energy, 2002.

[4] A.F. Burke, "Batteries and ultracapacitors for electric, hybrid, and fuel cell vehicles," in *Proc. of the IEEE*, 2007, pp. 806–820.

[5] M. Amrhein, and P.T. Krein, "Dynamic simulation for analysis of hybrid electric vehicle system and subsystem interactions, including power electronics," *IEEE Trans. Vehicular Technology*, vol. 54, pp. 825-836, May 2005.

[6] http://www.neahpower.com/powergap/overview.shtml.

[7] http://www.toshiba.co.jp/about/ press/2003_03/pr0501.htm.

[8] W. Choi, P. Enjeti, and J.W. Howze, "Fuel cell powered UPS systems: design considerations", in *Proc. IEEE-PESC*, 2003, pp. 385-390.

[9] Y. Watanabe, M. Matsumoto, and K. Takasu, "The market for utility-scale fuel cell plants," *Journal of Power Sources*, vol.61, pp. 53-59, Jul. 1996.

[10] G. Bernsten, "Scale-up experience with mega-watt class inverter topologies," *Solid State Energy Conversion Alliance Workshop*, May 2006, pp.122-128.

[11] S. Stevandic, and J. Jiang, "Standalone, reduced-order model and control of a grid-connected fuel cell power plant," in *IEEE Power Engineering Society General Meeting*, 2003, pp. 679-686.

[12] M. Uzunoglu, and M.S. Alam, "Dynamic modeling, design, and simulation of a combined PEM fuel cell and ultracapacitor system for stand-alone residential applications," *IEEE Trans. Energy Conversion*, vol. 21, pp. 767-775, Sep. 2006.

[13] B. Maher, "Use of ultracapacitors and fuel cells in both stationary and mobile applications," *Fuel Cell*, pp. 32-38, Dec. 2006/Jan. 2007.

[14] R. Smith, and W. Fuglevand, "Ultracapacitors and fuel cells make a perfect match for portable applications," *Portable Design*, Jan. 2004.

[15] J. Correa, F. Farret, L. Canha, and M. Simones, "An electrochemical–based fuel cell model suitable for electrical engineering automation approach," *IEEE Trans. Industrial Electronics*, vol. 51, pp. 1103-1112, Oct. 2004.

[16] R. Amphlett, R. Mann, B. Peppley, P. Roberge, and A. Rodigues, "A practical PEM fuel cell model for simulation vehicle power sources," in *Proc. Battery Conference on Applications and Advances*, 1995, pp. 221–226.

[17] M. Ceraolo, C. Miulli, and A. Pozio, "Modeling static and dynamic behavior of proton exchange membrane fuel cells on the basis of electro-chemical description," *Journal of Power Sources*, vol. 113, pp. 131-144, Jan. 2003.

[18] W. Lajnef, J.-M. Vinassa, S. Azzopardi, O. Briat, E. Woirgard, C. Zardini, and J.L. Aucouturier, "Ultracapacitors modeling improvement using an experimental

characterization based on step and frequency responses," in *Proc. IEEE-PESC*, 2004, pp. 131–134.

[19] W. Lajnef, J.-M. Vinassa, O. Briat, S. Azzopardi, and C. Zardini, "Study of ultracapacitors dynamic behavior using impedance frequency analysis on a specific test bench," in *Proc. IEEE Industrial Electronics*, 2004, pp. 839–844.

[20] L. Zubieta, and R. Bonert, "Characterization of double-layer capacitors for power electronics applications", *IEEE Trans. Industry Applications,* vol. 36, pp. 199–205, Jan.-Feb. 2000.

[21] R. Erickson, and D. Maksimović, *Fundamentals of Power Electronics*, 2nd ed. Boston: Kluwer Academic Publishers, 2001.

[22] T.L. Cleveland, "Bi-directional power system for laptop computers," in *Proc. IEEE-APEC*, 2005, pp. 199-203.

[23] B. Flipsen, and B. Coremans, "Fuel cells in consumer electronics, a case study of a fuel-cell powered laptop computer," in *Proc. International Power Sources Symposium*, 2005, Brighton (Great Britain). [Online] Available: http://www.io.tudelft.nl/live/pagina.jsp. "accessed on Feb. 2008".

[24] E. Santi, D. Franzoni, A. Monti, D. Patterson, F. Ponsi, and N. Barry, "A fuel cell based domestic uninterruptible power supply", in *Proc. IEEE-APEC*, 2002, pp. 605-613.

[25] G.V. Sukumara, A. Parthasarathy, and V.R. Shankar, "Fuel cell based uninterrupted power sources," in *Proc. IEEE International Conference on Power Electronics and Drive Systems*, 1997, pp. 728–733.

[26] N. Kato, T. Murao, K. Fujii, T. Aoiki, and S. Muroyama, "1 kW portable fuel cell system based on PEFCs," in *Proc. IEEE-TELESCON,* 2000, pp. 209–213.

[27] F.Z. Peng, J.S. Lai, J. McKeever, and J. VanCoevering, "A multilevel voltage-source inverter with separate DC sources for static VAr generation," *IEEE Trans. Industry Applications*, vol. 32, pp. 1130-1138, Oct. 1996.

[28] B. Ozpineci, L.M. Tolbert, and Z. Du, "Multiple input converters for fuel cells," in *Proc. IEEE-IAS*, 2004, pp. 791-797.

[29] B. Ozpineci, Z. Du, L.M. Tolbert, D.J. Adams, and D. Collins, "Integrating multiple solid oxide fuel cell modules," in *Proc. IEEE-IECON*, 2003, pp. 1568-1573.

[30] D.A. Rendusara, E. Cengelci, P.N. Enjeti, V.R. Stefanovic, and J.W. Gray, "Analysis of common mode voltage – 'Neutral shift' in medium voltage PWM adjustable speed drive (MV-ASD) systems," *IEEE Trans. Power Electronics*, vol. 15, pp. 1124-1133, Nov. 2000.

[31] L. Palma, and P. Enjeti, "An inverter output filter to mitigate dV/dt effects in PWM drive system," in *Proc. IEEE-APEC*, 2002, pp 550–556.

[32] S. Ogasawara, and H**.** Akagi, "Modeling and damping of high-frequency leakage currents in PWM inverter-fed AC motor drive systems," *IEEE Trans. Industry Applications*, vol. 32, pp. 1105–1114, Sep. 1996.

[33] P.C. Loh, D.G. Holmes, Y. Fukuta, and T.A. Lipo, "A reduced common mode hysteresis current regulation strategy for multilevel inverters," *IEEE Trans. Power Electronics*, vol. 19, pp. 192–200, Jan. 2004.

[34] P.C Loh, D.M. Vilathgamuwa, F. Gao, C.J. Gajanayake, L.W. Gay, and P.F. Leong, "Random pulse-width modulated neutral-point-clamped inverter with reduced common-mode switching," in *Proc. IEEE-PEDS,* 2005, pp. 1435–1440.

[35] H. Zhang, A. Von Jouanne, S. Dai, A.K. Wallace, and F. Wang**,** "Multilevel inverter modulation schemes to eliminate common-mode voltages**,**" *IEEE Trans. Industry Applications*, vol. 36, pp. 1645–1653, Nov. 2000.

[36] U. Dewald, "Micro-reformers turn methanol into hydrogen," Initiative Brennstoffzelle 12.03.2004 - micro devices. [Online] Available: http://www.initiative-brennstoffzelle.de/ibz/live/nachrichten/show.php3 "accessed on Feb. 2008".

[37] M. Harfman-Todorovic, L. Palma, and P. Enjeti, "Design of a wide input range DC-DC converter with a robust power control scheme suitable for fuel cell power conversion," in *Proc. IEEE-APEC,* 2004, pp.374-379.

[38] H.P. Dhar, "Medium-term stability testing of proton exchange membrane fuel cell stacks as independent power units," *Journal of Power Sources*, vol. 143, pp 185-190, Apr. 2005.

[39] S.B. Beikarov, and A. Emadi, "Uninterruptible power supplies: classification, operation, dynamics and control," in *Proc. IEEE-APEC,* 2002, pp. 597–604.

[40] S. Karve, "Three of a kind [UPS topologies, IEC standard]," *IEE Review*, vol. 46, pp. 27-31, Mar. 2000.

[41] M.S. Rauls, D.W. Novotny, and D.M. Divan, "Design considerations for high frequency coaxial winding power transformers," *IEEE Trans. Industrial Electronics*, vol. 29, pp. 375-381, Mar.-Apr. 1993.

[42] C. Pereira, S. Ahmed, S.H.D. Lee, and M. Krumpelt. Integrated fuel processor development. Presented at 2002 Future Car Congress. [Online] Available: http://www.ipd.anl.gov/anlpubs/2001/12/41460.pdf

[43] O.D. Patterson, and D.M. Divan, "Pseudo-resonant full-bridge DC/DC converter," *IEEE Trans. Power Electronics*, vol. 6, pp. 671-678, Oct. 1991.

[44] G. Hua, F.C. Lee, and M.M. Jovanovic, "An improved full-bridge zero-voltage-switched PWM converter using a saturable inductor," *IEEE Trans. Power Electronics*, vol. 8, pp. 530-534, Oct. 1993.

[45] N.H. Kutkut, D.M. Divan, and R.W. Gascoigne, "An improved full-bridge zero-voltage switching PWM converter using a two-inductor rectifier," *IEEE Trans. Industry Applications*, vol. 31, pp. 119-126, Jan.-Feb. 1993.

[46] Ballard Power Systems Inc, *NexaTM Power Module User's Manual MAN5100078*, Burnaby, BC, Canada: Ballard Power Systems Inc, Oct. 2005.

[47] M.W. Chase Jr., *NIST-JANAF Thermochemical Tables*, 4th ed., Washington D.C: American Institute of Physics for the NIST, 1998.

[48] J.H. Dymond, and E.B. Smith, *The Virial Coefficients of Pure Gases and Mixtures, A Critical Complication*, Oxford: Oxford University Press, 1980.

[49] J.M. Smith, H.C. Van Ness, and M.M. Abbott, *Introduction to Chemical Engineering Thermo Dynamics*, New York: McGraw-Hill, 1996.

[50] S.K. Mazumder, and R. Huang, "A high-power high-frequency and scalable multi-megawatt fuel-cell inverter for power quality and distributed generation," in *Proc. Power Electronics, Drives and Energy Systems,* 2006, pp. 1–5.

[51] J.S. Lai, and F. Z. Peng, "Multilevel converters–A new breed of power converters," *IEEE Trans. Industry Applications*, vol. 32, pp. 509–517, May/Jun. 1996.

[52] L. Tolbert, F.-Z. Peng, and T. Habetler, "Multilevel converters for large electric drives," *IEEE Trans. Industry Applications*, vol. 35, pp. 36–44, Jan./Feb. 1999.

[53] R. Teodorescu, F. Beaabjerg, J. K. Pedersen, E. Cengelci, S. Sulistijo, B. Woo, and P. Enjeti, "Multilevel converters — A survey," in *Proc. European Power Electronics Conf.*, Lausanne, Switzerland, 1999, CD-ROM.

[54] J. Rodríguez, J.-S. Lai, and F.Z. Peng, "Multilevel inverters: A survey of topologies, controls, and applications," *IEEE Trans. Industrial Electronics*, vol. 49, pp.724-738, Aug. 2002.

[55] P. Hammond, "A new approach to enhance power quality for medium voltage ac drives," *IEEE Trans. Industry Applications*, vol. 33, pp. 202–208, Jan./Feb. 1997.

[56] W.A. Hill, and C.D. Harbourt, "Performance of medium voltage multilevel inverters," in *Proc. IEEE-IAS*, 1999, pp. 1186–1192.

[57] B.J. Baliga, *Power Semiconductor Devices*. Boston, MA: PWS, 1996.

[58] M.D. Manjrekar, and T.A. Lipo, "A hybrid multilevel inverter topology for drive applications," in *Proc. IEEE-APEC*, 1998, pp. 523–529.

[59] M.D. Manjrekar, P.K. Steimer, and T.A. Lipo, *"*Hybrid multilevel power conversion system: A competitive solution for high-power applications," *IEEE Trans. Industry Applications*, vol. 36, pp. 834-841, May/Jun 2000.

[60] E. Cengelci, S.U. Sulistijo, B.O. Woom, P. Enjeti, R. Teodorescu, and F. Blaabjerge, "A new medium voltage PWM inverter topology for adjustable speed drives," *IEEE Trans. Industry Applications*, vol. 35, pp. 628-637, May/Jun 1999.

[61] U.S. Department of Energy, *Future Energy Challenge*, 2001. [Online]. Available: http://www.energychallenge.org.

[62] G.M. Martins; J.A. Pomilio, S. Buso, and G. Spiazzi, "Three-phase low-frequency commutation inverter for renewable energy systems," *IEEE Trans. Industrial Electronics*, vol. 53, pp. 1522-1528, Oct. 2006.

[63] G. Skibinski, J.Pankau, R. Sladky, and J. Campbell, "Generation, control and regulation of EMI from AC drives," in *Proc. IEEE-IAS*, 1997, pp. 1571–1583.

VITA

Maja Harfman Todorovic received her B.S. degree from University of Belgrade, Serbia in 2001 and, her M.S. degree from Texas A&M University, College Station, Texas in 2004, both in Electrical Engineering. She graduated with her Ph.D. in the Department of Electrical and Computer Engineering at Texas A&M University in May 2008. Her research interests include converters for fuel cells, green power, SMPS design, UPS systems, energy storage devices and digital control of power converters.

Ms. Harfman Todorovic may be reached through the Department of Electrical and Computer Engineering, Texas A&M University, College Station, TX 77843, mail stop 77843-3128. Her email is maja.harfman@gmail.com.